A MODEL FOR THE ESTIMATION OF RESIDUAL STRESSES IN SOFT TISSUES

A Dissertation

by

SUNNIE JOSHI

Submitted to the Office of Graduate Studies of
Texas A&M University
in partial fulfillment of the requirements for the degree of

DOCTOR OF PHILOSOPHY

August 2012

Major Subject: Mathematics

A MODEL FOR THE ESTIMATION OF RESIDUAL STRESSES IN SOFT TISSUES

A Dissertation

by

SUNNIE JOSHI

Submitted to the Office of Graduate Studies of
Texas A&M University
in partial fulfillment of the requirements for the degree of

DOCTOR OF PHILOSOPHY

Approved by:

Co–Chairs of Committee,	Jay R. Walton
	John C. Criscione
Committee Members,	Wolfgang Bangerth
	Joseph Ward
Head of Department,	Emil Straube

August 2012

Major Subject: Mathematics

ABSTRACT

A Model for the Estimation of Residual Stresses in Soft Tissues. (August 2012)

Sunnie Joshi, B.S.,Randolph College

Co–Chairs of Advisory Committee: Dr. Jay R. Walton
Dr. John C. Criscione

This dissertation focuses on a novel approach for characterizing the mechanical behavior of an elastic body. In particular, we develop a mathematical tool for the estimation of residual stress field in an elastic body that has mechanical properties similar to that of the arterial wall, by making use of intravascular ultrasound (IVUS) imaging techniques. This study is a preliminary step towards understanding the progression of a cardiovascular disease called atherosclerosis using ultrasound technology. It is known that residual stresses play a significant role in determining the overall stress distribution in soft tissues. The main part of this work deals with developing a nonlinear inverse spectral technique that allows one to accurately compute the residual stresses in soft tissues. Unlike most conventional experimental, both in vivo and in vitro, and theoretical techniques to characterize residual stresses in soft tissues, the proposed method makes fundamental use of the finite strain nonlinear response of the material to a quasi-static harmonic loading. The arterial wall is modeled as a nonlinear, isotropic, slightly compressible elastic body. A boundary value problem is formulated for the residually stressed arterial wall, the boundary of which is subjected to a constant blood pressure, and then an idealized model for the IVUS interrogation is constructed by superimposing small amplitude time harmonic infinitesimal vibrations on large deformations via an asymptotic construction

of its solution. We then use a semi-inverse approach to study the model for a specific class of deformations. The analysis leads us to a system of second order differential equations with homogeneous boundary conditions of Sturm-Liouville type. By making use of the classical theory of inverse Sturm-Liouville problems, and root finding and optimization techniques, we then develop several inverse spectral algorithms to approximate the residual stress distribution in the arterial wall, given the first few eigenfrequencies of several induced blood pressures.

To My Parents अच्युत लाल जोशी and संगीता जोशी

ACKNOWLEDGMENTS

First of all, I would like to express my deepest gratitude to my advisor Dr. Jay R. Walton for his invaluable support and motivation. I am truly honored to have him as a mentor and a teacher, and I am thankful to him for his continuous guidance, encouragement and advice. I am grateful to him for introducing me to this subject which I have learnt to love and appreciate. You are truly a source of inspiration.

I would like to thank Dr. Wolfgang Bangerth, Dr. John C. Criscione and Dr. Joe Ward for not only serving on my committee but also being my teachers. I have learnt so much from Dr. Criscione's biomechanics lectures, and I truly admire his enthusiasm and love for the subject. Dr. Bangerth's lectures on deal.II have been a tremendous help in finishing this project. I am indebted to Dr. Ward for his lectures on applied analysis and help with the qualifying exam.

I also wish to thank the Department of Mathematics at Texas A&M University for giving me the opportunity to pursue this degree and for creating such a conducive learning environment. I am especially thankful to Ms. Monique Stewart for all her help with the administrative tasks. I am very appreciative of the financial support provided by the Department of Mathematics and the Institute of Applied Mathematics and Computational Science through the grant KUS-C1-016-04 made by King Abdullah University of Science and Technology (KAUST).

Finally, I would like to thank my family and friends for their continuous support and encouragement through these years, and for always being there for me. My love and appreciation for Abishek Ghimire is difficult to put into words. Thank you for believing in me, and inspiring me. It would not have been possible without you.

Thank you all.

TABLE OF CONTENTS

LIST OF TABLES

LIST OF FIGURES

CHAPTER I

INTRODUCTION

A. Cardiovascular Disease: Atherosclerosis

Cardiovascular diseases are among the leading causes of death in the western world, and atherosclerosis is the most commonly acquired one among them. It is a chronic inflammatory process in which the arterial wall thickens as a result of the build up of cholesterol and other fatty materials in the interior surface of the wall. A soft fatty plaque is formed initially followed by the development of a calcified fibrous layer. The vulnerability of the plaque to rupture depends on the thickness of the layers of these lesions. A thin soft core covered by a thick fibrous cap is known to be stable, and it is less likely to rupture, whereas, a plaque with a thick fatty core and a thin fibrous layer is more susceptible to rupture. Rupture of the plaque predisposes the flowing blood to the highly thrombogenic constituents of the plaque, thereby leading to thrombus formation and possible embolization [43]. This obstruction in normal blood flow eventually leads to a heart attack or a stroke.

A vast literature has been dedicated toward understanding the initiation and progression of atherosclerosis [40]. It is now well-established that the mechanical response of the arterial wall plays a major role in understanding the mechanobiology and the growth of the disease [25]. For example, mechanical factors such as inner-wall shear stress and within-the-wall tensile stresses have major influence on growth and remodeling of the arterial wall, and the initiation and growth of atherosclerotic lesions. Attaining a deeper understanding of the mechanobiology of arteries requires the ability to more accurately estimate the material properties and the stresses the

---

The journal model is SIAM Journal of Numerical Analysis.

arterial wall experiences in vivo than current techniques allow. While there has been progress in modeling the development of pre-stresses and residual stresses in arteries as the natural outcome of growth and remodeling processes [8, 21], devising models and nondestructive experiments through which pre-stresses and residual stresses can be reliably estimated under either in vivo or in vitro conditions remains a very challenging task.

Soft tissues, in general, exhibit a very complex mechanical behavior. Arterial wall, in particular, is anisotropic, heterogeneous, layered, pre-stressed and residually stressed, exhibits an active and passive response and a highly non linear stress-strain behavior. Developing a model to understand the mechanical properties that takes into account all of these significant, but complicated factors is very challenging. The project proposed herein serves the purpose of a preliminary study towards developing a mathematical model that takes into account most, if not all, of the significant, but complicated properties of the material to characterize the residual stress distribution in the arterial wall. It is mainly concerned with developing a nonlinear inverse spectral technique to estimate the pre-stresses and the residual stresses by making a novel use of Intravascular Ultrasound (IVUS) techniques for imaging arteries. We adopt the modeling framework for the direct problem developed in [19] to formulate an inverse parameter identification problem. The direct problem is constructed in two stages. First a quasi-static boundary value problem is formulated modeling the large deformation of the residually stressed arterial wall, the boundary of which is subjected to a time-varying blood pressure. Then an idealized model for the IVUS interrogation is constructed to generate small amplitude time harmonic vibrations superimposed on the static large deformations. This is done by adding a small amplitude, time harmonic normal traction to the blood pressure induced, quasi-static traction on the inner arterial wall and constructing an asymptotic expansion of the

solution in powers of the amplitude of the superimposed ultrasound pressure wave. This leads to a sequence of boundary value problems to various orders of the amplitude. The zero-order boundary value problem governs the static finite deformation of the arterial wall due to blood pressure, and the first-order problem gives rises to a system of second order homogeneous differential equations of Sturm-Liouville type. We then use a semi-inverse approach to study the model for a specific class of deformations. In particular, two different model problems are studied and different numerical techniques are developed for each problem.

Most inverse spectral techniques for parameter identification use a single blood pressure to formulate a boundary value problem and use a large number of eigenfrequencies corresponding to the blood pressure as data to recover the parameters. It is important to note that unlike such traditional methods, our approach is based on formulating a sequence of boundary value problems for different blood pressures, and using only the first few eigenfrequencies of each boundary value problem as data to reconstruct the residual stresses. Making use of boundary value problems that correspond to different blood pressures makes our approach *nonlinear*. Such a nonlinear approach not only makes the algorithm more robust and accurate since the lower eigenfrequencies are the easiest to detect and measure accurately, it also allows us to over estimate the system and use non-linear least squares techniques to solve the problem.

B. Residual Stresses and Pre-Stresses in Soft Tissues

Pre-stress in a body is a stress that arises due to external forces, whereas residual stress exists in the absence of external loads [25]. A wide range of materials including polymers, composites and soft tissues possess residual stress. It is of interest to

FIGURE 7.9. The "opening up" (right) of an originally unloaded intact arterial ring (left) following the introduction of a radial cut. (From Fung, 1984, with permission.)

Fig. 1. Existence of Residual Stress in Arteries

note that a nonzero residual stress cannot be uniform [23]. It is widely known that residual stress exists in soft tissues through various growth and remodeling processes that occur in the living organism, and it affects the overall stress distribution in the arterial wall under external loads. As an important special case, predicting the distribution of residual stress is a fundamental step in understanding the response and behavior of healthy and diseased blood vessels.

Modeling residual stress in arteries has been widely studied in the past few decades [11, 17, 23, 24, 26]. That residual stress exists in soft tissues was demonstrated and studied by Fung [14] and Vaishnav et al [46]. Their results were based on experiments that involved cutting a thin segment of artery radially. The segment springs open, which shows that the unloaded arterial segment is stressed (See Figure 1). It has been hypothesized that this happens because the radial distribution of the circumferential stress in the aortic media is uniform in vivo, and as a result, the segment at no load has compressive residual stress near the inner wall and tensile near the outer, causing the opening-up of the ring-like segment [16]. It was also proposed that a single radial cut is sufficient to achieve a zero-stress state, an assumption that is made in most of the models developed so far [7, 33, 45]. However, it is well known

that this is not true due to the fact that the arterial wall is heterogeneous, and it takes an infinite number of cuts to achieve a natural stress free configuration. A good observation was made by Vossoughi et al [47] where they showed that if one cuts (circumferentially) the radially cut arterial segment into inner and outer rings, then the opening angles associated with each of the radially cut ring will be different, thus suggesting that one radial cut is not sufficient to relieve all of the residual stress [25]. Physically, this means that the residual stress does not arise through deformational processes.

Most experimental and theoretical attempts that have been made to characterize residual stresses in soft tissues over the past decade use the opening-angle method. In particular, various studies are devoted towards identifying residual strains instead of residual stresses. The model proposed herein is tailored towards using clinical *in vivo* IVUS data to estimate the residual stress distribution using a parameter identification process. This method avoids dissecting arterial segments and the models that we adopt from [19] to incorporate residual stress only requires the existence of some virtual natural configuration without having the need to specify it.

C. Intravascular Ultrasound (IVUS)

Intravascular Ultrasound is a tomographic medical technology that produces cross sectional images of the inner arterial wall. It is an invasive procedure that detects atherosclerosis plaques and blockages that cause narrowing of the vessels and obstruction of blood flow. As shown in Figure 2, IVUS is equipped with a catheter containing a transducer that emits high frequency sound waves with frequency in the range of $15 - 40$ MHz. When the catheter is inserted into the artery and the transducer emits the ultrasound waves, an echo is generated which is captured and returned to an

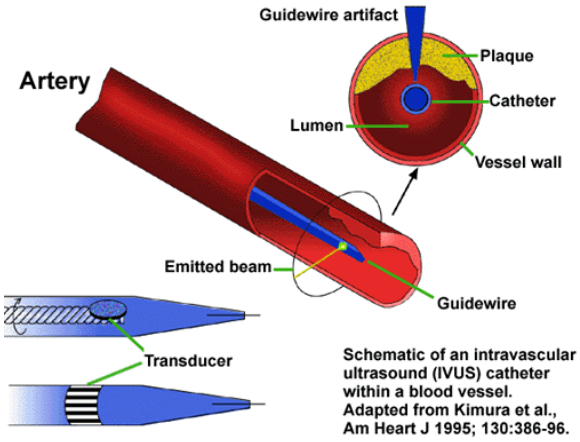

Fig. 2. IVUS Catheter

external computerized device which converts the information to real time images of the cross section of the arterial wall. Figure 3 shows an image generated by IVUS of a disease artery. The proximity of the ultrasound probe from the inner arterial walls makes it possible to use high frequency ultrasound waves and therefore obtain a high quality 360 degree image of the inner wall.

Unlike conventional models that allow characterization of the coronary plaques using IVUS imaging data [37, 44, 50], this project is focused towards using spectral characteristics of IVUS to understand the material behavior of the arterial wall. The ultrasound wave produces a time harmonic traction on the inner surface of the arterial wall causing the wall to vibrate at nanoscale [20]. One can adjust the frequency of the ultrasound wave to generate resonance of the arterial wall. This frequency, which gives an estimation of the natural eigenfrequencies of the wall tissue, is utilized to develop an inverse spectral method to reconstruct the residual stresses in the arterial wall. We note that due to the flexibility of the method, it can be generalized to study the response of any nonlinear elastic body that mimics the properties of arteries.

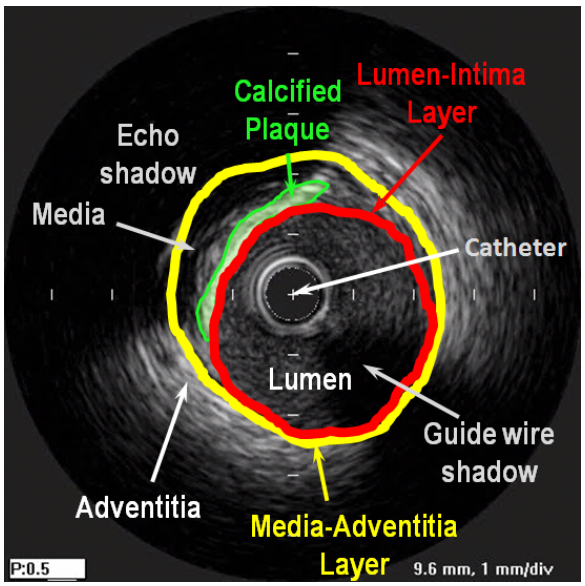

Fig. 3. Image Generated by IVUS

CHAPTER II

PRELIMINARIES

A. Basic Continuum Mechanics and Notation

Assume that a body occupies a connected open region $\mathcal{B}_t$ embedded in a three dimensional Euclidean space at time t. A particular configuration $\mathcal{B}$ is called the *reference configuration*. A point $\boldsymbol{X} \in \mathcal{B}$ is called a material point. A *motion* of $\mathcal{B}$ is a smooth mapping $\boldsymbol{\chi}$ that assigns to each material point $\boldsymbol{X}$ and time t a point $\boldsymbol{x} \in \mathcal{B}_t$ such that

$$\boldsymbol{x} = \boldsymbol{\chi}(\boldsymbol{X}, t).$$

$\boldsymbol{x}$ is referred to as the spatial point occupied by $\boldsymbol{X}$ at time t, and $\mathcal{B}_t$ is called the *current configuration* at time t. $\boldsymbol{\chi}(\boldsymbol{X}, t)$ for fixed t, is called the deformation at time t. We denote by $\boldsymbol{F}$ the *deformation gradient*

$$\boldsymbol{F}(\boldsymbol{X}) := \nabla \boldsymbol{\chi}(\boldsymbol{X}, t)$$

and assume that $J(\boldsymbol{X}, t) := \det \boldsymbol{F} > 0$. Also the *displacement* of $\boldsymbol{X}$ is denoted by

$$\boldsymbol{u}(\boldsymbol{X}, t) = \chi(\boldsymbol{X}, t) - \boldsymbol{X}.$$

A body is said to be *elastic* if there exists a symmetric tensor-valued function $\widehat{\boldsymbol{T}}(\boldsymbol{F})$, called the material *response function*, such that the Cauchy stress tensor $\boldsymbol{T}$ is given by

$$\boldsymbol{T} = \widehat{\boldsymbol{T}}(\boldsymbol{F}).$$

The first *Piola Kirchhoff stress* can then be defined as $\boldsymbol{S} = \widehat{\boldsymbol{S}}(\boldsymbol{F})$, where

$$\widehat{\boldsymbol{S}} = J \widehat{\boldsymbol{T}}(\boldsymbol{F}) \boldsymbol{F}^{-T}. \tag{2.1}$$

$\boldsymbol{\tau} := \widehat{\boldsymbol{T}}(\boldsymbol{I})$ corresponds to the residual stress in $\mathcal{B}$, where $\boldsymbol{I}$ is the Identity tensor. If $\widehat{\boldsymbol{T}}(\boldsymbol{I}) = 0$, then $\mathcal{B}$ is called the *natural configuration* or the *stress-free configuration*. It is important to note that since the reference configuration $\mathcal{B}$ is unloaded in the inner and outer wall, the residual stress $\boldsymbol{\tau}$ satisfies the following equilibrium condition:

$$\begin{cases} \text{Div}\,\boldsymbol{\tau} = 0 & \text{in} \qquad \mathcal{B} \\ \boldsymbol{\tau}\boldsymbol{n} = 0 & \text{on} \qquad \partial\mathcal{B}_I \cup \partial\mathcal{B}_O \end{cases} \tag{2.2}$$

where

$$\boldsymbol{\tau} = \sum_{i,j=1}^{3} \tau_{ij}(\boldsymbol{X})\boldsymbol{e}_i \otimes \boldsymbol{e}_j \ , \quad \boldsymbol{\tau} = \boldsymbol{\tau}^T \tag{2.3}$$

and $\boldsymbol{n}$ is the unit normal to the corresponding boundary.

An elastic body is said to be *hyperelastic* if there exists a scalar function $W = \widehat{W}(\boldsymbol{F})$ called the *strain energy function* per unit reference volume, such that

$$\boldsymbol{S} = \widehat{\boldsymbol{S}}(\boldsymbol{F}) = \partial_{\boldsymbol{F}}\widehat{W}(\boldsymbol{F}). \tag{2.4}$$

1. Balance of Linear Momentum

The equations of motion expressing the local form of balance of linear momentum in the referential frame [22] is given by

$$\text{Div}\ \boldsymbol{S} + \rho\boldsymbol{b} \ = \ \rho\ddot{\boldsymbol{u}} \qquad \text{in } \mathcal{B} \tag{2.5}$$

where Div denotes the divergence operator in $\mathcal{B}$, ρ is the mass density in $\mathcal{B}$, $\boldsymbol{b}$ is the body force, and the $\ddot{\boldsymbol{u}}$ represents the second derivative of $\boldsymbol{u}$ with respect to time.

B. Constitutive Model Incorporating Residual Stress

In order to model the constitutive response of the residually stressed arteries, one must first develop a model for the response of the material to the deformation $\boldsymbol{\chi}$

from the reference (unloaded) configuration to the current configuration i.e. find a suitable form for the strain energy function $\widehat{W}(\boldsymbol{F})$, and then address the issue of how to model the residual stress $\boldsymbol{\tau}$ in the unloaded configuration. A specific form for the *strain energy function* is chosen based on the assumptions one makes for the material such as isotropy, incompressibility, heterogeneity etc. Soft tissues exhibit a highly complex behavior and a nonlinear elastic response to external loads. In particular, an arterial wall is layered and highly anisotropic. However, considering that this is a preliminary study for reconstructing residual stress in arteries, we assume it to be isotropic and plan to incorporate anisotropy in subsequent studies. Healthy soft tissues are generally assumed in the literature to be incompressible, however, for a diseased artery, it is more reasonable to assume the response to be slightly compressible. To that end, we use the *compressible neo-Hookean* constitutive law to model the material behavior which is given by

$$\widehat{W}_N(\boldsymbol{F}) := \mu \left(\varphi(J) + \frac{1}{2}(|\boldsymbol{F}|^2 - 3) \right) \tag{2.6}$$

where $\varphi(\cdot)$ is a scalar-valued function given by

$$\varphi(r) = \frac{r^{-2\beta} - 1}{2\beta}, \quad \beta = \frac{\nu}{1 - 2\nu}. \tag{2.7}$$

μ and ν are the *shear modulus* and *Poisson's ratio* of the material respectively. Then, we have,

$$\widehat{S}_N(\boldsymbol{F}) = \mu \left(\psi(J) \boldsymbol{F}^{-T} + \boldsymbol{F} \right), \quad \text{where} \quad \psi(J) = \varphi'(J) J. \tag{2.8}$$

Here, $\widehat{W}_N(\boldsymbol{F})$ and $\widehat{S}_N(\boldsymbol{F})$ are the strain energy function and the response function corresponding to zero residual stresses and are called the *natural strain energy function* and the *natural response function* respectively.

In order to incorporate residual stress in the model, we use the additive form for

the *strain energy function* as described in [19]. The strain energy function and the Piola Kirchhoff stress are written as

$$\widehat{W}(\boldsymbol{C};\boldsymbol{\tau}) = \widehat{W}_N(\boldsymbol{C}) + \widehat{W}_\tau(\boldsymbol{C};\boldsymbol{\tau}), \tag{2.9}$$

$$\widehat{S}(\boldsymbol{F};\boldsymbol{\tau}) = \partial_{\boldsymbol{F}}\widehat{W}(\boldsymbol{C};\boldsymbol{\tau}) = \widehat{S}_N(\boldsymbol{F}) + \widehat{S}_\tau(\boldsymbol{F};\boldsymbol{\tau}). \tag{2.10}$$

$\widehat{W}(\boldsymbol{C};\boldsymbol{\tau})$ and $\widehat{S}(\boldsymbol{F};\boldsymbol{\tau})$ are both required to satisfy frame indifference. It has been emphasized that frame indifference cannot be examined before a choice of reference frame is made [29]. To that end, we consider two different formulations for $\widehat{W}_\tau(\boldsymbol{F};\boldsymbol{\tau})$ that correspond to different frames of reference.

1. Strain Energy Function $\widehat{W}_{\tau_1}(F)$

Let the frame of reference be the natural configuration, that is, the unloaded stress-free configuration. Consider the strain energy function

$$\widehat{W}_{\tau_1}(\boldsymbol{F};\boldsymbol{\tau}) = \frac{1}{2}\boldsymbol{C}\cdot\boldsymbol{\tau}, \tag{2.11}$$

where $\boldsymbol{C} = \boldsymbol{F}^T\boldsymbol{F}$, the right Cauchy-Green strain tensor. The corresponding Piola Kirchhoff stress is given by

$$\widehat{S}_\tau(\boldsymbol{F};\boldsymbol{\tau}) = \partial_{\boldsymbol{F}}\widehat{W}_\tau(\boldsymbol{C};\boldsymbol{\tau}) = \boldsymbol{F}\boldsymbol{\tau}. \tag{2.12}$$

Note that this particular form of strain energy function and the Piola Kirchhoff stress satisfy frame indifference for this choice of reference frame.

2. Strain Energy Function $\widehat{W}_{\tau_2}(F)$

Let the frame of reference be the unloaded but residually stressed configuration. Consider the strain energy function

$$\widehat{W}_{\tau_2}(\boldsymbol{F};\boldsymbol{\tau}) = \frac{1}{2}\boldsymbol{\tau}\cdot\boldsymbol{C}, \tag{2.13}$$

with the associated first Piola-Kirchoff stress given by

$$\widehat{S}_{\tau}(\boldsymbol{F};\boldsymbol{\tau}) = \partial_{\boldsymbol{F}}\widehat{W}_{\tau}(\boldsymbol{C};\boldsymbol{\tau}) = \boldsymbol{\tau}\boldsymbol{F}. \tag{2.14}$$

Again, this particular form of strain energy function and the Piola Kirchhoff stress satisfy frame indifference for this choice of reference frame.

C. Problem Description

The arterial wall is modeled as a nonlinear, isotropic, slightly compressible elastic body. The model that is proposed considers the arterial wall to be of a rectangular slab geometry. The reason for this assumption is that the mathematical equations and algorithms that are developed for this particular geometry can be validated through experiments that are being performed by some of our colleagues in the University of Strathclyde and the University of Edinburgh on phantom materials. In particular, for the experiments to be consistent with the specific class of deformations that are studied herein, the rectangular slab is required to have pre-stress in the form of tractions on the lateral boundaries along with residual stress, in the absence of applied pressure. For our purposes, we define the unloaded configuration to be one in which the pressure in the inner and outer wall is zero but the tractions on the lateral sides are non zero, and the residual stress field in the rectangular slab to be the stress field present in the unloaded configuration. Soft tissues is widely accepted to be a

nonlinear viscoelastic material. However, for frequencies as high as that used for IVUS, one can ignore the time-dependence viscoelastic effects and simply consider the material response to be elastic [19].

We consider the arterial wall to be a rectangular slab of unit length across the thickness and infinitely long in the transverse directions. Referring to our definition of residual stress, we consider the reference configuration $\mathcal{B}$ to be unloaded and residually stressed. Let $\partial\mathcal{B}_I$ and $\partial\mathcal{B}_O$ denote the boundaries in the reference configuration. In order to model the propagation of high frequency IVUS waves on the nonlinear elastic body that undergoes finite strain, we adopt the theory of time harmonic small amplitude vibrations superimposed upon a quasi static large deformation.

A constant pressure is applied on one side of the boundary in the deformed configuration. The corresponding boundary value problem is given by

$$\begin{cases} \text{Div } \boldsymbol{S} = \rho\ddot{\boldsymbol{u}}, & \text{in} \quad \mathcal{B} = [0,1]\times(-\infty,\infty)\times(-\infty,\infty), \\ \boldsymbol{S}\boldsymbol{e}_j = -\pi J\boldsymbol{F}^{-\top}\boldsymbol{e}_j, & \text{on} \quad \partial\mathcal{B}_I\ (X_1 = 0), \end{cases} \tag{2.15}$$

where $\boldsymbol{e}_j$ denotes the outward unit normal to the boundary in the reference configuration.

Different boundary conditions may be applied to $\partial\mathcal{B}_O$ depending on whether one is interested in in vivo or in vitro behavior. One could impose

$$\boldsymbol{S}\boldsymbol{e}_j = -k\boldsymbol{u} \qquad \text{on} \qquad \partial\mathcal{B}_O\ (X_1 = 1) \tag{2.16}$$

where $k \in [0,\infty)$. Note that $k \to 0$ and $k \to \infty$ correspond to a traction-free and fixed grip boundary conditions respectively. Alternatively, one could also apply an equal pressure on $\partial\mathcal{B}_O$

$$\boldsymbol{S}\boldsymbol{e}_j = -\pi J\boldsymbol{F}^{-\top}\boldsymbol{e}_j, \qquad \text{on} \qquad \partial\mathcal{B}_O\ (X_1 = 1). \tag{2.17}$$

1. Small Vibrations Superimposed upon a Finite Deformation

We derive the governing equations for small amplitude time harmonic waves linearized in the neighborhood of a static, finite deformation from the BVP (2.15) by subjecting the rectangular domain to a time harmonic pressure given by

$$\pi_t = \pi_0(1 + \epsilon e^{i\omega t})$$

and constructing an asymptotic expansion for the solution of the form

$$\begin{aligned}
\boldsymbol{u}(\boldsymbol{X}, t) &= \boldsymbol{u}_0(\boldsymbol{X}) + \epsilon \boldsymbol{u}_1(\boldsymbol{X}) e^{i\omega t} + o(\epsilon) && (2.18)\\
\boldsymbol{F}(X, t) &= \boldsymbol{I} + \nabla(\boldsymbol{u}_0(\boldsymbol{X}) + \epsilon \boldsymbol{u}_1(\boldsymbol{X}) e^{i\omega t} + o(\epsilon)) \\
&= (\boldsymbol{I} + \nabla \boldsymbol{u}_0(\boldsymbol{X})) + \epsilon \nabla \boldsymbol{u}_1(\boldsymbol{X}) e^{i\omega t} + o(\epsilon) \\
&= \boldsymbol{F}_0(\boldsymbol{X}) + \epsilon \boldsymbol{F}_1(\boldsymbol{X}) e^{i\omega t} + o(\epsilon) && (2.19)\\
\boldsymbol{S}(\boldsymbol{X}, t) &= \boldsymbol{S}_0(\boldsymbol{X}) + \epsilon \boldsymbol{S}_1(\boldsymbol{X}) e^{i\omega t} + o(\epsilon) && (2.20)
\end{aligned}$$

where ω and ϵ are the frequency and the maximum amplitude of the pressure wave generated by IVUS respectively. Also note that $\epsilon << 1$.

Asymptotic expansion of the boundary value problem (2.15)–(2.17) of the form (2.18)–(2.20) generates a sequence of quasi static boundary value problems to all orders in ϵ. To zero-order in ϵ, $\boldsymbol{u}_0$ satisfies the following boundary value problem

$$\begin{cases}
\mathrm{Div}\, \boldsymbol{S}_0 = 0, & \text{in} \quad \mathcal{B}, \\
\boldsymbol{S}_0 \boldsymbol{e}_j = -\pi_0 J_0 \boldsymbol{F}_0^{-T} \boldsymbol{e}_j, & \text{on} \quad \partial\mathcal{B}_I, \\
\boldsymbol{S}_0 \boldsymbol{e}_j = -k \boldsymbol{u}_0 \quad \text{or,} \quad \boldsymbol{S}_0 \boldsymbol{e}_j = -\pi_0 J_0 \boldsymbol{F}_0^{-T} \boldsymbol{e}_j & \text{on} \quad \partial\mathcal{B}_O.
\end{cases} \tag{2.21}$$

The BVP (2.21) governs the static finite deformation of the elastic body due to blood

pressure. To first-order in ϵ, $\boldsymbol{u}_1$ satisfies

$$\mathrm{Div}\boldsymbol{S}_1 = -\rho\omega^2\boldsymbol{u}_1 \qquad \text{in } \mathcal{B} \tag{2.22}$$

with appropriate boundary conditions. In order to construct $\boldsymbol{S}$ and the boundary conditions, we need the following asymptotic expansions for J and $\boldsymbol{F}^{-T}$

$$J = J_0\left(1 + \epsilon e^{i\omega t}\boldsymbol{F}_0^{-T}\cdot\nabla\boldsymbol{u}_1 + o(\epsilon)\right) \tag{2.23}$$

$$\boldsymbol{F}^{-T} = \boldsymbol{F}_0^{-T} - \epsilon e^{i\omega t}\boldsymbol{F}_0^{-T}\nabla\boldsymbol{u}_1\boldsymbol{F}_0^{-T} + o(\epsilon). \tag{2.24}$$

Linearizing the first Piola-Kirchhoff stress about the zero-order deformation gives us

$$\widehat{\boldsymbol{S}}(\boldsymbol{F};\boldsymbol{\tau}) \;=\; \widehat{\boldsymbol{S}}(\boldsymbol{F}_0;\boldsymbol{\tau}) + \epsilon\,\mathbb{E}\left(\boldsymbol{F}_0;\boldsymbol{\tau}\right)[\nabla\boldsymbol{u}_1]e^{i\omega t} + o(\epsilon) \tag{2.25}$$

where $\mathbb{E}\left(\boldsymbol{F}_0;\boldsymbol{\tau}\right)[\boldsymbol{H}] := \mathbb{D}_{\boldsymbol{F}}\widehat{\boldsymbol{S}}(\boldsymbol{F}_0;\boldsymbol{\tau})[\boldsymbol{H}]$, the fourth-order elasticity tensor. The zero order stress tensor is then given by

$$\boldsymbol{S}_0 = \widehat{\boldsymbol{S}}(\boldsymbol{F}_0;\boldsymbol{\tau}). \tag{2.26}$$

Plugging in (2.23)–(2.25) into (2.15)-(2.17), the first-order BVP then becomes

$$\mathrm{Div}\mathbb{E}\left(\boldsymbol{F}_0;\boldsymbol{\tau}\right)[\nabla\boldsymbol{u}_1] = -\rho\omega^2\boldsymbol{u}_1 \tag{2.27}$$

with boundary conditions

$$\mathbb{E}\left(\boldsymbol{F}_0;\boldsymbol{\tau}\right)[\nabla\boldsymbol{u}_1]\boldsymbol{e}_j \;=\; -\pi_0\boldsymbol{F}_0^{-T}J_0\left(\left(1+\boldsymbol{F}_0^{-T}\cdot\nabla\boldsymbol{u}_1\right) - \nabla\boldsymbol{u}_1^T\boldsymbol{F}_0^{-T}\right)\boldsymbol{e}_j \text{ on } \partial\mathcal{B}_I, \tag{2.28}$$

$$\mathbb{E}\left(\boldsymbol{F}_0;\boldsymbol{\tau}\right)[\nabla\boldsymbol{u}_1]\boldsymbol{e}_j = -k\boldsymbol{u}_1$$
$$\text{or, } -\pi_0\boldsymbol{F}_0^{-T}J_0\left(\left(1+\boldsymbol{F}_0^{-T}\cdot\nabla\boldsymbol{u}_1\right) - \nabla\boldsymbol{u}_1^T\boldsymbol{F}_0^{-T}\right)\boldsymbol{e}_j \text{ on } \partial\mathcal{B}_O. \tag{2.29}$$

(2.8) and (2.10) give

$$\begin{aligned}\mathbb{E}\left(\boldsymbol{F}_0;\boldsymbol{\tau}\right)[\boldsymbol{H}] &= \mathbb{D}_{\boldsymbol{F}}\left(\widehat{S}_N(\boldsymbol{F}_0)+\widehat{S}_\tau(\boldsymbol{F}_0;\boldsymbol{\tau})\right)[\boldsymbol{H}] \\ &= \mathbb{E}_N\left(\boldsymbol{F}_0\right)[\boldsymbol{H}]+\mathbb{E}_\tau\left(\boldsymbol{F}_0;\boldsymbol{\tau}\right)[\boldsymbol{H}], \end{aligned} \tag{2.30}$$

where

$$\mathbb{E}_N\left(\boldsymbol{F}_0\right)[\boldsymbol{H}] = \mu\left(\psi'(J_0)J_0\left(\boldsymbol{F}_0^{-T}\cdot\boldsymbol{H}\right)\boldsymbol{F}_0^{-T}-\psi(J_0)\boldsymbol{F}_0^{-T}\boldsymbol{H}^T F_0^{-T}\right)+\mu\boldsymbol{H}. \tag{2.31}$$

Appealing to the *compressible neo-Hookean* constitutive model described in (2.6)–(2.8), one gets the natural stress response function

$$\widehat{S}_N(\boldsymbol{F}_0) = \mu\left(-J^{-2\beta}\boldsymbol{F}_0^{-T}+\boldsymbol{F}_0\right) \tag{2.32}$$

and the natural linear elasticity tensor

$$\mathbb{E}_N(\boldsymbol{F}_0)[\boldsymbol{H}] = \mu J_0^{-2\beta}\left(2\beta[\boldsymbol{F}_0^{-T}\cdot\boldsymbol{H}]\boldsymbol{F}_0^{-T}+\boldsymbol{F}_0^{-T}\boldsymbol{H}^T\boldsymbol{F}_0^{-T}\right)+\mu\boldsymbol{H}. \tag{2.33}$$

In order to formulate the first order eigenvalue problem, we need to calculate $\mathrm{Div}(\mathbb{E}_N(\boldsymbol{F}_0)[\nabla\boldsymbol{u}_1])$. The computations below make use of the following formulae:

$$\begin{aligned}\mathrm{Div}(\phi\boldsymbol{u}) &= \phi\mathrm{Div}\boldsymbol{u}+\boldsymbol{u}\cdot\nabla\phi \\ \mathrm{Div}(\phi\boldsymbol{S}) &= \phi\mathrm{Div}\boldsymbol{S}+\boldsymbol{S}\nabla\phi \\ \mathrm{Div}(\boldsymbol{S}^T\boldsymbol{u}) &= \boldsymbol{S}\cdot\nabla\boldsymbol{u}+\boldsymbol{u}\cdot\mathrm{Div}\boldsymbol{S} \\ \nabla\left(\boldsymbol{u}\cdot\boldsymbol{v}\right) &= \left(\nabla\boldsymbol{u}\right)^T\boldsymbol{v}+\left(\nabla\boldsymbol{v}\right)^T\boldsymbol{u} \\ \mathrm{Div}(\boldsymbol{u}\otimes\boldsymbol{v}) &= \boldsymbol{u}\mathrm{Div}\boldsymbol{v}+\left(\nabla\boldsymbol{u}\right)\boldsymbol{v}. \end{aligned}$$

We then get,

$$\mathrm{Div}(\mathbb{E}_N(\boldsymbol{F}_0)[\nabla \boldsymbol{u}_1]) = 2\beta\mu \mathrm{Div}\left(J_0^{-2\beta}\left(\boldsymbol{F}_0^{-T}\cdot\nabla\boldsymbol{u}_1\right)\boldsymbol{F}_0^{-T}\right) + \mu\mathrm{Div}\left(J_0^{-2\beta}(\boldsymbol{F}_0^{-T}(\nabla\boldsymbol{u}_1)^T\boldsymbol{F}_0^{-T})\right) + \mu\mathrm{Div}\left(\nabla\boldsymbol{u}_1\right), \quad (2.34)$$

where

$$\mathrm{Div}\left(J_0^{-2\beta}[\boldsymbol{F}_0^{-T}\cdot\nabla\boldsymbol{u}_1]\boldsymbol{F}_0^{-T}\right) = J_0^{-2\beta}[\boldsymbol{F}_0^{-T}\cdot\nabla\boldsymbol{u}_1]\mathrm{Div}\left(\boldsymbol{F}_0^{-T}\right) + \boldsymbol{F}_0^{-T}(\nabla J_0^{-2\beta}[\boldsymbol{F}_0^{-T}\cdot\nabla\boldsymbol{u}_1] + J_0^{-2\beta}\nabla[\boldsymbol{F}_0^{-T}\cdot\nabla\boldsymbol{u}_1]) \quad (2.35)$$

and

$$\mathrm{Div}\left(J_0^{-2\beta}(\boldsymbol{F}_0^{-T}(\nabla\boldsymbol{u}_1)^T\boldsymbol{F}_0^{-T})\right) = J_0^{-2\beta}\mathrm{Div}\left(\boldsymbol{F}_0^{-T}(\nabla\boldsymbol{u}_1)^T\boldsymbol{F}_0^{-T}\right) + \left(\boldsymbol{F}_0^{-T}(\nabla\boldsymbol{u}_1)^T\boldsymbol{F}_0^{-T}\right)\nabla J_0^{-2\beta}. \quad (2.36)$$

In the following sections, we formulate two model problems and derive the corresponding static boundary value problems and eigenvalue problems.

D. Model Problem I

Let $\mathcal{B}$ be a rectangular domain in the unloaded residually stressed configuration as described in Section C and $\boldsymbol{X} = (X_1, X_2, X_3) \in \mathcal{B}$. In an effort to use the semi-inverse approach for the algorithm development and simulations, we now consider a model problem to determine the residual stress when the material is subjected to a specific class of deformations of the form

$$\boldsymbol{\chi}(X,t) = \widehat{\chi}(X_1,t)\boldsymbol{e}_1 + \lambda(X_1,t)X_2\boldsymbol{e}_2 + \eta(X_1,t)X_3\boldsymbol{e}_3, \quad (2.37)$$

where $\{\boldsymbol{e}_1, \boldsymbol{e}_2, \boldsymbol{e}_3\}$ is the natural Euclidean orthonormal basis, $\widehat{\chi}(X_1, t)$ is the deformation in $\boldsymbol{e}_1$, and $\lambda(X_1, t)$ and $\eta(X_1, t)$ are the stretches in $\boldsymbol{e}_2$ and $\boldsymbol{e}_3$ respectively and $\lambda, \eta > 0$. For this particular model problem, we adopt the constitutive equation in which the strain energy is given in (2.11). Our goal is to derive the static boundary value problem (2.21) and the eigenvalue problem (2.27)–(2.29) for this particular model problem, and develop an inverse spectral algorithm to estimate the residual stresses. To that end, we construct an asymptotic expansion of the deformation and the stretches in the following way:

$$\widehat{\chi}(X_1, t) = \chi_0(X_1) + \epsilon\chi_1(X_1)e^{i\omega t} + o(\epsilon), \tag{2.38}$$

$$\lambda(X_1, t) = \lambda_0(X_1) + \epsilon\lambda_1(X_1)e^{i\omega t} + o(\epsilon), \tag{2.39}$$

$$\eta(X_1, t) = \eta_0(X_1) + \epsilon\eta_1(X_1)e^{i\omega t} + o(\epsilon). \tag{2.40}$$

In the following sections, we derive the static boundary value problem and the eigenvalue problem when the body is subjected to the deformation given by (2.37).

1. Static Large Deformation Boundary Value Problem

It follows from (2.37) that the deformation gradient $\boldsymbol{F}_0$ is given by

$$\begin{aligned} \boldsymbol{F}_0(\boldsymbol{X}) &= \chi_0' \boldsymbol{e}_1 \otimes \boldsymbol{e}_1 + \lambda_0' X_2 \boldsymbol{e}_2 \otimes \boldsymbol{e}_1 + \lambda_0 \boldsymbol{e}_2 \otimes \boldsymbol{e}_2 \\ &+ \eta_0' X_3 \boldsymbol{e}_3 \otimes \boldsymbol{e}_1 + \eta_0 \boldsymbol{e}_3 \otimes \boldsymbol{e}_3 \end{aligned} \tag{2.41}$$

and

$$J_0 = \lambda_0 \eta_0 \chi_0'.$$

We then get

$$\boldsymbol{F}_0^{-T} = \frac{1}{\chi_0'} \boldsymbol{e}_1 \otimes \boldsymbol{e}_1 - \frac{\lambda_0' X_2}{\chi_0' \lambda_0} \boldsymbol{e}_1 \otimes \boldsymbol{e}_2 - \frac{\eta_0' X_3}{\chi_0' \eta_0} \boldsymbol{e}_1 \otimes \boldsymbol{e}_3 + \frac{1}{\lambda_0} \boldsymbol{e}_2 \otimes \boldsymbol{e}_2 + \frac{1}{\eta_0} \boldsymbol{e}_3 \otimes \boldsymbol{e}_3 \tag{2.42}$$

where $'$ denotes differentiation with respect to X_1. From (2.10), (2.12) and (2.26), we get,

$$\mathrm{Div}\boldsymbol{S}_0 = \mathrm{Div}\left(\widehat{\boldsymbol{S}}_N(\boldsymbol{F}_0) + \boldsymbol{F}_0\boldsymbol{\tau}\right). \tag{2.43}$$

By making use of (2.8),

$$\begin{aligned}\mathrm{Div}\widehat{\boldsymbol{S}}_N(\boldsymbol{F}_0) &= \mu\mathrm{Div}\left(\psi(J_0)\boldsymbol{F}_0^{-T}\right) + \mu\mathrm{Div}\boldsymbol{F}_0 \\ &= \mu\left(\psi(J_0)\mathrm{Div}\boldsymbol{F}_0^{-T} + \boldsymbol{F}_0^{-T}\nabla\psi(J_0) + \mathrm{Div}\ \boldsymbol{F}_0\right). \end{aligned}\tag{2.44}$$

We deduce the following from (2.41):

$$\mathrm{Div}\boldsymbol{F}_0 = \chi_0''\boldsymbol{e}_1 + \lambda_0''X_2\boldsymbol{e}_2 + \eta_0''X_3\boldsymbol{e}_3 \tag{2.45}$$

$$\mathrm{Div}\boldsymbol{F}_0^{-T} = \left(\left(\frac{1}{\chi_0'}\right)' - \frac{\lambda_0'}{\lambda_0\chi_0'} - \frac{\eta_0'}{\eta_0\chi_0'}\right)\boldsymbol{e}_1 \tag{2.46}$$

$$\begin{aligned}\nabla\psi(J_0) &= \psi'(J_0)\nabla_{\boldsymbol{X}}\det\boldsymbol{F}_0 \\ &= \psi'(J_0)\left(J_0\boldsymbol{F}_0^{-T}\cdot\boldsymbol{F}_0'\right)\boldsymbol{e}_1 \\ &= 2\beta J_0^{-2\beta}\left(\frac{\chi_0''}{\chi_0'} + \frac{\lambda_0'}{\lambda_0} + \frac{\eta_0'}{\eta_0}\right)\boldsymbol{e}_1 \end{aligned}\tag{2.47}$$

$$\boldsymbol{F}_0^{-T}\nabla\psi(J_0) = \frac{2\beta J_0^{-2\beta}}{\chi_0'}\left(\frac{\chi_0''}{\chi_0'} + \frac{\lambda_0'}{\lambda_0} + \frac{\eta_0'}{\eta_0}\right)\boldsymbol{e}_1. \tag{2.48}$$

Hence, from (2.44)-(2.48),

$$\begin{aligned}\mathrm{Div}\widehat{\boldsymbol{S}}_N(\boldsymbol{F}_0) = \mu\Bigg(&-J_0^{-2\beta}\left(\left(\frac{1}{\chi_0'}\right)' - \frac{\lambda_0'}{\lambda_0\chi_0'} - \frac{\eta_0'}{\eta_0\chi_0'}\right) + \frac{2\beta J_0^{-2\beta}}{\chi_0'}\left(\frac{\chi_0''}{\chi_0'} + \frac{\lambda_0'}{\lambda_0} + \frac{\eta_0'}{\eta_0}\right) \\ &+\chi_0''\Bigg)\boldsymbol{e}_1 + \mu\,\lambda_0''X_2\boldsymbol{e}_2 + \mu\,\eta_0''X_3\boldsymbol{e}_3. \end{aligned}\tag{2.49}$$

In order to calculate $\mathrm{Div}(\boldsymbol{F}_0\boldsymbol{\tau})$, we appeal to the following definition of the Divergence operator:

Definition 1. The divergence of a second order tensor $\boldsymbol{A}$ is the unique vector $\mathrm{Div}(\boldsymbol{A})$

satisfying

$$\boldsymbol{k} \cdot \mathrm{Div}(\boldsymbol{A}) = \mathrm{Div}(\boldsymbol{A}^T \boldsymbol{k}) \tag{2.50}$$

for all vectors $\boldsymbol{k}$.

Then,

$$\begin{aligned} \boldsymbol{k} \cdot \mathrm{Div}(\boldsymbol{F}_0 \boldsymbol{\tau}) &= \mathrm{Div}\left(\boldsymbol{\tau}(\boldsymbol{F}_0{}^T \boldsymbol{k})\right) \\ &= (\boldsymbol{F}_0{}^T \boldsymbol{k}) \cdot \mathrm{Div}(\boldsymbol{\tau}) + \boldsymbol{\tau} \cdot \nabla \left(\boldsymbol{F}_0{}^T \boldsymbol{k}\right) \\ &= \boldsymbol{\tau} \cdot \nabla \left(\boldsymbol{F}_0{}^T\right)[\boldsymbol{k}] \\ &= \boldsymbol{k} \cdot \nabla \left(\boldsymbol{F}_0{}^T\right)^T \boldsymbol{\tau}. \end{aligned}$$

Hence,

$$\mathrm{Div}(\boldsymbol{F}_0 \boldsymbol{\tau}) = \nabla \left(\boldsymbol{F}_0{}^T\right)^T \boldsymbol{\tau}. \tag{2.51}$$

Here we have used the fact that $\boldsymbol{\tau} \in Sym$ and the equilibrium condition (2.2) satisfied by $\boldsymbol{\tau}$. For the model (2.37), one can show that

$$\mathrm{Div}(\boldsymbol{F}_0 \boldsymbol{\tau}) = \tau_{11} \chi_0'' \boldsymbol{e}_1 + (\tau_{11} X_2 \lambda_0'' + 2\tau_{12} \lambda_0') \boldsymbol{e}_2 + (\tau_{11} X_3 \eta_0'' + 2\tau_{13} \eta_0') \boldsymbol{e}_3. \tag{2.52}$$

Using $\boldsymbol{\tau} \boldsymbol{e}_1 = 0$ from (2.2),

$$\left(\widehat{\boldsymbol{S}}_N(\boldsymbol{F}_0) + (\boldsymbol{F}_0 \tau)\right) \boldsymbol{e}_1 = \widehat{\boldsymbol{S}}_N(\boldsymbol{F}_0) \boldsymbol{e}_1. \tag{2.53}$$

The boundary condition on $\partial \mathcal{B}_I$ reduces to

$$\mu \left(\frac{-J_0^{-2\beta}}{\chi_0'} + \chi_0' \right) \boldsymbol{e}_1 + \mu \lambda_0' X_2 \boldsymbol{e}_2 + \mu \eta_0' X_3 \boldsymbol{e}_3 = -\pi_0 \lambda_0 \eta_0 \boldsymbol{e}_1 \tag{2.54}$$

and the outer boundary condition on $\partial\mathcal{B}_O$ is (2.53)–(2.54) or

$$\mu\left(\frac{-J_0^{-2\beta}}{\chi_0'}+\chi_0'\right)\boldsymbol{e}_1+\mu\lambda_0'X_2\boldsymbol{e}_2+\mu\eta_0'X_3\boldsymbol{e}_3 \\ =-k\left(\left(\chi_0-X_1\right)\boldsymbol{e}_1+\left(\lambda_0-1\right)X_2\boldsymbol{e}_2+\left(\eta_0-1\right)X_3\boldsymbol{e}_3\right) \quad (2.55)$$

depending on if one chooses (2.16) or (2.17). Appealing to (2.26), (2.49), (2.52) and (2.54)–(2.55), χ_0 satisfies the following static boundary value problem:

$$\mu J_0^{-2\beta}(1+2\beta)\left(\chi_0''+\chi_0'\left(\frac{\lambda_0'}{\lambda_0}+\frac{\eta_0'}{\eta_0}\right)\right)+\left(\mu+\tau_{11}\right)\chi_0''(\chi_0')^2=0 \quad \text{on} \quad \mathcal{B} \quad (2.56)$$

$$\frac{-J_0^{-2\beta}}{\chi_0'}+\chi_0'=-\frac{\pi_0}{\mu}\lambda_0\eta_0 \quad \text{on} \quad \partial\mathcal{B}_I \quad (2.57)$$

$$\frac{-J_0^{-2\beta}}{\chi_0'}+\chi_0'=-k\frac{(\chi_0-X_1)}{\mu} \quad \text{or,} \quad \frac{-J_0^{-2\beta}}{\chi_0'}+\chi_0'=-\frac{\pi_0}{\mu}\lambda_0\eta_0 \quad \text{on} \quad \partial\mathcal{B}_O. \quad (2.58)$$

The stretches in the $\boldsymbol{e}_2$ and $\boldsymbol{e}_3$ direction, λ_0 and η_0, satisfy the following BVPs:

$$\begin{cases}(\mu+\tau_{11}(\boldsymbol{X})X_2\lambda_0''+2\tau_{12}(\boldsymbol{X})\lambda_0'=0 & \text{on} \quad \mathcal{B}\\ \lambda_0'=0 & \text{on} \quad \partial\mathcal{B}_I\\ \lambda_0'=-k\frac{\lambda_0-1}{\mu} \quad \text{or,} \quad \lambda_0'=0 & \text{on} \quad \partial\mathcal{B}_O\end{cases} \quad (2.59)$$

$$\begin{cases}(\mu+\tau_{11}(\boldsymbol{X})X_3\eta_0''+2\tau_{13}(\boldsymbol{X})\eta_0'=0 & \text{on} \quad \mathcal{B}\\ \eta_0'=0 & \text{for} \quad \partial\mathcal{B}_I\\ \eta_0'=-k\frac{\eta_0-1}{\mu} \quad \text{or,} \quad \eta_0'=0 & \text{on} \quad \partial\mathcal{B}_O.\end{cases} \quad (2.60)$$

Note that the two ordinary differential equations shown above are linear, first-order equations in λ_0' and η_0' respectively. Hence, from the boundary conditions on $\partial\mathcal{B}_I$, we

get

$$\lambda_0' = 0, \;\; \eta_0' = 0 \quad \text{on} \quad \mathcal{B}. \tag{2.61}$$

Thus, λ_0 and η_0 are constants which need to be obtained from experimental measurements. (2.56) then reduces to

$$\chi_0'' = 0 \quad \text{or,} \tag{2.62}$$

$$\frac{\mu(2\beta+1)J_0^{-2\beta}}{(\chi_0')^2} + \mu + \tau_{11} = 0. \tag{2.63}$$

The latter is equivalent to

$$(\chi_0')^{-2(\beta+1)} = -\frac{(\lambda_0\eta_0)^{2\beta}}{1+2\beta}\left(1+\frac{\tau_{11}}{\mu}\right).$$

Since $\beta > 0$ and $|\tau_{11}/\mu| < 1$ [19], the latter equation suggests that the derivative of the deformation is a complex function, which is not possible. Thus, χ_0 satisfies (2.62) and from (2.57), χ_0' is a constant given by

$$\frac{-J_0^{-2\beta}}{\chi_0'} + \chi_0' = -\frac{\pi_0}{\mu}\lambda_0\eta_0 \quad \text{on } \mathcal{B}. \tag{2.64}$$

The above analysis shows that the static deformation for the model problem (2.37) is homogeneous. Note that the residual stress does not appear in any explicit form in the boundary value problems derived above for the static deformation. This does not mean that the stress distribution is independent of the residual stress, but that the experiments performed within such class of deformations do not indicate the presence or absence of residual stress.

2. The Linearized Vibrations Eigenvalue Problem

Recall that the first order eigenvalue problem was derived in (2.27)–(2.29) with the natural elasticity tensor $\mathbb{E}_N(\boldsymbol{F}_0)[\boldsymbol{H}]$ given by (2.31). Also from (2.12) and (2.30),

$$\mathbb{E}_\tau\left(\boldsymbol{F}_0;\boldsymbol{\tau}\right)[\boldsymbol{H}] = \boldsymbol{H}\boldsymbol{\tau}. \tag{2.65}$$

Now, we would like to study the linearized eigenvalue problem within the class of displacements of the form

$$\boldsymbol{u}_1(\boldsymbol{X}) = \chi_1(X_1)\boldsymbol{e}_1 + \lambda_1(X_1)X_2\boldsymbol{e}_2 + \eta_1(X_1)X_3\boldsymbol{e}_3. \tag{2.66}$$

The following formulae will be used to formulate the eigenvalue problem:

$$\begin{aligned}
\nabla\boldsymbol{u}_1 &= \chi_1'\boldsymbol{e}_1\otimes\boldsymbol{e}_1 + \lambda_1'X_2\boldsymbol{e}_2\otimes\boldsymbol{e}_1 + \lambda_1(X_1)\boldsymbol{e}_2\otimes\boldsymbol{e}_2 \\
&\quad +\eta_1'X_3\boldsymbol{e}_3\otimes\boldsymbol{e}_1 + \eta_1(X_1)\boldsymbol{e}_3\otimes\boldsymbol{e}_3 && (2.67)\\
\operatorname{Div}\nabla\boldsymbol{u}_1 &= \chi_1''\boldsymbol{e}_1 + \lambda_1''X_2\boldsymbol{e}_2 + \eta_1''X_3\boldsymbol{e}_3 && (2.68)\\
\left(\boldsymbol{F}_0^{-T}\cdot\nabla\boldsymbol{u}_1\right) &= \operatorname{tr}\left(\frac{\chi_1'}{\chi_0'}\boldsymbol{e}_1\otimes\boldsymbol{e}_1 + \frac{X_2\lambda_1'}{\lambda_0}\boldsymbol{e}_2\otimes\boldsymbol{e}_1 + \frac{\lambda_1(X_1)}{\lambda_0(X_1)}\boldsymbol{e}_2\otimes\boldsymbol{e}_2\right. \\
&\quad \left. +\frac{X_3\eta_1'}{\eta_0}\boldsymbol{e}_3\otimes\boldsymbol{e}_1 + \frac{\eta_1(X_1)}{\eta_0(X_1)}\boldsymbol{e}_3\otimes\boldsymbol{e}_3\right) \\
&= \frac{\chi_1'}{\chi_0'} + \frac{\lambda_1(X_1)}{\lambda_0(X_1)} + \frac{\eta_1(X_1)}{\eta_0(X_1)} && (2.69)\\
\nabla\left(\boldsymbol{F}_0^{-T}\cdot\nabla\boldsymbol{u}_1\right) &= \left(\frac{\chi_1'}{\chi_0'} + \frac{\lambda_1(X_1)}{\lambda_0(X_1)} + \frac{\eta_1(X_1)}{\eta_0(X_1)}\right)'\boldsymbol{e}_1 && (2.70)\\
(\boldsymbol{F}_0^{-T}\nabla\boldsymbol{u}_1^T\boldsymbol{F}_0^{-T}) &= \frac{\chi_1'}{(\chi_0')^2}\boldsymbol{e}_1\otimes\boldsymbol{e}_1 + \frac{X_2\lambda_1'}{\lambda_0\chi_0'}\boldsymbol{e}_1\otimes\boldsymbol{e}_2 + \frac{X_3\eta_1'}{\eta_0\chi_0'}\boldsymbol{e}_1\otimes\boldsymbol{e}_3 \\
&\quad +\frac{\lambda_1}{\lambda_0^2}\boldsymbol{e}_2\otimes\boldsymbol{e}_2 + \frac{\eta_1}{\eta_0^2}\boldsymbol{e}_3\otimes\boldsymbol{e}_3 && (2.71)\\
\operatorname{Div}(\boldsymbol{F}_0^{-T}\nabla\boldsymbol{u}_1^T\boldsymbol{F}_0^{-T}) &= \left(\left(\frac{\chi_1'}{(\chi_0')^2}\right)' + \frac{\lambda_1'}{\lambda_0\chi_0'} + \frac{\eta_1'}{\eta_0\chi_0'}\right)\boldsymbol{e}_1 && (2.72)\\
\operatorname{Div}((\nabla\boldsymbol{u}_1)\boldsymbol{\tau}) &= \tau_{11}\chi_1''\boldsymbol{e}_1 + \left(\tau_{11}X_2\lambda_1'' + 2\tau_{12}\lambda_1'\right)\boldsymbol{e}_2 \\
&\quad +\left(\tau_{11}X_3\eta_1'' + 2\tau_{13}\eta_1'\right)\boldsymbol{e}_3. && (2.73)
\end{aligned}$$

Substituting (2.67)–(2.73) into (2.35)–(2.36), we get

$$\begin{aligned}
\mathrm{Div}\left(J_0^{-2\beta}[\boldsymbol{F}_0^{-T}\cdot\nabla\boldsymbol{u}_1]\boldsymbol{F}_0^{-T}\right) &= \frac{J_0^{-2\beta}}{\chi_0'}\left(\left(\frac{\chi_1''}{\chi_0'}\right)+\left(\frac{\lambda_1'}{\lambda_0}\right)+\left(\frac{\eta_1'}{\eta_0}\right)\right)\boldsymbol{e}_1 \quad (2.74)\\
\mathrm{Div}\left(J_0^{-2\beta}(\boldsymbol{F}_0^{-T}\left(\nabla\boldsymbol{u}_1\right)^T\boldsymbol{F}_0^{-T})\right) &= J_0^{-2\beta}\left(\frac{\chi_1''}{(\chi_0')^2}+\frac{\lambda_1'}{\lambda_0\chi_0'}+\frac{\eta_1'}{\eta_0\chi_0'}\right)\boldsymbol{e}_1. \quad (2.75)
\end{aligned}$$

Note that (2.61) and (2.62) were used to derive the above formulas. Substituting (2.67)–(2.75) into (2.27)–(2.34) gives the boundary value problem governing the superimposed small amplitude vibrations in the $\boldsymbol{e}_1$ direction

$$\begin{aligned}
&\left(\frac{\mu(1+2\beta)J_0^{-2\beta}}{(\chi_0')^2}+\mu+\tau_{11}\right)\chi_1''\\
&\qquad+\frac{\mu(1+2\beta)J_0^{-2\beta}}{(\chi_0')}\left(\frac{\lambda_1'}{\lambda_0}+\frac{\eta_1'}{\eta_0}\right)=-\rho\omega^2\chi_1 \quad \text{on } \mathcal{B} \quad (2.76)
\end{aligned}$$

with boundary conditions

$$\begin{aligned}
&\mu\left(J_0^{-2\beta}(1+2\beta)\frac{1}{(\chi_0')^2}+1\right)\chi_1'+2\beta\mu J_0^{-2\beta}\left(\frac{\lambda_1}{\lambda_0}+\frac{\eta_1}{\eta_0}\right)\frac{1}{\chi_0'}\\
&\qquad=\pi_0 J_0\left(\frac{\lambda_1}{\lambda_0}+\frac{\eta_1}{\eta_0}+1\right)\frac{1}{\chi_0'} \quad \text{on } \partial\mathcal{B}_I \quad (2.77)
\end{aligned}$$

and

$$\begin{aligned}
&\mu\left(J_0^{-2\beta}(1+2\beta)\frac{1}{(\chi_0')^2}+1\right)\chi_1'+2\beta\mu J_0^{-2\beta}\left(\frac{\lambda_1}{\lambda_0}+\frac{\eta_1}{\eta_0}\right)\frac{1}{\chi_0'}\\
&\qquad=\pi_0 J_0\left(\frac{\lambda_1}{\lambda_0}+\frac{\eta_1}{\eta_0}+1\right)\frac{1}{\chi_0'} \quad \text{or,} \quad -k\chi_1 \quad \text{on } \partial\mathcal{B}_O. \quad (2.78)
\end{aligned}$$

It follows from (2.76) that

$$\tau_{11}(X)=\tau_{11}(X_1).$$

Remark 1. The only non-zero components of the residual stress appearing in the linearized eigenvalue problem within the class of deformations (2.37) is τ_{11}. This

means that the experiments performed within such class of deformations only allow one to recover the tensile stress τ_{11}. The above method can be generalized to recover the other two normal residual stresses τ_{22} and τ_{33} by utilizing the eigenfrequencies obtained from a similar experiment with the body rotated about the corresponding direction.

Remark 2. In order to reconstruct the shear residual stresses such as τ_{12}, τ_{13} and τ_{23}, one needs to conduct experiments that involve shearing the material as opposed to just extension and compression.

The boundary value problem (2.76)–(2.78) is an eigenvalue problem for χ_1 that governs forced vibrations and has solutions for all frequencies ω except for a discrete spectrum of resonant frequencies. We assume that the resonant frequencies in each of the three orthogonal directions are different. If the driving frequency ω hits one of the pure resonant frequencies along $\boldsymbol{e}_1$, then the vibrations in the lateral directions $\boldsymbol{e}_j$, $j = 2, 3$, are negligible, i.e. $\lambda_1 = \eta_1 = 0$. This is governed by the unforced system

$$\left(\frac{\mu(2\beta+1)J_0^{-2\beta}}{(\chi_0')^2} + \mu + \tau_{11} \right) \chi_1'' = -\rho\omega^2 \chi_1 \text{ on } \mathcal{B} \tag{2.79}$$

with homogeneous boundary conditions

$$\chi_1' = 0 \quad \text{on } \partial\mathcal{B}_I \tag{2.80}$$

$$\chi_1' = -\frac{k}{\mu\left(J_0^{-2\beta}(1+2\beta)\frac{1}{(\chi_0')^2}+1\right)}\chi_1 \quad \text{on } \partial\mathcal{B}_O \tag{2.81}$$

where $k \in [0, \infty)$.

E. Model Problem II

Let $\mathcal{B}$ be a rectangular domain in the unloaded residually stressed configuration as described in Section (C) and $\boldsymbol{X} = (X_1, X_2, X_3) \in \mathcal{B}$. The next class of deformations

that we consider is of the following form

$$\boldsymbol{\chi}(X,t) = \widehat{\chi}(X_1,t)\boldsymbol{e}_1 + \alpha(t)X_2\boldsymbol{e}_2 + \alpha(t)X_3\boldsymbol{e}_3 \tag{2.82}$$

where $\{\boldsymbol{e}_1, \boldsymbol{e}_2, \boldsymbol{e}_3\}$ is the natural Euclidean orthonormal basis, $\widehat{\chi}(X_1)$ is the deformation in $\boldsymbol{e}_1$, and $\alpha > 0$ is the stretch in $\boldsymbol{e}_2$ and $\boldsymbol{e}_3$ directions. Note that in contrast to the model problem considered in Section D, α is a function of time and does not vary spatially. For this particular model problem we adopt the constitutive equation in which the strain energy function is given by (2.13). Our goal is again to derive the boundary value problems (2.21) and (2.27)–(2.29) for this particular model problem, and develop an inverse spectral algorithm to estimate the residual stresses.

1. Static Large Deformation Boundary Value Problem

We perform an asymptotic expansion of $\widehat{\chi}(\boldsymbol{X},t)$ as in (2.38) and expand $\alpha(t)$ in the following way

$$\alpha(t) = \alpha_0 + \epsilon\alpha_1 e^{i\omega t} + o(\epsilon)$$

where α_0 and α_1 are constants. The static displacement $\boldsymbol{u}_0$ and the deformation gradient $\boldsymbol{F}_0$ for (2.82) are given by

$$\boldsymbol{u}_0(\boldsymbol{X},t) = (\chi_0(X_1,t) - X_1)\boldsymbol{e}_1 + (\alpha_0 - 1)X_2\boldsymbol{e}_2 + (\alpha_0 - 1)X_3\boldsymbol{e}_3 \tag{2.83}$$

$$\boldsymbol{F}_0(\boldsymbol{X}) = \chi_0'\boldsymbol{e}_1 \otimes \boldsymbol{e}_1 + \alpha_0\boldsymbol{e}_2 \otimes \boldsymbol{e}_2 + \alpha_0\boldsymbol{e}_3 \otimes \boldsymbol{e}_3 \tag{2.84}$$

with $J_0 = \alpha_0^2 \chi_0'$. In order to derive the static boundary value problem, the following formulae are required:

$$\boldsymbol{F}_0^{-T} = \frac{1}{\chi_0'}\boldsymbol{e}_1 \otimes \boldsymbol{e}_1 + \frac{1}{\alpha_0}\boldsymbol{e}_2 \otimes \boldsymbol{e}_2 + \frac{1}{\alpha_0}\boldsymbol{e}_3 \otimes \boldsymbol{e}_3 \tag{2.85}$$

$$\mathrm{Div}\boldsymbol{F}_0 = \chi_0''\boldsymbol{e}_1 \tag{2.86}$$

$$\mathrm{Div}\boldsymbol{F}_0^{-T} = \left(\frac{1}{\chi_0'}\right)'\boldsymbol{e}_1 \tag{2.87}$$

$$\nabla\psi(J_0) = 2\beta J_0^{-2\beta}\frac{\chi_0''}{\chi_0'}\boldsymbol{e}_1. \tag{2.88}$$

From (2.10), (2.14) and (2.26), we get,

$$\mathrm{Div}\boldsymbol{S}_0 = \mathrm{Div}\left(\widehat{\boldsymbol{S}}_N(\boldsymbol{F}_0) + \boldsymbol{\tau}\boldsymbol{F}_0\right) \tag{2.89}$$

where $\widehat{\boldsymbol{S}}_N(\boldsymbol{F}_0)$ is given in (2.32). Appealing to (2.44) and (2.85)–(2.88), we get

$$\mathrm{Div}\widehat{\boldsymbol{S}}_N(\boldsymbol{F}_0) = \mu\left(-J_0^{-2\beta}\left(\frac{1}{\chi_0'}\right)' + \frac{2\beta J_0^{-2\beta}}{(\chi_0')^2}\chi_0'' + \chi_0''\right)\boldsymbol{e}_1. \tag{2.90}$$

In order to calculate $\mathrm{Div}(\boldsymbol{\tau}\boldsymbol{F}_0)$, we refer to Definition 1. Then

$$\begin{aligned}
\boldsymbol{k}\cdot\mathrm{Div}(\boldsymbol{\tau}\boldsymbol{F}_0) &= \mathrm{Div}\left({\boldsymbol{F}_0}^T(\boldsymbol{\tau}\boldsymbol{k})\right)\\
&= \boldsymbol{\tau}\boldsymbol{k}\cdot\mathrm{Div}\left({\boldsymbol{F}_0}^T\right) + {\boldsymbol{F}_0}^T\cdot\nabla(\boldsymbol{\tau}\boldsymbol{k})\\
&= \boldsymbol{k}\cdot\boldsymbol{\tau}\mathrm{Div}\left({\boldsymbol{F}_0}^T\right) + {\boldsymbol{F}_0}^T\cdot\nabla\boldsymbol{\tau}[\boldsymbol{k}]\\
&= \boldsymbol{k}\cdot\left(\boldsymbol{\tau}\mathrm{Div}\left({\boldsymbol{F}_0}^T\right) + (\nabla\boldsymbol{\tau})^T{\boldsymbol{F}_0}^T\right)
\end{aligned}$$

where we have used the fact that $\boldsymbol{\tau} \in Sym$. Hence,

$$\mathrm{Div}(\boldsymbol{\tau}\boldsymbol{F}_0) = \boldsymbol{\tau}\mathrm{Div}\left({\boldsymbol{F}_0}^T\right) + (\nabla\boldsymbol{\tau})^T{\boldsymbol{F}_0}^T. \tag{2.91}$$

For the model (2.82), one can show, using (2.2), that

$$\mathrm{Div}(\boldsymbol{\tau}\boldsymbol{F}_0) = \left(\tau_{11}'\chi_0' - \alpha_0\tau_{11}' + \tau_{11}\chi_0''\right)\boldsymbol{e}_1. \tag{2.92}$$

Substituting (2.90) and (2.92) into (2.89) and simplifying, one gets

$$\mathrm{Div}\boldsymbol{S}_0 = \mu\left(J_0^{-2\beta}(1+2\beta)\left(\frac{\chi_0''}{(\chi_0')^2}\right)+\chi_0''\right)+\tau_{11}'\left(\chi_0'-\alpha_0\right)+\tau_{11}\chi_0''. \tag{2.93}$$

The boundary conditions remain the same as (2.53)–(2.55) since $\boldsymbol{\tau}\boldsymbol{F}_0\boldsymbol{e}_1 = \chi_0'\boldsymbol{\tau}\boldsymbol{e}_1 = 0$. Hence, the static finite boundary value problem in $\boldsymbol{e}_1$ is given by

$$\left(\mu(1+2\beta)+(\mu+\tau_{11})\,\alpha_0^{4\beta}(\chi_0')^{2(1+\beta)}\right)\chi_0'' + \alpha_0^{4\beta}\tau_{11}'(\chi_0')^{2(1+\beta)}\left(\chi_0'-\alpha_0\right)=0 \quad \text{on } \mathcal{B} \tag{2.94}$$

$$\frac{-J_0^{-2\beta}}{\chi_0'}+\chi_0' = -\frac{\pi_0}{\mu}\alpha_0^2 \qquad \text{on} \quad \partial\mathcal{B}_I \tag{2.95}$$

$$\frac{-J_0^{-2\beta}}{\chi_0'}+\chi_0' = -k\frac{(\chi_0-X_1)}{\mu} \quad \text{or,} \quad \frac{-J_0^{-2\beta}}{\chi_0'}+\chi_0' = -\frac{\pi_0}{\mu}\alpha_0^2 \qquad \text{on} \quad \partial\mathcal{B}_O. \tag{2.96}$$

2. The Linearized Vibrations Eigenvalue Problem

In this section, we derive the linearized eigenvalue problem (2.27)–(2.29) for the class of displacements of the form

$$\boldsymbol{u}_1(\boldsymbol{X}) = \chi_1(X_1)\boldsymbol{e}_1+\alpha_1X_2\boldsymbol{e}_2+\alpha_1X_3\boldsymbol{e}_3 \tag{2.97}$$

with the natural elasticity tensor $\mathbb{E}_N(\boldsymbol{F}_0)[\boldsymbol{H}]$ given by (2.31) and

$$\mathbb{E}_\tau(\boldsymbol{F}_0;\boldsymbol{\tau})[\boldsymbol{H}] = \boldsymbol{\tau}\boldsymbol{H}$$

from (2.14) and (2.30). The following formulae corresponding to (2.97) will be used to formulate the eigenvalue problem:

$$\nabla \boldsymbol{u}_1 = \chi_1' \boldsymbol{e}_1 \otimes \boldsymbol{e}_1 + +\alpha_1 \boldsymbol{e}_2 \otimes \boldsymbol{e}_2 + \alpha_1 \boldsymbol{e}_3 \otimes \boldsymbol{e}_3 \tag{2.98}$$

$$\operatorname{Div} \nabla \boldsymbol{u}_1 = \chi_1'' \boldsymbol{e}_1 \tag{2.99}$$

$$\left(\boldsymbol{F}_0^{-T} \cdot \nabla \boldsymbol{u}_1\right) = \frac{\chi_1'}{\chi_0'} + \frac{\alpha_1}{\alpha_0} + \frac{\alpha_1}{\alpha_0} \tag{2.100}$$

$$\nabla \left(\boldsymbol{F}_0^{-T} \cdot \nabla \boldsymbol{u}_1\right) = \left(\frac{\chi_1'}{\chi_0'}\right)' \boldsymbol{e}_1 \tag{2.101}$$

$$(\boldsymbol{F}_0^{-T} \nabla \boldsymbol{u}_1^T \boldsymbol{F}_0^{-T}) = \frac{\chi_1'}{(\chi_0')^2} \boldsymbol{e}_1 \otimes \boldsymbol{e}_1 + \frac{\alpha_1}{\alpha_0^2} \boldsymbol{e}_2 \otimes \boldsymbol{e}_2 + \frac{\alpha_1}{\alpha_0^2} \boldsymbol{e}_3 \otimes \boldsymbol{e}_3$$

$$\operatorname{Div}(\boldsymbol{F}_0^{-T} \nabla \boldsymbol{u}_1^T \boldsymbol{F}_0^{-T}) = \left(\frac{\chi_1'}{(\chi_0')^2}\right)' \boldsymbol{e}_1 \tag{2.102}$$

$$\operatorname{Div}(\boldsymbol{\tau} \nabla \boldsymbol{u}_1) = \left(\tau_{11}' \chi_1' - \alpha_1 \tau_{11}' + \tau_{11} \chi_1''\right) \boldsymbol{e}_1. \tag{2.103}$$

Substituting (2.98)–(2.103) into (2.35)–(2.36), we get

$$\operatorname{Div}\left(J_0^{-2\beta} [\boldsymbol{F}_0^{-T} \cdot \nabla \boldsymbol{u}_1] \boldsymbol{F}_0^{-T}\right) = -J_0^{-2\beta} (1 + 2\beta) \frac{\chi_0''}{(\chi_0')^2} \left(\frac{\chi_1'}{\chi_0'} + 2\frac{\alpha_1}{\alpha_0}\right) + J_0^{-2\beta} \frac{1}{\chi_0'} \left(\frac{\chi_1'}{\chi_0'}\right)' \tag{2.104}$$

$$\operatorname{Div}\left(J_0^{-2\beta} (\boldsymbol{F}_0^{-T} (\nabla \boldsymbol{u}_1)^T \boldsymbol{F}_0^{-T})\right) = J_0^{-2\beta} \left(\frac{\chi_1'}{(\chi_0')^2}\right)' - 2\beta J_0^{-2\beta} \frac{\chi_0'' \chi_1'}{(\chi_0')^3} \tag{2.105}$$

and substituting (2.104) and (2.105) into (2.27)–(2.34) we get the following eigenvalue problem that governs the superimposed small amplitude vibrations in $\boldsymbol{e}_1$

$$J_0^{-2\beta} \left(\mu(1 + 2\beta) \frac{1}{(\chi_0')^2} \chi_1'' - 2\mu(1 + \beta)(1 + 2\beta) \frac{\chi_0''}{(\chi_0')^3} \chi_1' - 4\beta\mu(1 + 2\beta) \frac{\alpha_1}{\alpha_0} \frac{\chi_0''}{(\chi_0')^2}\right) + (\mu + \tau_{11}) \chi_1'' + \tau_{11}' \chi_1' = -\rho\omega^2 \chi_1 \quad \text{on } \mathcal{B} \tag{2.106}$$

with boundary conditions

$$\mu\left(J_0^{-2\beta}(1+2\beta)\frac{1}{(\chi_0')^2}+1\right)\chi_1'+4\beta\mu J_0^{-2\beta}\frac{\alpha_1}{\alpha_0}\frac{1}{\chi_0'} = \pi_0 J_0\left(2\frac{\alpha_1}{\alpha_0}+1\right)\frac{1}{\chi_0'} \quad \text{on } \partial\mathcal{B}_I \quad (2.107)$$

and

$$\mu\left(J_0^{-2\beta}(1+2\beta)\frac{1}{(\chi_0')^2}+1\right)\chi_1'+4\beta\mu J_0^{-2\beta}\frac{\alpha_1}{\alpha_0}\frac{1}{\chi_0'} = \pi_0 J_0\left(2\frac{\alpha_1}{\alpha_0}+1\right)\frac{1}{\chi_0'} \quad \text{or,} \quad -k\chi_1 \quad \text{on } \partial\mathcal{B}_O. \quad (2.108)$$

Note that *Remark* 1 and *Remark* 2 both apply to this model problem.

Remark 3. The first-order eigenvalue problem depends on the residual stress τ_{11} and its derivatives both directly in the differential equation, and indirectly in the differential equation and the boundary conditions through the zero order stretch χ_0. Such is not the case for Model Problem I.

The boundary value problem (2.106)–(2.108) is an eigenvalue problem for χ_1 that governs forced vibrations and has solutions for all frequencies ω except for a discrete spectrum of resonant frequencies. We assume that the resonant frequencies in each of the three orthogonal directions are different. If the driving frequency ω hits one of the pure resonant frequencies along $\boldsymbol{e}_1$, then the vibrations in the lateral directions $\boldsymbol{e}_j$, $j=2,3$, are negligible, i.e. $\alpha_1=0$. This is governed by the unforced system

$$\left(\mu(1+2\beta)J_0^{-2\beta}\frac{1}{(\chi_0')^2}+\tau_{11}+\mu\right)\chi_1''-\left(2\mu(1+\beta)(1+2\beta)J_0^{-2\beta}\frac{\chi_0''}{(\chi_0')^3}-\tau_{11}'\right)\chi_1' = -\rho\omega^2\chi_1 \quad \text{on } \mathcal{B} \quad (2.109)$$

with homogeneous boundary conditions

$$\chi_1' = 0 \quad \text{on } \partial\mathcal{B}_I \tag{2.110}$$

$$\chi_1' = -\frac{k}{\mu\left(J_0^{-2\beta}(1+2\beta)\frac{1}{(\chi_0')^2}+1\right)}\chi_1 \quad \text{on } \partial\mathcal{B}_O \tag{2.111}$$

where $k \in [0,\infty)$. In Chapter 3, we present several numerical algorithms to reconstruct τ_{11} for Model Problem I and II given the resonant frequencies ω and all the other involved material parameters. We call such a problem an *inverse spectral problem*.

CHAPTER III

STURM-LIOUVILLE THEORY

In this chapter, we give a brief introduction to the direct [49] and inverse [32, 39] Sturm-Liouville problems.

A. Direct Sturm-Liouville Problem

Definition 2. A classical *Sturm-Liouville problem* (SLP) is defined to be a second order differential equation given by

$$-\left(p(x)y'(x)\right)' + q(x)y(x) = \lambda w(x)y(x), \infty < a < x < b < \infty \tag{3.1}$$

with boundary conditions

$$a_0y'(a) - a_1y(a) = 0 \tag{3.2}$$

$$b_0y'(b) + b_1y(b) = 0, \tag{3.3}$$

where $r(x) = 1/p(x)$, $q(x)$ and $w(x) \in L^2[a,b]$. a_0, a_1, b_0 and b_1 are real constants satisfying $a_0a_1 \neq 0$ and $b_0b_1 \neq 0$. λ is a parameter called the eigenvalue of the SLP.

The problem of finding the eigenvalues $\{\lambda_n\}_{n=1}^{\infty}$ and the eigenfunctions $\{u_n\}_{n=1}^{\infty}$ given $p(x)$, $q(x)$ and $w(x)$ is called the direct Sturm-Liouville problem.

Theorem 1. *A SLP can be obtained from any second order linear homogeneous differential equation.*

Proof. Consider a second order homogeneous differential equation given by

$$A(x)y''(x) + B(x)y'(x) + C(x)y(x) = \lambda D(x)y(x) \tag{3.4}$$

where $A(x) \neq 0$ for any $x \in [a,b]$. Dividing (3.4) by $A(x)$ and then multiplying it by

$e^{\int (B/A)dx}$ yields

$$-\left(e^{\int (B/A)dx}y'\right)' + \left(-\frac{C}{A}e^{\int (B/A)dx}\right)y = \lambda\left(-\frac{D}{A}e^{\int (Q/F)dx}\right)y, \tag{3.5}$$

which is in the form of (3.1). □

Definition 3. The endpoint a is said to be regular if

1. $r, q, w \in L^2(a, d)$ for some (and hence any) $d \in (a, b)$.

A similar definition holds for the end point b. Next we state a classical theorem that characterizes the eigenvalues and eigenfunctions of a SLP with regular endpoints and some positivity assumptions on the coefficients [49].

Theorem 2. *Consider a SLP* (3.1) *with boundary conditions* (3.2)–(3.3). *Let* $p > 0$, $w > 0$ *a.e on* (a, b). *Then*

1. *All eigenvalues are real and simple.*
2. *There are an infinite but countable number of eigenvalues* $\{\lambda_n : n \in \mathbb{N}_0\}$, *they are bounded below and can be ordered in the following way.*

$$-\infty < \lambda_0 < \lambda_1 < \lambda_2 < \lambda_3 < ...$$

3. *If* $u_n = u_n(\cdot, \lambda_n)$ *is an eigenfunction of* λ_n, *the* u_n *has exactly n zeros in the open interval* (a, b).
4. *The sequence of eigenfunctions* $\{u_n(\cdot, \lambda_n) : n \in \mathbb{N}_0\}$ *can be normalized to be an orthonormal sequence in* $L^2(a, b)$ *i.e.*

$$\int_a^b u_n u_m w dx = \delta_{mn}.$$

Furthermore, the orthonormal sequence u_n *is complete on* $L^2(a, b)$ *i.e. any*

$g \in L^2(a,b)$ can be expressed as

$$g = \sum_0^\infty c_n u_n, \quad c_n = \int_a^b g\, u_n\, w.$$

In other words, the sequence $\{u_n(\cdot, \lambda_n) : n \in \mathbb{N}_0\}$, after normalization, forms an orthonormal basis in $L^2(a,b)$.

5. *The eigenvalues λ_n satisfy the following asymptotic formula:*

$$\frac{\lambda_n}{n^2} \to \pi^2 \left(\int_a^b \sqrt{\frac{w}{p}} \right)^{-2}, \text{ as } n \to \infty. \tag{3.6}$$

Next, we state two theorems that shows that the eigenvalues of a regular SLP depend continuously on the coefficients $p(x)$, $q(x)$ and $w(x)$ (Theorem 2.1, [30]), and are Frechet differentiable with respect to the coefficients (Theorem 4.2, [31]), assuming the hypotheses of Theorem 2 hold. Recall the definition of the Frechet derivative:

Definition 4. Let V and W be Banach spaces, and $U \subset V$ be an open subset of V. A map $f : U \to W$ is called *Frechet differentiable* at $x \in U$ if there exists a bounded linear operator $df_x : V \to W$ such that for $h \in V$

$$\lim_{h \to 0} \frac{\|f(x+h) - f(x) - df_x\|_W}{\|h\|_V} = 0$$

Let $\mathbf{\Omega} = \{\boldsymbol{v} = (1/p, q, w)\} \subset L^2(a,b) \times L^2(a,b) \times L^2(a,b)$ with the induced norm

$$||w|| = \left(\int_a^b \left(|1/p|^2 + |q|^2 + |w|^2 \right) \right)^2$$

such that $p > 0$, $w > 0$ a.e on (a,b).

Theorem 3. *Let $\boldsymbol{v}_0 = (1/p_0, q_0, w_0) \in \mathbf{\Omega}$. Let $\lambda = \lambda_n(\boldsymbol{v}_0)$ be the n-th eigenvalue of the SLP 3.1–3.3. Then λ is a continuous function at $\boldsymbol{v}_0$ i.e. given any $\epsilon > 0$, there exists a $\delta > 0$ such that if $\boldsymbol{v} \in \mathbf{\Omega}$ satisfies*

$$||\boldsymbol{v} - \boldsymbol{v}_0|| < \delta, \quad \textit{then,}$$

$$|\lambda(\boldsymbol{v}) - \lambda(\boldsymbol{v}_0)| < \epsilon.$$

Theorem 4. *Assume that the hypotheses in Theorem 3 hold, and let* $u = u_n(\cdot, \boldsymbol{v})$ *be the normalized eigenfunction of the boundary value problem* (3.1)–(3.3). *Then* λ *is continuously differentiable with respect to each variable* $1/p$, q, *and* w. *In particular,*

1. *If all the variables of* $\boldsymbol{v}$ *are fixed except* $1/p$, *and* λ *is considered as a function of* $1/p \in L^2(a,b)$, *then* λ *is Frechet differentiable and its derivative is given by*

$$d\lambda_{(1/p)}[h] = \int_a^b |pu'|^2 h, \;\; h \in L^2(a,b) \tag{3.7}$$

2. *If all the variables of* $\boldsymbol{v}$ *are fixed except* q, *and* λ *is considered as a function of* $q \in L^2(a,b)$, *then* λ *is Frechet differentiable and its derivative is given by*

$$d\lambda_{(q)}[h] = \int_a^b |u|^2 h, \;\; h \in L^2(a,b) \tag{3.8}$$

3. *If all the variables of* $\boldsymbol{v}$ *are fixed except* w, *and* λ *is considered as a function of* $w \in L^2(a,b)$, *then* λ *is Frechet differentiable and its derivative is given by*

$$d\lambda_{(w)}[h] = -\lambda \int_a^b |u|^2 h, \;\; h \in L^2(a,b) \tag{3.9}$$

The following theorem states the monotonicity of the eigenvalues (Theorem 4.9.1 [49]):

Theorem 5. *Let* $\boldsymbol{v} = (1/p, q, w) \in \Omega$ *and let* $p > 0$, $w > 0$ *a.e on* (a,b). *Let* $\lambda_n(\boldsymbol{v})$ *be the n-th eigenvalue of the SLP* (3.1)–(3.3).

1. *Fix p,w. Suppose* $Q \in L^2(a,b)$ *and assume that* $Q \geq q$ *a.e. on* $[a,b]$. *Then* $\lambda_n(Q) \geq \lambda_n(q)$ *for any* $n \in N_0$. *If* $Q > q$ *on a subset of* $[a,b]$ *having positive Lebesgue measure, then* $\lambda_n(Q) > \lambda_n(q)$.

2. *Fix q,w. Suppose* $1/P \in L^2(a,b)$ *and assume that* $0 < P \leq p$ *a.e. on* $[a,b]$.

Then $\lambda_n(1/P) \geq \lambda_n(1/p)$ *for any* $n \in N_0$. *If* $1/P < 1/p$ *on a subset of* $[a, b]$ *having positive Lebesgue measure, then* $\lambda_n(1/P) < \lambda_n(1/p)$.

3. *Fix p,q. Suppose* $W \in L^2(a, b)$ *and assume that* $W \geq w > 0$ *a.e. on* $[a, b]$. *Then for any* $n \in N_0$, $\lambda_n(W) \geq \lambda_n(w)$ *if* $\lambda_n(W) < 0$ *and* $\lambda_n(w) < 0$, *and* $\lambda_n(W) \leq \lambda_n(w)$ *if* $\lambda_n(W) > 0$ *and* $\lambda_n(w) > 0$. *Furthermore, if* $W > w > 0$ *on a subset of* $[a, b]$ *having positive Lebesgue measure, then* $\lambda_n(W) > \lambda_n(w)$ *if* $\lambda_n(W) < 0$ *and* $\lambda_n(w) < 0$, *and* $\lambda_n(W) < \lambda_n(w)$ *if* $\lambda_n(W) > 0$ *and* $\lambda_n(w) > 0$.

B. Inverse Sturm-Liouville Problem

The problem of finding the eigenvalues $\{\lambda_n\}_{n=0}^{\infty}$ and eigenfunctions $\{u_n\}_{n=0}^{\infty}$, given the coefficients $p(x)$, $q(x)$ and $w(x)$ of the SLP (3.1)–(3.3), is known as the forward or direct Sturm-Liouville problem. On the other hand, the problem of recovering the coefficients $p(x)$, $q(x)$ and $w(x)$, given the the eigenvalues $\{\lambda_n\}_{n=0}^{\infty}$, is called the *Inverse Sturm-Liouville Problem.*

Reconstructing all of the three coefficients in the SLP (3.1) from the knowledge of $\{\lambda_n\}_{n=0}^{\infty}$ is a very complicated task. Most algorithms proposed to solve the inverse Sturm-Liouville problem usually deals with the reconstruction of either of the three coefficients [1, 9, 41]. A common method is to transform (3.1)–(3.3), via the Liouville transformation [9], into the following equation:

$$\mathcal{L}[u_n] := -u_n''(x) + q(x)u_n(x) = \mu_n u_n(x), \quad x \in (0, 1) \tag{3.10}$$

$$u_n'(0) - hu_n(0) = 0, \tag{3.11}$$

$$u_n'(1) + Hu_n(1) = 0, k = 1, 2 \ldots \infty \tag{3.12}$$

(3.10)–(3.12) is called the Sturm-Liouville problem of normal form and $q(x)$ is called the potential. $\{\mu_n\}_{n=0}^{\infty}$ and $\{u_n\}_{n=0}^{\infty}$ are the eigenvalues and the eigenfunctions of

the problem respectively. The inverse problem then reduces to recovering $q(x)$ from given spectral data. (3.10)–(3.12) has been extensively studied in the past few decades [6, 13, 18, 32, 39]. It was proved by Borg in 1946 that a single spectrum is insufficient to uniquely recover $q(x)$. He also showed that if the potential $q(x)$ is symmetric about the mid point i.e. $q(x) = q(1-x)$, then it can be uniquely recovered by a sequence of eigenvalues $\{\mu_n\}_{n=1}^{\infty}$ of (3.1). Additional spectral information such as a sequence of eigenvalues $\{\tilde{\mu}_n\}_{n=1}^{\infty}$ with H replaced by $\tilde{H}$, a sequence of terminal velocities $\{\kappa_n\}_{n=1}^{\infty}, \kappa_n = \ln\left(|u_n'|_{x=1}/|u_n'|_{x=0}\right)$ for $h, H = \infty$ or $\{\kappa_n\}_{n=1}^{\infty}, \kappa_n = \ln\left(|u_n|_{x=1}/|u_n|_{x=0}\right)$ for $h, H = 0$, or a sequence of norming constants $\{\|u_n\|_{L_2}^2/(u_n)^2|_{x=0}\}_{n=1}^{\infty}$ for $h, H = 0$ or $\{||u_n||_{L_2}^2/(u_n')^2|_{x=0}\}_{n=1}^{\infty}$ for $h, H \neq 0$ is needed in order to reconstruct a general potential [13].

A number of constructive algorithms have been developed for the recovery of $q(x)$ with finite spectral data [9, 13, 42, 38]. We emphasize that such algorithms that reconstruct the coefficients using a number of eigenfrequencies and other spectral data correspond to using spectral data from a single blood pressure as mentioned in Chapter I, and hence, cannot be implemented for our problem of reconstructing residual stress using data from different blood pressures. In the next chapter, we present several numerical algorithms that meet our goal.

For the model problems described in Sections D and E of Chapter II, the eigenvalue problems that describe the small amplitude vibrations due to IVUS are of Sturm-Liouville type and given by the following:

For Model Problem I: The linearized eigenvalue problem is given by (3.1) where $[a, b] = [0, 1]$, $u(x) = \chi_1(X_1), X_1 \in [0, 1]$, $\lambda = \omega^2$ and

$$p(X_1) = 1, \quad q(X_1) = 0, \quad w(X_1) = \left(\frac{1}{\frac{\mu(1+2\beta)J_0^{-2\beta}}{(\chi_0')^2} + \mu + \tau_{11}} \right). \tag{3.13}$$

Here, χ_0' is a constant. The boundary conditions for this particular model is (3.2)–(3.3), where

$$a_0, b_0 = 1,\ a_1 = 0 \text{ and } b_1 = \frac{k}{\mu\left(\frac{J_0^{-2\beta}(1+2\beta)}{(\chi_0')^2}+1\right)}. \tag{3.14}$$

For Model Problem II: The linearized eigenvalue problem is given by (3.1) where $[a,b] = [0,1]$, $u(x) = \chi_1(X_1), X_1 \in [0,1]$, $\lambda = \omega^2$ and

$$p(X_1) = e^{\int_0^{X_1}\left(\frac{\tau_{11}'-2\mu(1+\beta)(1+2\beta)J_0^{-2\beta}\frac{\chi_0''}{(\chi_0')^3}}{\mu(1+2\beta)J_0^{-2\beta}\frac{1}{(\chi_0')^2}+\tau_{11}+\mu}\right)dX}, \quad q(X_1) = 0, \tag{3.15}$$

and

$$w(X_1) = p(X_1)\left(\frac{1}{\frac{\mu(1+2\beta)J_0^{-2\beta}}{(\chi_0')^2}+\mu+\tau_{11}}\right). \tag{3.16}$$

In this case, χ_0 is a solution to the boundary value problem (2.94)–(2.96). The boundary condition remains unchanged and is also given by (3.14).

Note that $p(X_1) > 0$ for both the problems. Also, from (2.63) and the fact that $\mu, \beta > 0$ and $|\tau_{11}/\mu| < 1$, we conclude that the $w(X_1)$ given in (3.13) and (3.16) satisfy $0 < w(X_1) < \infty$.

Our interest lies in the reconstruction of the residual stress τ_{11} using the Inverse Sturm-Liouville Theory, where the coefficients $p(x)$, $q(x)$ and/or $w(x)$ of the eigenvalue problems described above depend on τ_{11}.

Lemma 1. *The eigenvalues* $\{\lambda_n : n \in \mathbb{N}_0\}$ *of the SLP* (3.1)–(3.3) *for the Model Problems I and II given by* (3.13) *and* (3.15)–(3.16) *respectively are non-negative.*

Proof. Let $u_n(x)$ be the eigenfunction corresponding to the n^{th} eigenvalue of (3.1)–(3.3). Multiplying the differential equation (3.1) by $u_n(x)$ and integrating from $x = 0$ to $x = 1$ we obtain

$$-\int_0^1 \left(p(x)u_n'(x)\right)' u_n(x) + \int_0^1 q(x)u_n^2(x) = \int_0^1 \lambda_n w(x)u_n^2(x),$$

Note that $q(x) = 0$. Integrating by parts and rearranging the terms gives,

$$\lambda_n = \frac{-\left(pu_n'\right) u_n \,|_0^1 + \int_0^1 p(x)(u_n'(x))^2}{\int_0^1 w(x)u_n^2(x)}. \tag{3.17}$$

Applying the boundary conditions, we obtain

$$\lambda_n = \frac{\frac{\left(p(u_n')^2\right)(1)}{b_1} + \int_0^1 (u_n'(x))^2}{\int_0^1 w(x)u_n^2(x)} \tag{3.18}$$

which is non-negative, since $p > 0$ and $b_1 > 0$ from (3.14). □

Lemma 2. *The n^{th} eigenvalues $\{\lambda = \lambda_n(1/p, q, w) : n \in \mathbb{N}_0\}$ of the SLP* (3.1)–(3.3) *for the Model Problems I and II given by* (3.13) *and* (3.15)–(3.16) *respectively is a continuous function of τ_{11}.*

Proof. By Theorem 3, λ is a continuous function of $\boldsymbol{v} = (1/p, q, w) \in \boldsymbol{\Omega}$. Furthermore, p, q and w are continuous functions of $\tau_{11}(X_1)$. Hence, λ is a continuous function of τ_{11} and can be written as $\lambda = \lambda(\tau_{11})$. □

Proposition 1. *The eigenvalues $\{\lambda(\tau_{11}) = \lambda_n(1/p, q, w) : n \in \mathbb{N}_0\}$ are continuously differentiable with respect to τ_{11}. Furthermore, for the Model Problem I, λ_n is an increasing function of τ_{11}.*

Proof. By the chain rule, we get,

$$d\lambda_{\tau_{11}}[h] = \left((D\lambda_{1/p})(Dp) + (D\lambda_q)(Dq) + (D\lambda_w)(Dw)\right)[h].$$

Recall that p, q and r given in (3.13) for Model Problem I and (3.15)-(3.13) for Model Problem II are smooth functions of τ. Then by Theorem 4, $d\lambda_{\tau_{11}}[h]$ is well defined and continuous. In particular, for Model Problem I, we get, from (3.13) and the chain rule,

$$d\lambda_{\tau_{11}}[h] = (D\lambda)(Dw)[h]$$

where

$$Dw[h] = -\int \frac{1}{\left(\frac{\mu(1+2\beta)J_0^{-2\beta}}{(\chi_0')^2} + \mu + \tau_{11}\right)^2} h = -\int w^2(\cdot, \tau_{11})h.$$

Appealing to the Frechet derivative of (3.9) and Lemma 1, we get,

$$d\lambda_{\tau_{11}}[h] = \lambda \int |u^2(z,w)| w^2(z,\tau_{11}) h \, dz, \;\; h \in L^2(0,1).$$

To prove the second part of the proposition, let $w(x) = 1/(A(x) + \tau_{11})$ and $W(x) = 1/(A(x) + \tilde{\tau}_{11})$ and $\tau_{11} \geq \tilde{\tau}_{11}$ a.e on $[0,1]$. Then, $W(x) \geq w(x) > 0$ a.e on $[0,1]$. Also, from Lemma 1, $\lambda_n(\tau_{11}) > 0$ and $\lambda_n(\tilde{\tau}_{11}) > 0$. Then, according to part 3. of Theorem 5, $\lambda_n(\tau_{11}) \geq \lambda_n(\tilde{\tau}_{11})$. □

CHAPTER IV

CONSTRUCTIVE ALGORITHMS

A. Cubic Spline Approximation

Recall that the main goal of this project is to estimate the residual stress τ_{11} from the spectral data of a system of boundary value problems that correspond to different blood pressures π occurring during a cardiac cycle. To that note, we make the following observation:

- The dependence of the problem to π is through the zero order stretch $\chi_0 = \chi_0(X_1, \pi)$.
- The first order stretch χ_1 depends on χ_0, and hence is a function of π.
- For Model Problem II, both χ_0 and χ_1 are functions of τ_{11} and τ_{11}'. As a result, χ_0 is solved numerically for different blood pressures, and the solution is used in the eigenvalue problem to estimate τ_{11}.

It was shown that τ_{11} only varies in the radial direction i.e. $\tau_{11} = \tau_{11}(X_1)$. From here on, for notational convenience, we simply replace X_1 by x and τ_{11} by τ. To that end, we assume that $\tau(x)$ is continuously differentiable and can be accurately approximated using cubic splines. More specifically, the algorithm estimates τ at the finite degrees of freedom which are the nodal points of the spline interpolation, and a series of cubic polynomials are fitted between each of the data points.

We partition the domain $[0, 1]$ into $N - 1$ uniform sub-intervals. The nodes are denoted as x_i, $0 \leq i \leq N$ and the value of τ at x_i are denoted by τ_i, $0 \leq i \leq N$. Define a piecewise function of the form

$$P(x) = \begin{cases} p_1(x) & if \quad x_1 \leq x < x_2 \\ p_2(x) & if \quad x_2 \leq x < x_3 \\ & \vdots \\ p_{N-1}(x) & if \quad x_{N-1} \leq x < x_N \end{cases}$$

where p_i is a third degree polynomial defined by

$$p_i(x) = a_i\,(x - x_i)^3 + b_i\,(x - x_i)^2 + c_i\,(x - x_i) + d_i, \;\; 0 \leq i \leq N - 1.$$

The N data points are then interpolated using this piecewise function, which means

$$\tau(x) = P(x)$$

and

$$P(x_i) = \tau_i\,, \;\; 0 \leq i \leq N - 1.$$

In addition, the spline should satisfy the following conditions:

- $P(x)$ is continuous on the interval $[x_0, x_N]$, which means

$$p_i(x_i) = p_{i-1}(x_i);$$

- $P'(x)$ is continuous on the interval $[x_0, x_N]$, which means

$$p_i'(x_i) = p_{i-1}'(x_i);$$

- $P''(x)$ is continuous on the interval $[x_0, x_N]$, which means

$$p_i''(x_i) = p_{i-1}''(x_i).$$

Figure 4 shows a cubic spline interpolation of 5 data points $(0, 0.5)$, $(0.25, 0.27)$, $(0.5, 0.35)$, $(0.75, 0.1875)$ and $(1, 0.2)$.

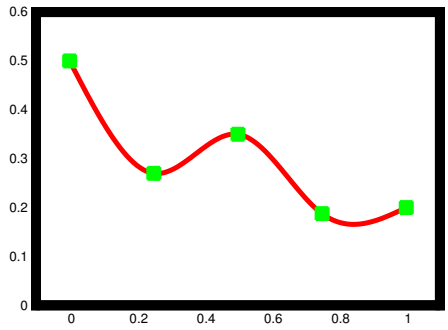

Fig. 4. Cubic Spline Interpolation of 5 Nodes

Our focus lies in finding $\tau = (\tau_1, \tau_2, \ldots \tau_N)$, and the cubic spline interpolation of these N nodes gives us an approximation to the residual stress τ.

B. Basic Algorithms

The numerical solution of the static problem and the eigenvalue problem require several basic algorithms, including Newton's method and the secant method for solving a non-linear equation, the fourth-order Runge-Kutta method for solving an initial value problem and the shooting method for finding the solution of a two-point boundary value problem. We present these algorithms below.

1. Newton's Method

Suppose we have a function $f : \mathbb{R} \to \mathbb{R}$. The Newton's method can be used to find the roots of a non-linear equation $f(y) = 0$. Given an initial guess y_0, the iteration formula is given by

$$y_{k+1} = y_k - f'(y_k)^{-1} f(y_k), \;\; k = 0, 1, 2, \ldots$$

The same formula also works for solving a system of nonlinear equations.

2. Secant Method

Suppose we have a function $f : \mathbb{R} \to \mathbb{R}$. Like the Newton's method, the one dimensional secant method can be used to find the roots of a non-linear equation $f(y) = 0$. Given two initial guess y_0 and y_1, the recurrence relation is given by [10]

$$y_{k+1} = y_k - \frac{y_{k-1} - y_k}{f(y_{k-1}) - f(y_k)} f(y_k), \ k = 0, 1, 2, \ldots$$

It is known that the secant method converges superlinearly with order $\alpha = 1.618$, provided that the two initial guesses are close to the solution and f is twice continuously differentiable [27]. Although the secant method requires more iterations to converge than the Newton's method, it has the advantage that the derivative $f'(y)$ is not required for the iteration, and it only requires one function evaluation per iteration.

3. Fourth Order Runge-Kutta Method for Initial Value Problems

The Runge-Kutta method is a numerical method to solve initial value problems of such type

$$Y'(t) = F(Y, t), \quad Y(t_0) = Y_0, \quad Y \in \mathbb{R}^N. \tag{4.1}$$

In particular, the fourth order Runge-Kutta method is given by [10]

$$Y(t + h) = Y(t) + \frac{1}{6}(F_1 + 2F_2 + 2F_3 + F_4), \tag{4.2}$$

where

$$F_1 = hF(Y),$$
$$F_2 = hF(Y + \frac{1}{2}F_1),$$
$$F_3 = hF(Y + \frac{1}{2}F_2),$$
$$F_4 = hF(Y + F_3).$$

Now consider a second order initial value problem given by

$$y''(t) = f(t, y, y'), \quad \text{for} \quad t \geq t_0, \tag{4.3}$$
$$y(t_0) = \alpha, \tag{4.4}$$
$$y'(t_0) = \beta, \tag{4.5}$$

where f is a known function and α and β are given constants. We set

$$y_1 = t, \quad y_2 = y(t), \quad y_3 = y'(t). \tag{4.6}$$

This yields

$$y_1' = 1, \quad y_2' = y_3, \quad y_3' = f(y_1, y_2, y_3). \tag{4.7}$$

Define vectors $Y = (y_1, y_2, y_3)^T$, $F(Y) = (1, y_3, f(y_1, y_2, y_3))^T$ and $Y_0 = (t_0, \alpha, \beta)^T$. This gives an initial value problem for Y given in (4.1). The fourth-order Runga-Kutta method described above can then be used to find the solution $y(t)$ of the initial value problem (4.3)–(4.5).

4. Shooting Method for Boundary Value Problems

Consider a boundary value problem of the form

$$y''(t) = f(t, y, y'), \quad t \in [a, b] \tag{4.8}$$

$$F_a(a, y(a), y'(a)) = 0, \tag{4.9}$$

$$F_b(b, y(b), y'(b)) = 0. \tag{4.10}$$

A shooting method combined with the Runge-Kutta method and the secant method can be used to find the solution to (4.8)–(4.10). Set $y'(a) = \alpha$, where α is any number. (4.9) can then be solved for $y(a) = g(\alpha)$ using the secant method described in 2. Formulate an initial value problem given by

$$y''(t) = f(t, y, y') \tag{4.11}$$

$$y(a) = g(\alpha), \quad y'(a) = \alpha. \tag{4.12}$$

(4.11)–(4.12) is then solved using the Runge-Kutta method described in 3, and the solution is expressed as $Y(t, \alpha)$. Finally, α is found by making use of (4.10), that is, the secant method is used to solve the equation

$$F_b(b, y(b, \alpha), y'(b, \alpha)) = 0$$

for α.

5. Generalized Secant Method for a System of Equations

The one-dimensional secant method described in 2 can be generalized to find a solution of a system of linear or non-linear equations [48]. Suppose we have a system of n equations with n unknowns:

$$\boldsymbol{f}(\boldsymbol{x}) = 0, \tag{4.13}$$

where $\boldsymbol{f} = (f_1, f_2, \ldots f_n)$ and $\boldsymbol{x} = (x_1, x_2, \ldots x_n)$. Just as in the single variable secant method, we require $n+1$ trial solutions or initial guesses for the method to work. Let us denote the $n+1$ trial solutions by

$$\begin{aligned} \boldsymbol{X}_1 &= (x_1^{(1)}, x_2^{(1)}, \ldots x_n^{(1)}), \\ \boldsymbol{X}_2 &= (x_1^{(2)}, x_2^{2)}, \ldots x_n^{(2)}), \\ &\ldots \\ \boldsymbol{X}_{n+1} &= (x_1^{(n+1)}, x_2^{(n+1)}, \ldots x_n^{(n+1)}). \end{aligned} \tag{4.14}$$

There are several generalizations of the secant method to solve n equations. We describe the one introduced in [48].

The first step is to find a set of numbers $\eta_1, \ldots \eta_{n+1}$ such that

$$\sum_{j=1}^{n+1} \eta_j = 1 \tag{4.15}$$

and

$$\sum_{j=1}^{n+1} \eta_j f_i(x_1^{(j)}, x_2^{(j)}, \ldots x_n^{(j)}) = 0 \quad \text{for} \quad i = 1, 2 \ldots n. \tag{4.16}$$

Construct a new vector

$$\widehat{\boldsymbol{X}} = \sum_{j=1}^{n+1} \eta_j \boldsymbol{X}_j. \tag{4.17}$$

Compute the $n+1$ values

$$b_j = \sum_{i=1}^{n} |f_i(\boldsymbol{X}_j)|^\alpha \quad \text{for} \quad j = 1, 2, \ldots n+1, \tag{4.18}$$

where $\alpha > 0$ is a chosen parameter. Find $m \in [1, n+1]$ such that

$$b_m := \max_{1 \le j \le n+1} b_j.$$

Finally, update the set of trial solutions by replacing $\boldsymbol{X}_m$ with $\widehat{\boldsymbol{X}}$. The iteration is

repeated til we have

$$\|\widehat{\boldsymbol{X}}_{n+1} - \widehat{\boldsymbol{X}}_n\| < \varepsilon_1,$$

where ε_1 is the tolerance number, $\varepsilon_1 << 1$. Note that when $n = 1$, the above method reduces to the one dimensional secant method. One can show that the method converges superlinearly with order $\alpha = 1.618$ if the solutions to (4.15)–(4.16) remain bounded at each iteration, and the $n + 1$ trial solutions are sufficiently close to the solution [48].

6. Eigenspectrum Solver

In order to develop an algorithm for the Inverse Spectral problem, we need to solve the forward problem of finding the eigenvalues and the eigenfunctions of the (3.1)–(3.3). We describe a method that uses finite element bases to discretize the problem to a matrix eigenvalue problem, and then utilizes the Krylov-Schur methods in a package called SLEPc to find the eigenpairs $(\lambda_i, \boldsymbol{\Psi}_i)_{i=1}^{M}$, where λ_i and $\boldsymbol{\Psi}_i$ are the eigenvalues and the eigenvectors respectively [3, 4].

Let $\{x_j\}_{j=0}^{N'}$ be a uniform partition of the interval $[0, 1]$. Let $\{\phi_i\}_{i=0}^{N}$ be a piecewise smooth finite element basis for $\boldsymbol{\Psi}$ such that $\phi_i(x_j) = \delta_{ij}$ [12]. We can write $\boldsymbol{\Psi}(x) = \sum_{j=0}^{N} \psi_j \phi_j(x)$ where $\boldsymbol{\psi} = (\psi_1, \psi_2 \dots \psi_N)$ is a vector of expansion coefficients. Multiplying (3.1) with a test function ϕ_i and integrating by parts, we get

$$\sum_{j=0}^{N} \left(-p(x)\phi_i\phi_j'\psi_j \,\big|_{x=0}^{1} + \int_0^1 p(x)\phi_i'\phi_j'\psi_j + \int_0^1 q(x)\phi_i\phi_j\psi_j \right) = \lambda \sum_{j=0}^{N} \int_0^1 w(x)\phi_i\phi_j\psi_j, \quad i = 1 \dots N. \tag{4.19}$$

In matrix and vector notation, this equation can be rewritten as

$$\boldsymbol{A}\boldsymbol{\psi} = \lambda \boldsymbol{M}\boldsymbol{\psi} \tag{4.20}$$

where $\boldsymbol{A}$ is the stiffness matrix given by

$$[A]_{ij} = \int_0^1 \left(-p(x)\phi_i\phi_j' \,|_{x=0}^1 + p(x)\phi_i'\phi_j' + q(x)\phi_i\phi_j\right)$$

and $\boldsymbol{B}$ is the mass matrix given by

$$[B]_{ij} = \int_0^1 w(x)\phi_i\phi_j.$$

The matrix eigenvalue problem (4.20) is solved for $(\lambda_i, \boldsymbol{\Psi}_i)_{i=1}^M$ using the Krylov-Schur solver which is implemented in the SLEPc library.

C. Secant Method for the Inverse Spectral Problem

We develop an algorithm for the inverse Sturm-Liouville problem, in particular, the problem of recovering the residual stress τ, by making use of the algorithms described above. Our goal is to recover the N unknowns $\tau_1, \tau_2, \ldots \tau_N$ by deriving N equations from N different blood pressures $\pi_1, \pi_2, \ldots \pi_N$. We postulate obtaining a selection of eigenfrequencies from experimental measurements for each π_j, and denote them by $\{\tilde{\lambda}_n^{(j)}\}_{n=1}^{N'}$. The multi dimensional secant method requires an initial guess of $N+1$ trial solutions $\tau^{(k)} = (\tau_1^{(k)}, \tau_2^{(k)}, \ldots \tau_N^{(k)}), k = 1 \ldots N+1$. For each initial guess $\tau = (\tau_1, \tau_2, \ldots \tau_N)$, from which we know the corresponding cubic spline function $\tau(x)$, we find an approximation for $\tau'(x)$, since the static problem (2.94)–(2.96) and the eigenvalue problem (2.109)–(2.111) for Model Problem II both depend on $\tau'(x)$. This is achieved using a second order central difference scheme which is given by

$$\tau'(x) = \frac{\tau(x+h) - \tau(x-h)}{2h} + O(h^2) \tag{4.21}$$

where h is sufficiently small. For each π_j and an initial guess $\tau = (\tau_1, \tau_2, \ldots \tau_N)$, we find the solution $\chi_0(\tau, x)$ from (2.94)–(2.96) using the shooting method described in 4.

Then substitute $\chi_0(\tau, x)$, $\tau(x)$, $\tau'(x)$ and blood pressure π_j into (2.109)–(2.111), and use the Eigenspectrum solver described in 6 to find the sequence of eigenvalues which depend on τ and π_j and denote them as $\{\lambda_n^{(j)}(\tau)\}_{n=0}^{N'}$ where N' is the total number of eigenvalues computed for each blood pressure. Then we define N equations of N unknowns as

$$d_j(\tau) = \sum_{n=0}^{N'} |\lambda_n^{(j)}(\tau) - \tilde{\lambda}_n^{(j)}|^{\Gamma}, \tag{4.22}$$

where Γ is a parameter specific to the problem. We then find $\tau_1, \tau_2, \ldots \tau_N$ such that $d_j(\tau) \approx 0$ by using the secant method described in 5 to solve the resulting equations.

We know from Theorem 2 that the eigenfrequencies $\{\lambda_n^{(j)}\}_{n=1}^{\infty}$, for a fixed j, are increasing with n and in practice, only the first few lower eigenfrequencies can be measured accurately from experiments. However, these lower eigenfrequencies can be accurately measured for a large number of blood pressures occurring in a cardiac cycle. Hence, we only require the first few eigenfrequencies corresponding to different blood pressures to get a good reconstruction for τ. In fact, in our numerical examples, we substitute (4.22) with

$$d_j(\tau) = |\lambda_0^{(j)}(\tau) - \tilde{\lambda}_0^{(j)}|^{\Gamma} \tag{4.23}$$

and use only the smallest eigenvalue for each blood pressure π_j. The detailed algorithm is given as follows:

Algorithm 1.

1. Provide $N+1$ trial solutions $\tau^{(1)}$, $\tau^{(2)}$,$\ldots \tau^{(N+1)}$ for τ, where each $\tau^{(k)}$ is a N dimensional vector given by $\tau^{(k)} = (\tau_1^{(k)}, \tau_2^{(k)}, \ldots \tau_N^{(k)}), k = 1 \ldots N+1$. Note that the initial guesses are required to be close enough to the true solution in order for the method to converge.

2. For each $\tau^{(k)}$, find the cubic spline interpolation function.

3. Find the numerical derivative $\tau'^{(k)}$ of each $\tau^{(k)}$ using (4.21).

4. For each $\tau^{(k)}$ (the cubic spline interpolation from Step 2) and each blood pressure π_j, where $1 \leq j \leq N$, find the numerical solution $\chi_0^{(j)}(x, \tau^{(k)})$ from (2.94)–(2.96). The secant method and the shooting methods are used for solving the boundary value problems. Note that for the Model Problem I, where $\chi_0 = \chi_0(\pi_j)$, simply use the secant method to find $\chi_0^{(j)}(x)$.

5. Substitute $\chi_0^{(j)}(x, \tau^{(k)})$, $\tau^{(k)}$, $\tau'^{(k)}$ and π_j into (2.109)–(2.111) and find the first eigenvalues for the SLP (3.1) for each j and k and denote it as $\lambda_0^{(j)}(\tau^k)$.

6. Substitute $\lambda_0^{(j)}(\tau^{(k)})$ into (4.23) to get $d_j(\tau^{(k)})$ for each j and k.

7. Form a $(N+1) \times (N+1)$ square matrix D given by

$$\boldsymbol{D} = \begin{bmatrix} d_1(\tau^{(1)}) & d_1(\tau^{(2)}) & \dots & d_1(\tau^{(N+1)}) \\ d_2(\tau^{(1)}) & d_2(\tau^{(2)}) & \dots & d_2(\tau^{(N+1)}) \\ \vdots & \vdots & \vdots & \vdots \\ d_N(\tau^{(1)}) & d_N(\tau^{(2)}) & \dots & d_N(\tau^{(N+1)}) \\ 1 & 1 & \dots & 1 \end{bmatrix}. \tag{4.24}$$

8. Find the vector $\eta = (\eta_1, \eta_2, ...\eta_{(N+1)})$ by solving the matrix-vector equation $\boldsymbol{D}\eta^T = (0, 0, \dots, 0, 1)^T$, where the superscript T stands for transpose.

9. Find an updated $\widehat{\tau}$ using (4.17).

10. Compute b_i for $1 \leq i \leq N+1$ by taking $f_i(\boldsymbol{X}_j) = d_i(\tau^{(j)})$ in (4.18), where $d_i(\tau^{(j)})$ is given by (4.23).

11. Find the value m such that (5) is satisfied and replace $\tau^{(m)}$ by $\widehat{\tau}$ and form an updated $N+1$ solutions $\tau^{(1)}$, $\tau^{(2)}$,..., $\tau^{(m-1)}$, $\widehat{\tau}$, $\tau^{(m+1)}$...$\tau^{(N+1)}$.

12. Repeat Steps 2 – 11 until $|\widehat{\tau}_{new} - \widehat{\tau}_{old}| < \varepsilon_1$, where ε_1 is a given tolerance and $\widehat{\tau}_{new}$ and $\widehat{\tau}_{old}$ are the $\widehat{\tau}$ from the current and the previous iteration respectively.

D. Numerical Examples

In this section, we present various numerical examples corresponding to the algorithm developed in Section C. The density ρ is chosen to be 1 gm/cm^3. The inner and outer radius of the unloaded but residually stressed arterial wall is assumed to be 1.39 mm and 1.99 mm respectively [25]. The values of other parameters used in the numerical simulations are chosen to be: $\mu = 27$ kPa, $\nu = 0.4$, the stretches $\lambda_0 = \eta_0 = \alpha_0 = 1.5$. The parameter Γ in the algorithm is chosen to be 2. In each of the tables, the first row represents the blood pressure used for that example, and the second row represents the corresponding first eigenfrequency for the pressure. Each table contains a particular set of initial guesses for τ at the nodes $x_1, x_2 \dots x_N$ for the secant method. Note that the number of initial guesses depend on the number of blood pressures used. The true value and the returned value of τ at each node is given along with the absolute error computed in the L^2 norm and the value $\|\widehat{\tau}_{new} - \widehat{\tau}_{old}\|_{L^2}$ for the last iteration. A corresponding plot of the true τ and the iterated τ for each table is presented. Note that in the figures, the solid line represents the true τ and the dotted line represents the iterated τ.

Example 1. The function we want to approximate is $\tau = 1 - \left(\frac{x-x_0}{x_1-x_0}\right)^2$. We use the cubic spline interpolation of the function at 3 nodes and 5 nodes and the first eigenvalue $\{\lambda_0\}$ as given data. The reconstructions are given in Figure 5 and the iteration input and output data are given in Tables I and II.

Example 2. The function we want to approximate is $\tau = \frac{x-x_0}{x_1-x_0}\left(1 - \frac{x-x_0}{x_1-x_0}\right)$. We use the cubic spline interpolation with 3, 5 and 7 nodes. The function reconstructions are given in Figures 6, 7 and 8 and the iteration input and output data are given in Tables III, IV and V respectively. For 3 and 7 nodes problems, the first eigenvalue $\{\lambda_0\}$ was assumed as data, and for the 5 nodes case, we compare the results for given

Table I. Numerical Example 1 with 3 Nodes

pressure(mmHg)	5	93	130
frequency($\times 10^4$Hz)	4.462	6.9143	7.7945
initial guess 1 (kPa)	1.1	0.8	0.001
initial guess 2 (kPa)	1.3	0.97	0.01
initial guess 3 (kPa)	1.02	0.73	0.01
initial guess 4 (kPa)	0.99	0.71	0.05
true value (kPa)	1.0	0.75	0.0
returned value (kPa)	1.0005	0.7193	0.0423
iteration number	23		
absolute L^2 error	$5.22\text{e}-02$		
$\|\widehat{\tau}_{new} - \widehat{\tau}_{old}\|_{L^2}$	$8.26\text{e}-06$		

Table II. Numerical Example 1 with 5 Nodes

pressure(mmHg)	45	93	120	130	150
frequency($\times 10^4$Hz)(λ_0)	5.6967	6.9143	7.5612	7.7945	8.2512
initial guess 1 (kPa)	1.01	0.8	0.67	0.5	0.001
initial guess 2 (kPa)	0.9	0.85	0.82	0.6	0.001
initial guess 3 (kPa)	0.8	0.75	0.625	0.35	0.002
initial guess 4 (kPa)	1.1	0.9	0.7	0.45	0.01
initial guess 5 (kPa)	1.2	1.01	0.9	0.62	0.003
initial guess 6 (kPa)	0.75	0.65	0.6	0.54	0.001
true value (kPa)	1.0	0.9375	0.75	0.4375	0.0
returned value (kPa)	0.9994	0.9528	0.7994	0.4242	0.0098
iteration number	40				
absolute L^2 error	$5.42\text{e}-02$				
$\|\widehat{\tau}_{new} - \widehat{\tau}_{old}\|_{L^2}$	$5.21\text{e}-06$				

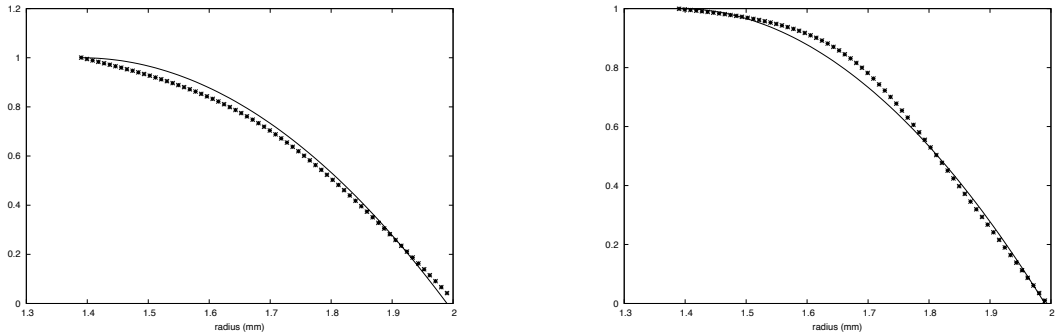

Fig. 5. Reconstruction of Example 1 with 3 Nodes (left figure) and 5 Nodes (right figure)

Table III. Numerical Example 2 with 3 Nodes

pressure(mmHg)	10	93	130
frequency($\times 10^4$Hz)	3.999	6.671	7.5996
initial guess 1 (kPa)	0.01	0.2	0.001
initial guess 2 (kPa)	0.001	0.32	0.01
initial guess 3 (kPa)	0.02	0.22	0.01
initial guess 4 (kPa)	0.01	0.4	0.1
true value (kPa)	0.0	0.25	0.0
returned value (kPa)	-0.02	0.2597	0.01
iteration number	25		
absolute L^2 error	$2.8e-02$		
$\|\widehat{\tau}_{new} - \widehat{\tau}_{old}\|_{L^2}$	$4.86e-06$		

Table IV. Numerical Example 2 with 5 Nodes

pressure(mmHg)	45	93	120	130	150
frequency($\times 10^4$Hz)(λ_0)	5.357	6.671	7.3549	7.5996	8.0762
frequency($\times 10^5$Hz)(λ_1)	1.0709	1.3339	1.4707	1.5197	1.615
initial guess 1 (kPa)	0.001	0.18	0.2	0.18	0.001
initial guess 2 (kPa)	0.01	0.21	0.32	0.21	0.01
initial guess 3 (kPa)	0.002	0.2	0.39	0.2	0.002
initial guess 4 (kPa)	0.01	0.18	0.3	0.18	0.01
initial guess 5 (kPa)	0.001	0.15	0.3	0.15	0.001
initial guess 6 (kPa)	0.955	0.92	0.875	0.71	0.49
true value (kPa)	0.0	0.1875	0.25	0.1875	0.0
returned value (kPa)(with λ_0)	0.0009	0.1876	0.2497	0.1876	0.0009
iteration number	27				
absolute L^2 error	1.3e − 03				
$\|\widehat{\tau}_{new} - \widehat{\tau}_{old}\|_{L^2}$	9.18e − 07				
returned value (kPa) (with λ_0 and λ_1)	-0.0006	0.1876	0.2494	0.1876	-0.0006
iteration number	44				
absolute L^2 error	1.1e − 03				
$\|\widehat{\tau}_{new} - \widehat{\tau}_{old}\|_{L^2}$	9.51e − 06				

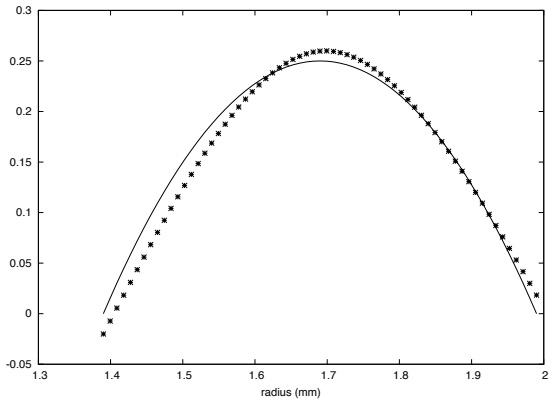

Fig. 6. Reconstruction of Example 2 with 3 Nodes

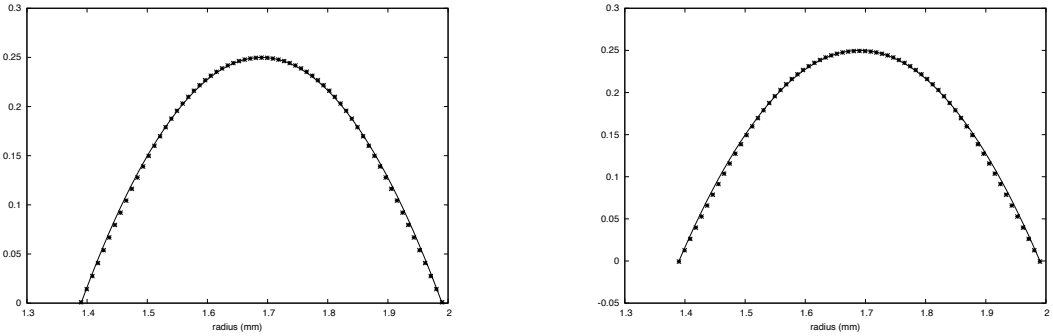

Fig. 7. Reconstruction of Example 2 with 5 Nodes using λ_0 (left figure) and λ_0 and λ_1 (right figure)

Table V. Numerical Example 2 with 7 Nodes

pressure(mmHg)	10	45	93	100	120	130	150
frequency($\times 10^4$Hz)	3.999	5.357	6.671	6.8516	7.3549	7.5996	8.0762
initial guess 1 (kPa)	0.01	0.15	0.28	0.4	0.18	0.14	0.001
initial guess 2 (kPa)	-0.01	0.17	0.25	0.4	0.24	0.12	-0.0001
initial guess 3 (kPa)	-0.01	0.12	0.15	0.27	0.24	0.1	- 0.002
initial guess 4 (kPa)	0.01	0.2	0.3	0.4	0.3	0.19	0.01
initial guess 5 (kPa)	0.0003	0.1	0.25	0.35	0.15	0.17	0.0003
initial guess 6 (kPa)	0.001	0.14	0.22	0.28	0.2	0.2	0.1
initial guess 7 (kPa)	0.1	0.16	0.2	0.275	0.24	0.11	0.001
initial guess 8 (kPa)	0.001	0.175	0.29	0.31	0.26	0.15	0.001
true value (kPa)	0.0	0.1389	0.2222	0.25	0.2222	0.1389	0.0
returned value (kPa)	-0.0004	0.1159	0.2502	0.2477	0.1980	0.1593	0.0039
iteration number	76						
absolute L^2 error	4.83e − 02						
$\|\widehat{\tau}_{new} - \widehat{\tau}_{old}\|_{L^2}$	9.59e − 05						

data $\{\lambda_0\}$ and $\{\lambda_0, \lambda_1\}$ for each blood pressure.

Example 3. The function we want to approximate is $\tau = \sin 2\pi \left(\frac{x-x_0}{x_1-x_0}\right)$. Cubic spline interpolations with 5 and 7 nodes were used and $\{\lambda_0\}$ was assumed to be given. Reconstructions are given in Figure 9 and the iteration input and output data are given in Tables VI and VII.

The numerical examples suggest that the algorithm is only locally convergent and the initial guesses need to be close to the original function. The number of nodes N that gives the most accurate results is specific to the problem and depends on the shape of the function that is being approximated. For instance, for Example 1, $N = 3$ gives a better approximation than $N = 5$ whereas for Example 3, $N = 3$ is not enough

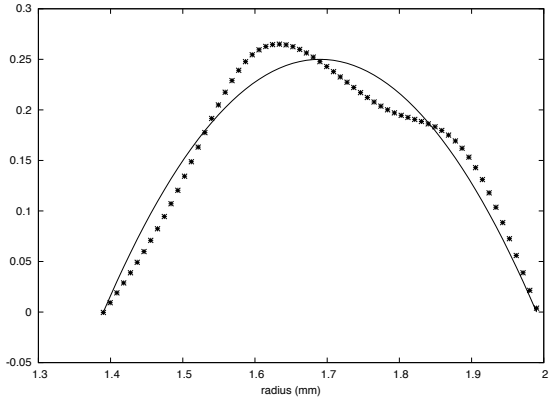

Fig. 8. Reconstruction of Example 2 with 7 Nodes

Table VI. Numerical Example 3 with 5 Nodes

pressure(mmHg)	45	93	120	130	150
frequency($\times 10^4$Hz)(λ_0)	5.3685	6.6819	7.3655	7.61	8.0865
initial guess 1 (kPa)	0.1	1.04	0.002	-0.98	0.001
initial guess 2 (kPa)	-0.0001	0.9	-0.03	-1.02	-0.0001
initial guess 3 (kPa)	-0.002	0.85	-0.02	-1.04	- 0.002
initial guess 4 (kPa)	0.01	1.04	0.003	-0.8	0.01
initial guess 5 (kPa)	0.0003	1.1	0.04	-0.9	0.0003
initial guess 6 (kPa)	0.001	1.15	0.001	-0.9	0.001
true value (kPa)	0.0	1.0	0.0	-1.0	0.0
returned value (kPa)	-0.0028	1.0401	0.0089	-1.0352	0.005
iteration number	49				
absolute L^2 error	$5.44e-02$				
$\|\widehat{\tau}_{new} - \widehat{\tau}_{old}\|_{L^2}$	$1.64e-07$				

Table VII. Numerical Example 3 with 7 Nodes

pressure(mmHg)	10	45	93	100	120	130	150
frequency($\times 10^4$Hz)	3.999	5.3657	6.6794	6.8601	7.3631	7.6077	8.0842
initial guess 1 (kPa)	0.1	0.9	0.98	0.002	-0.98	-0.8	0.001
initial guess 2 (kPa)	-0.0001	0.5	0.6	-0.03	-0.7	-0.82	-0.0001
initial guess 3 (kPa)	-0.002	0.85	0.95	-0.02	-1.04	-0.9	- 0.002
initial guess 4 (kPa)	0.01	0.5	0.89	0.003	-0.8	-1.1	0.01
initial guess 5 (kPa)	0.0003	1.1	0.92	0.04	-0.9	-0.7	0.0003
initial guess 6 (kPa)	0.001	1.15	0.7	0.001	-0.9	-0.9	0.001
initial guess 7 (kPa)	0.1	1.1	1.3	0.001	-0.9	-1.1	0.001
initial guess 8 (kPa)	0.001	1.15	0.7	0.001	-1.1	-0.9	0.001
true value (kPa)	0.0	0.866	0.866	0.0	-0.866	-0.866	0.0
returned value (kPa)	-0.01	1.0044	0.7147	-0.0404	- 0.8508	-1.0114	-0.0038
iteration number	93						
absolute L^2 error	$2.76\text{e}-01$						
$\|\widehat{\tau}_{new} - \widehat{\tau}_{old}\|_{L^2}$	$8.53\text{e}-05$						

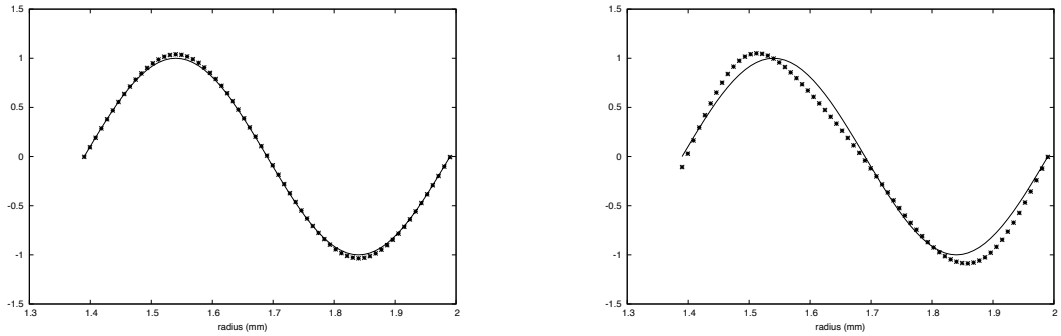

Fig. 9. Reconstruction of Example 3 with 5 Nodes (left figure) and 7 Nodes (right figure)

to predict the shape of the function and hence, the algorithm does not converge. On the other hand, the absolute error for Example 2 and 3 with $N = 5$ is lower than $N = 7$. In addition, observe that the number of iterations increase as N increases for all the examples. This is because choosing more nodes imply solving a larger system of equations that require more initial guesses which may deviate away from the true solution. The above observations suggest that one needs to have an estimation of the shape of the function to select a reasonable N. Although this information might not be available beforehand, one can test for several values of N and choose the smallest one that allows convergence of the algorithm with acceptable accuracy. Table IV of Example 2 also implies that considering the first 2 eigenfrequencies as data does not give a better approximation than considering only the first eigenfrequency as data. In fact, it takes fewer iterations for the latter to converge, suggesting that the lowest eigenfrequency for each of the blood pressure is enough to accurately approximate the function. This feature also makes the algorithm stable since the lowest eigenfrequencies are the easiest to measure with minimum error.

As we see from the above tables, the eigenfrequencies (ω) of the problem that we consider are in the order of 10^4. The actual eigenvalues λ that we compute using SLEPc are in the order of ω^2, that is, 10^8, and they increase with increase in the pressure. In order to avoid using such large numbers that compromises the accuracy of the algorithm, we scale the eigenvalues of the problem. We multiply both sides of 3.1 by a parameter ϵ where $\epsilon << 1$, and compute the scaled eigenvalue $\lambda\epsilon$ instead of the actual eigenvalue λ. This makes the algorithm more robust and the reconstructions more accurate. For the numerical examples above, ϵ was chosen to be 10^{-6}.

The secant method for the inverse spectral problem is not superlinearly convergent like the generalized secant method as suggested in [48]. This is because errors

from several factors of the algorithm accumulate such as the error due to estimating the eigenvalues, the error due to approximating the zero order stretch χ_0 using the shooting method and the error due to approximating $\tau'(x)$ using finite difference schemes.

CHAPTER V

OPTIMIZATION ALGORITHM

In the previous chapter, we developed a method for estimating the residual stress by solving a system of nonlinear equations using various algorithms including the generalized secant method. The advantage of such methods over Newton-like methods is that the Jacobian matrix $f'(y)$ need not be computed. An alternative approach is to formulate the inverse problem of approximating the residual stress $\boldsymbol{\tau}$ as a minimization problem and use least squares techniques. In this chapter, we give a brief introduction to least squares problems and develop an algorithm using such methods to solve the inverse spectral problem.

A. Nonlinear Least Squares Problem

Let $r_1, r_2 \dots r_M$ be M functions of N variables $\boldsymbol{\beta} = (\beta_1, \beta_2 \dots \beta_N)$. Define an objective functional F given by [28]

$$F(\boldsymbol{\beta}) = \frac{1}{2} \sum_{i=1}^{M} |r_i(\boldsymbol{\beta})|^2. \tag{5.1}$$

The vector $\boldsymbol{R} = (r_1, r_2, \dots r_M)$ is called the residual. (5.1) can be rewritten as

$$F(\boldsymbol{\beta}) = \frac{1}{2} \boldsymbol{R}(\boldsymbol{\beta})^T \boldsymbol{R}(\boldsymbol{\beta}) \tag{5.2}$$

where T represents the transpose of a vector. Nonlinear least squares problem involve finding a $\boldsymbol{\beta}^* \in \mathbb{R}^N$ that minimizes $F(\boldsymbol{\beta})$. M is the number of observations and N is the number of unknowns. If $M > N$, the system is overdetermined and if $M < N$, the system is underdetermined. If $M = N$, it is a system of nonlinear equations. We

define the $M \times N$ Jacobian matrix $\boldsymbol{R}'$ of $\boldsymbol{R}$ by

$$[\boldsymbol{R}'(\boldsymbol{\beta})]_{ij} = \frac{\partial r_i}{\partial \beta_j},\ 1 \le i \le M,\ 1 \le j \le N.$$

The gradient of $F(\boldsymbol{\beta}) \in \mathbb{R}^N$ can then be written as

$$\nabla F = \boldsymbol{R}'(\boldsymbol{\beta})^T \boldsymbol{R}(\boldsymbol{\beta}). \tag{5.3}$$

A necessary condition for $\boldsymbol{\beta}^*$ to be a minimizer is

$$\boldsymbol{R}'(\boldsymbol{\beta}^*)^T \boldsymbol{R}(\boldsymbol{\beta}^*) = 0. \tag{5.4}$$

If $\nabla^2 F$ is positive definite, then $\boldsymbol{\beta}^*$ is the unique solution to (5.4). If $\boldsymbol{\beta}$ is close to the minimum, (5.4) can be solved using Newton's method. This is equivalent to solving

$$\nabla^2 F(\boldsymbol{\beta})\boldsymbol{s} = -\nabla F(\boldsymbol{\beta}), \tag{5.5}$$

$$\boldsymbol{\beta}_{k+1} = \boldsymbol{\beta}_k + \boldsymbol{s}. \tag{5.6}$$

In order to solve the above equation, one needs to compute the $N \times N$ Hessian matrix which is given by

$$\nabla^2 F(\boldsymbol{\beta}) = \boldsymbol{R}'(\boldsymbol{\beta})^T \boldsymbol{R}'(\boldsymbol{\beta}) + \sum_{i=1}^{M} r_i(\boldsymbol{\beta})^T \nabla^2 r_i(\boldsymbol{\beta}). \tag{5.7}$$

The second derivative can be rewritten as

$$\sum_{i=1}^{M} r_i(\boldsymbol{\beta})^T \nabla^2 r_i(\boldsymbol{\beta}) = \boldsymbol{R}''(\boldsymbol{\beta})^T \boldsymbol{R}(\boldsymbol{\beta}),$$

where $\boldsymbol{R}''(\boldsymbol{\beta})^T \boldsymbol{R}(\boldsymbol{\beta})$ is a third order tensor such that for any $\boldsymbol{p} \in \mathbb{R}^N$, $\boldsymbol{R}''(\boldsymbol{\beta})^T \boldsymbol{p}$ is a $N \times N$ matrix

$$(\boldsymbol{R}'')^T \boldsymbol{p} = \sum_{i=1}^{N} p_i \nabla^2 r_i.$$

Note that the computation of (5.7) requires the computation of the M Hessians

$\nabla^2 r_i(\boldsymbol{\beta})$. In practice, this is too costly and often not possible to compute analytically. One way to avoid having to compute (5.7) is by using the *Gauss-Newton Iteration* which simply discards the second order term in $\nabla^2 F(\boldsymbol{\beta})$ and approximates the Hessian by

$$\nabla^2 F(\boldsymbol{\beta}) \approx \boldsymbol{R}'(\boldsymbol{\beta})^T \boldsymbol{R}'(\boldsymbol{\beta}). \tag{5.8}$$

Definition 5. Let $f : \mathbb{R}^M \to \mathbb{R}^N$. Then f is said to be Lipschitz continuous if there exists a $\alpha > 0$ such that

$$\|f(x) - f(y)\| \leq \alpha \|x - y\|.$$

Assumption 1. *If $\boldsymbol{\beta}^*$ is a minimizer of $F(\boldsymbol{\beta})$,*

1. *$\boldsymbol{R}$ is Lipschitz continuously differentiable near $\boldsymbol{\beta}^*$.*
2. *$\boldsymbol{R}'(\boldsymbol{\beta}^*)^T \boldsymbol{R}'(\boldsymbol{\beta}^*)$ has maximal rank. This is equivalent to*
   - *$\boldsymbol{R}'(\boldsymbol{\beta}^*)$ is non-singular.*
   - *$\boldsymbol{R}'(\boldsymbol{\beta}^*)$ has full column-rank if $M > N$.*
   - *$\boldsymbol{R}'(\boldsymbol{\beta}^*)$ has full row rank if $M < N$.*

If Assumption 1 holds, the *Gauss-Newton Iteration* step is given by

$$\begin{aligned} \boldsymbol{s} &= -\left(\boldsymbol{R}'(\boldsymbol{\beta}_k)^T \boldsymbol{R}'(\boldsymbol{\beta}_k)\right)^{-1} \nabla F \\ &= -\left(\boldsymbol{R}'(\boldsymbol{\beta}_k)^T \boldsymbol{R}'(\boldsymbol{\beta}_k)\right)^{-1} \boldsymbol{R}'(\boldsymbol{\beta}_k)^T \boldsymbol{R}(\boldsymbol{\beta}_k). \end{aligned} \tag{5.9}$$

It is clear that $\boldsymbol{R}'(\boldsymbol{\beta}_k)^T \boldsymbol{R}'(\boldsymbol{\beta}_k)$ is symmetric and positive definite. Observe that the second order term in (5.7) vanishes for zero residual problems where $F(\boldsymbol{\beta}^*)$ is zero, and can be negligible for small residual problems where $F(\boldsymbol{\beta}^*)$ is small, or for problems with very small $\boldsymbol{R}''(\boldsymbol{\beta})$. Hence, the Gauss Newton iteration converges well for zero residual problems or small residual problems with good initial data. Moreover, the rate of convergence for small residual problems is q-quadratic [28]. For a large residual

problem, convergence can be fast if the problem is not very nonlinear, that is, if $\boldsymbol{R}''(\boldsymbol{\beta})$ is small.

B. Line Search Algorithms

Definition 6. Let $\boldsymbol{d} \in \mathbb{R}^N$. $\boldsymbol{d}$ is a descent direction for F at $\boldsymbol{\beta}$ if

$$\left.\frac{dF(\boldsymbol{\beta} + t\boldsymbol{d})}{dt}\right|_{t=0} = \nabla F(\boldsymbol{\beta})^T \boldsymbol{d} < 0.$$

A line search algorithm is an algorithm that searches for decrease in the objective functional F in the descent direction $\boldsymbol{d}$ by controlling the step length of the iteration [5, 28, 36]. The step length is controlled such that there is *sufficient decrease* in F. The general *sufficient decrease* condition is

$$F(\boldsymbol{\beta}_k + \eta_k \boldsymbol{d}) - F(\boldsymbol{\beta}_k) < \theta \eta_k \nabla F(\boldsymbol{\beta}_k)^T \boldsymbol{d} < 0. \tag{5.10}$$

Here $\theta \in (0, 1)$ is an algorithm parameter. The goal is to find a parameter η_k in each iteration such that (5.10) is satisfied. The iterate is then updated as

$$\boldsymbol{\beta}_{k+1} = \boldsymbol{\beta}_k + \eta_k \boldsymbol{d}. \tag{5.11}$$

One way to find the step length η_k is using the Armijo rule [2]. For fixed k, let $\eta_k = \xi^j$, where $\xi \in (0, 1)$ and $j \in \mathbb{Z}^+$. Fix ξ and find the smallest j such that (5.10) is satisfied. This strategy of repeatedly finding sufficient decrease in F and updating the step size if (5.10) fails is also called *backtracking*.

An example of a line search method is the *method of steepest descent* where the iteration is updated by

$$\boldsymbol{\beta}_{k+1} = \boldsymbol{\beta}_k - \eta_k \nabla F(\boldsymbol{\beta}_k).$$

Clearly, $\boldsymbol{d} = -\nabla F(\boldsymbol{\beta}_k)$ is a descent direction. Although the steepest descent method

is very easy to implement, the local convergence of such methods is very poor [28]. The *method of steepest descent* is often combined with a good locally convergent scheme such as the Newton's Method or the Gauss-Newton method to get good convergence properties.

Recall that the Gauss Newton direction is given by

$$\boldsymbol{d}_k = -\left(\boldsymbol{R}'(\boldsymbol{\beta}_k)^T \boldsymbol{R}'(\boldsymbol{\beta}_k)\right)^{-1} \boldsymbol{R}'(\boldsymbol{\beta}_k)^T \boldsymbol{R}(\boldsymbol{\beta}_k). \tag{5.12}$$

If Assumption 1 holds, then $\left(\boldsymbol{R}'(\boldsymbol{\beta}_k)^T \boldsymbol{R}'(\boldsymbol{\beta}_k)\right)$ is positive definite, and hence,

$$\boldsymbol{d}_k^T \nabla F(\boldsymbol{\beta}_k) = -\left(\boldsymbol{R}'(\boldsymbol{\beta}_k)^T \boldsymbol{R}(\boldsymbol{\beta}_k)\right)^T \left(\boldsymbol{R}'(\boldsymbol{\beta}_k)^T \boldsymbol{R}'(\boldsymbol{\beta}_k)\right)^{-1} \boldsymbol{R}'(\boldsymbol{\beta}_k)^T \boldsymbol{R}(\boldsymbol{\beta}_k) < 0 \tag{5.13}$$

and the Gauss Newton direction is a descent direction. The Armijo rule can also be combined with the Gauss Newton method, and the method is called the *damped Gauss Newton* method.

Lemma 3. *Let $\nabla F(\boldsymbol{\beta})$ be Lipschitz continuous with Lipschitz constant L. Let $\boldsymbol{\beta}_k$ be the damped Gauss Newton iteration with the steps*

$$\boldsymbol{s}_k = \boldsymbol{\beta}_{k+1} - \boldsymbol{\beta}_k = \eta_k \boldsymbol{d}_k = \eta_k \boldsymbol{H}_k^{-1} \nabla F(\boldsymbol{\beta}_k), \tag{5.14}$$

and $\boldsymbol{H}_k = \boldsymbol{R}'(\boldsymbol{\beta}_k)^T \boldsymbol{R}'(\boldsymbol{\beta}_k)$ at each iteration k. Let $\kappa(\boldsymbol{H}_k)$ denote the condition number $\boldsymbol{H}_k$ such that

$$\kappa(\boldsymbol{H}_k) = \frac{\lambda_{max}}{\lambda_{min}} \leq \hat{\kappa},$$

where λ_{min} and λ_{max} are the smallest and the largest eigenvalues of $\boldsymbol{H}_k$ respectively. Then

$$\eta_k \geq \hat{\eta} = \frac{2\xi\lambda_{min}(1-\theta)}{L\hat{\kappa}} \tag{5.15}$$

and the maximum number of stepsize reductions is

$$j = \frac{log\left(\frac{2\lambda_{min}(1-\theta)}{L\hat{\kappa}}\right)}{log(\nu)}. \tag{5.16}$$

The above lemma implies that the the sufficient decrease condition (5.10) can be satisfied in finitely many steps for all k and the step lengths are bounded away from zero. It also holds for other line search methods such as the Levenberg-Marquardt algorithm that is described below [28].

Theorem 6. *Let the assumptions from Lemma 3 hold and let* $\|\boldsymbol{R}'\|$ [1] *be uniformly bounded for all* k*. Then either* $F(\boldsymbol{\beta}_k)$ *is unbounded from below or*

$$\lim_{k\to\infty} \nabla F(\boldsymbol{\beta}_k) = 0 \tag{5.17}$$

and hence, any limit point of the sequence of iterates $\{\boldsymbol{\beta}_k\}$ *produced by the damped Gauss Newton Method is a stationary point. Moreover, the stationary point is a minimum.*

Theorem 6 (Theorem 3.2.4 [28]) says that if the condition numbers of $\boldsymbol{H}_k$ and the norm of the iterates remain bounded, then there will be a limit point. However, uniqueness of the limit point is not guaranteed. In order for Theorem 6 to hold, the matrices $\boldsymbol{H}_k$ need not only be non-singular, but also must be well-conditioned and uniformly bounded, which are strong assumptions. One way to guarantee these conditions are satisfied is by regularizing the matrices $\boldsymbol{H}_k$. The *Levenberg-Marquardt*

[1] *In this chapter, we use the Euclidean norm* $\|\boldsymbol{x}\| = \sqrt{\sum_{i=1}^{N} (x_i)^2}$ *if* $\boldsymbol{x} \in \mathbb{R}^N$*. When we refer to a matrix norm, we will mean the matrix norm induced by the Euclidean norm given by*

$$\|\boldsymbol{A}\| = \max_{\boldsymbol{x}\neq 0} \frac{\|\boldsymbol{A}\boldsymbol{x}\|}{\|\boldsymbol{x}\|}.$$

method [34] adds a regularization parameter $\gamma > 0$ to $\boldsymbol{R}'(\boldsymbol{\beta}_k)^T\boldsymbol{R}'(\boldsymbol{\beta}_k)$ to obtain

$$\boldsymbol{H}_k = \gamma_k \boldsymbol{I} + \boldsymbol{R}'(\boldsymbol{\beta}_k)^T\boldsymbol{R}'(\boldsymbol{\beta}_k), \tag{5.18}$$

where I is the $N \times N$ Identity matrix and γ is called the Levenberg-Marquardt parameter. The iteration is then given by

$$\begin{aligned} \boldsymbol{\beta}_{k+1} &= \boldsymbol{\beta}_k + \boldsymbol{d}_k, & (5.19)\\ \boldsymbol{d}_k &= -\left(\boldsymbol{H}_k\right)^{-1}\boldsymbol{R}'(\boldsymbol{\beta}_k)^T\boldsymbol{R}(\boldsymbol{\beta}_k). & (5.20) \end{aligned}$$

Note that the matrix $\gamma_k \boldsymbol{I} + \boldsymbol{R}'(\boldsymbol{\beta}_k)^T\boldsymbol{R}'(\boldsymbol{\beta}_k)$ is symmetric and positive definite. The parameter γ is chosen such that the $\gamma_k \boldsymbol{I} + \boldsymbol{R}'(\boldsymbol{\beta}_k)^T\boldsymbol{R}'(\boldsymbol{\beta}_k)$ is well conditioned. The *Levenberg-Marquardt* method can be combined with the Armijo rule, that is, find η_k such that (5.10) is satisfied where $\boldsymbol{d}_k$ is given by (5.20), and update the iteration using (5.14). This method is called the *Levenberg-Marquardt-Armijo* algorithm. The following theorem is a special case of Theorem 6 applied to the *Levenberg-Marquardt-Armijo* method [28].

Theorem 7. *Let $\boldsymbol{R}'(\boldsymbol{\beta})$ be Lipschitz continuous. Let $\boldsymbol{\beta}_k$ be the Levenberg-Marquardt-Armijo iteration with the steps*

$$\boldsymbol{d}_k = \boldsymbol{\beta}_{k+1} - \boldsymbol{\beta}_k = -\eta_k \boldsymbol{H}_k^{-1}\nabla F(\boldsymbol{\beta}_k),$$

where $\boldsymbol{H}_k = \gamma_k \boldsymbol{I} + \boldsymbol{R}'(\boldsymbol{\beta}_k)^T\boldsymbol{R}'(\boldsymbol{\beta}_k)$. Assume that $\|\boldsymbol{R}'\|$ be uniformly bounded for all k and γ_k is chosen such that $\kappa(\boldsymbol{H}_k)$ is bounded. Then

$$\lim_{k\to\infty} \nabla F(\boldsymbol{\beta}_k) = \lim_{k\to\infty} \boldsymbol{R}'(\boldsymbol{\beta})\boldsymbol{R}(\boldsymbol{\beta}) = 0. \tag{5.21}$$

Moreover, if $\boldsymbol{\beta}^*$ is a limit point of $\{\boldsymbol{\beta}_k\}$ such that $\boldsymbol{R}(\boldsymbol{\beta}^*) = 0$, $\boldsymbol{R}'(\boldsymbol{\beta}_k)^T\boldsymbol{R}'(\boldsymbol{\beta}_k)$ has maximal rank and $\gamma_k \to 0$, then $\boldsymbol{\beta}_k \to \boldsymbol{\beta}^*$ q superlinearly. If $\gamma_k = O\left(\|\boldsymbol{R}(\boldsymbol{\beta}_k)\|\right)$ as

$k \to \infty$, then the convergence is q-quadratic.

The Levenberg-Marquardt method can be thought of as the combination of steepest descent method and the Gauss Newton method. Both of these methods have complimentary properties and the Levenberg-Marquardt method is designed to take advantage of both the methods. When γ_k is large, the first term in $\boldsymbol{H}_k$ dominates and the method behaves like the steepest descent method, and as γ_k decreases, it behaves like the Gauss Newton method. Since the steepest descent method exhibits good global convergence and slower local convergence, γ_k is chosen to be large when $\boldsymbol{\beta}_k$ is further away from the minimum. γ_k is gradually decreased as the iterate gets closer to the minimum so that the iteration behaves like the Gauss Newton method. The above algorithm has the disadvantage that if the value of γ_k is large, the calculated Hessian $\boldsymbol{H}_k$ is not used at all. Marquardt proposed to replace the Identity matrix in (5.18) with the diagonal of the Hessian resulting in

$$\boldsymbol{H}_k = \gamma_k \, diag\,[\boldsymbol{R}'(\boldsymbol{\beta}_k)^T \boldsymbol{R}'(\boldsymbol{\beta}_k)] + \boldsymbol{R}'(\boldsymbol{\beta}_k)^T \boldsymbol{R}'(\boldsymbol{\beta}_k), \tag{5.22}$$

$$\boldsymbol{d}_k = -\boldsymbol{H}_k^{-1} \boldsymbol{R}'(\boldsymbol{\beta}_k)^T \boldsymbol{R}(\boldsymbol{\beta}_k). \tag{5.23}$$

Since the Hessian is a measure of the curvature of $F(\boldsymbol{\beta})$, (5.22)–(5.23) implies that the iteration takes a large step in the direction with low curvature (an almost flat region) and a small step in the direction with high curvature (a steep incline). There are several approaches to find the parameter γ_k [28, 34]. The first parameter γ_0 is found using a trial and error method and the rest of the γ_k's are found using

$$\gamma_k = \min\{1, \|\boldsymbol{R}(\boldsymbol{\beta}_k)\|^{\delta}\},$$

where $\delta \in (0, 2)$. This is an appropriate choice because clearly, the residual $\|\boldsymbol{R}(\boldsymbol{\beta}_k)\|$ decreases with the iteration number by the way we constructed the algorithm.

Another important aspect of developing algorithms is the termination of the iteration. Let $\boldsymbol{e} = (\boldsymbol{\beta} - \boldsymbol{\beta}^*)$, where $\boldsymbol{\beta}^*$ is the minimizer of (5.1). If Assumption 1 holds, then for any gradient based iterative method, termination on small gradients is reasonable [27]. This is because if the Hessian $\nabla^2 F(\boldsymbol{\beta}^*)$ is well-conditioned, then the gradient norm and the error norm are equivalent, that is,

$$c_1\|e\| \leq \|\nabla F(\boldsymbol{\beta})\| \leq c_2\|e\|, \tag{5.24}$$

where c_1 and c_2 are constants. Hence, a natural termination condition would be

$$\|\nabla F(\boldsymbol{\beta}_k)\| \leq t_r\|\nabla F(\boldsymbol{\beta}_0)\|. \tag{5.25}$$

If the initial iterate $\boldsymbol{\beta}_0$ is close to the solution, then depending on t_r, (5.25) may be difficult to satisfy and the iteration may not terminate at all. Hence, we add an absolute measure t_a and terminate the iteration when

$$\|\nabla F(\boldsymbol{\beta}_k)\| \leq t_r\|\nabla F(\boldsymbol{\beta}_0)\| + t_a. \tag{5.26}$$

Here, t_r and t_a are given tolerances and varies with the problem.

C. Least Squares Algorithm for the Inverse Spectral Problem

In this section, we develop a least squares algorithm for the inverse spectral problem described in Chapter III of estimating the residual stress $\boldsymbol{\tau}$ from the spectral data of a system of boundary value problems that correspond to different blood pressures π occurring during a cardiac cycle. We first formulate the least squares problem and then make use of the algorithms described in Chapter IV and the least squares methods described in the previous section to reconstruct $\boldsymbol{\tau}$.

Suppose we are given the spectral data for m blood pressures $\pi_1, \pi_2 \ldots \pi_m$ and

for each π_i, the first n eigenfrequencies are given. Consider the functional

$$D(\boldsymbol{\tau}) = \frac{1}{2}\sum_{i=1}^{m}\sum_{j=1}^{n}|\lambda_{\pi_i}^{j}(\boldsymbol{\tau}) - \tilde{\lambda}_{\pi_i}^{j}|^2 = \frac{1}{2}\sum_{k=1}^{m*n}|\lambda_k(\boldsymbol{\tau}) - \tilde{\lambda}_k|^2, \tag{5.27}$$

where $\tilde{\lambda}_{\pi_i}^{j}$ is the j^{th} eigenfrequency corresponding to the pressure π_i obtained from IVUS, and $\{\lambda_{\pi_i}^{j}(\boldsymbol{\tau})\}$ are the eigenvalues achieved from the model. Recall that the goal is to reconstruct the residual stress $\boldsymbol{\tau} = \boldsymbol{\tau}(x)$ from the IVUS eigenfrequencies. We assume that $\boldsymbol{\tau}$ is continuously differentiable and approximate it using cubic spline interpolation. Just as in the algorithm developed in Chapter IV, the optimization algorithm estimates $\boldsymbol{\tau} = \tau_1, \tau_2 \ldots \tau_N$ at the nodal points $x_1, x_2 \ldots x_N$ and the function is approximated using cubic splines. It is evident that F cannot completely vanish since the eigenfrequencies obtained from experiments contain noise and the eigenfrequencies that are achieved from the algorithm contain numerical and round-off errors, and hence, they cannot be equal. The best one can do is to find a $\boldsymbol{\tau}$ that minimizes $D(\boldsymbol{\tau})$. Note that the functional $D(\boldsymbol{\tau})$ is similar to the functional described in (5.1). It is also important to note that the least squares problem (5.27) is non-linear. Moreover, it is different from the usual non-linear least squares problems due to the fact that the quantities $\{\lambda_{\pi_i}^{j}(\boldsymbol{\tau})\}$ are not defined explicitly but only implicitly as a solution to the eigenvalue problem (3.1). As a result, it does not have an analytical expression and its evaluation relies on numerical methods.

The advantage of least squares method over methods for non-linear equations is that one can overestimate the number of eigenvalues and solve the overdetermined problem to achieve more accuracy. To that end, we assume that the total number of eigenfrequencies $M = m * n$ is greater than or equal to the number of unknowns N. Define $\boldsymbol{R} \in \mathbb{R}^M$

$$\boldsymbol{R}(\boldsymbol{\tau}) = \left(\lambda_k(\boldsymbol{\tau}) - \tilde{\lambda}_k\right). \tag{5.28}$$

Then (5.27) can be rewritten as

$$D(\boldsymbol{\tau}) = \frac{1}{2}\boldsymbol{R}(\boldsymbol{\tau})^T\boldsymbol{R}(\boldsymbol{\tau}). \tag{5.29}$$

Note that by Proposition 1, $\lambda_k(\boldsymbol{\tau})$ is continuously differentiable with respect to $\boldsymbol{\tau}$, and hence, $R(\boldsymbol{\tau})$ is continuously differentiable with respect to $\boldsymbol{\tau}$. The gradient of $D(\boldsymbol{\tau}) \in \mathbb{R}^N$ can then be written as

$$\nabla D(\boldsymbol{\tau}) = \boldsymbol{R}'(\boldsymbol{\tau})^T\boldsymbol{R}(\boldsymbol{\tau}) \tag{5.30}$$

and the Hessian is approximated as

$$\nabla^2 D(\boldsymbol{\tau}) \approx \boldsymbol{R}'(\boldsymbol{\tau})^T\boldsymbol{R}'(\boldsymbol{\tau}), \tag{5.31}$$

where $R'(\boldsymbol{\tau}) \in \mathbb{R}^{M\times N}$ is the Jacobian matrix

$$[\boldsymbol{R}'(\boldsymbol{\tau})]_{ij} = \frac{\partial\lambda_i(\boldsymbol{\tau})}{\partial\tau_j},\ 1 \le i \le M,\ 1 \le j \le N. \tag{5.32}$$

Provided that $\boldsymbol{R}(\boldsymbol{\tau})$ has maximal column rank, we can adopt the gradient based algorithms such as damped Gauss-Newton Method and Levenberg-Marquardt-Armijo method described above to solve the minimization problem. Note that $\boldsymbol{R}'(\boldsymbol{\tau})$ and hence $\nabla D(\boldsymbol{\tau})$ do not have an analytical expression and can only be solved numerically. Due to this, the rank condition needs to be checked separately for each problem. $\boldsymbol{R}'(\boldsymbol{\tau})$ is approximated using the directional derivative. Let $\boldsymbol{u}$ be a unit vector in $\mathbb{R}^N$. Then the approximated directional derivative along $\boldsymbol{u}$ is given by

$$\nabla_u\boldsymbol{R}(\boldsymbol{\tau}) = \frac{\boldsymbol{R}(\boldsymbol{\tau}+\epsilon\boldsymbol{u}) - \boldsymbol{R}(\boldsymbol{\tau})}{\epsilon} \tag{5.33}$$

where ϵ is a small number. Then $\boldsymbol{R}'(\boldsymbol{\tau})$ is the unique $M \times N$ matrix such that

$$\nabla_u\boldsymbol{R}(\boldsymbol{\tau}) = \boldsymbol{R}'(\boldsymbol{\tau})\boldsymbol{u}, \quad \forall\boldsymbol{u} \in \mathbb{R}^N. \tag{5.34}$$

In order to solve the least squares problem, an initial guess for $\boldsymbol{\tau}$, $\boldsymbol{\tau}^{(0)} = \tau_1^0, \tau_2^0 \dots \tau_N^0$ is required for the iteration to execute. The corresponding cubic spline interpolation $\boldsymbol{\tau}^{(0)}(x)$ of $\boldsymbol{\tau}^{(0)}$ is calculated and used to approximate $\boldsymbol{\tau}'(x)$ using the central difference scheme given in (4.21) since the static problem (2.94)–(2.96) and the eigenvalue problem (2.109)–(2.111) for Model Problem II both depend on $\boldsymbol{\tau}'(x)$. For each π_i, we use the initial guess to find the solution $\chi_0(\boldsymbol{\tau}, x)$ from (2.94)–(2.96) using the shooting method described in Chapter IV. Then substitute $\chi_0(\boldsymbol{\tau}, x)$, $\boldsymbol{\tau}(x)$, $\boldsymbol{\tau}'(x)$ and blood pressure π_j into (2.109)–(2.111), and use the Eigenspectrum solver described in Chapter IV to find a sequence of eigenvalues $\{\lambda_{\pi_i}^j(\boldsymbol{\tau})\}_{j=0}^n$ for each π_i. We then use the damped Gauss-Newton Method or the Levenberg-Marquardt-Armijo method to find a $\boldsymbol{\tau}$ that minimizes D.

The detailed algorithm is given as follows:

Algorithm 2.

1. Let the iteration number be k. Set $k = 0$. Provide an initial guess $\boldsymbol{\tau}^{(k)} = (\tau_1^{(k)}, \tau_2^{(k)}, ...\tau_N^{(k)})$ for $\boldsymbol{\tau}$, and find the cubic spline interpolation function for $\boldsymbol{\tau}^{(k)}$. Note that the initial guess is required to be close enough to the true solution.
2. Find the numerical derivative $\boldsymbol{\tau}'^{(k)}$ of $\boldsymbol{\tau}^{(k)}$ using (4.21).
3. For each blood pressure π_i, where $1 \leq i \leq N$, find the numerical solution $\chi_0^{(i)}(x, \boldsymbol{\tau}^{(k)}, \boldsymbol{\tau}'^{(k)})$ from (2.64) for Model Problem I and (2.94)–(2.96) for Model Problem II. The secant method and the shooting methods described in Chapter IV are used for solving the boundary value problems. Note that for Model Problem I, simply use the secant method to find $\chi_0^{(i)}(x)$, since χ_0 does not depend on $\boldsymbol{\tau}$.
4. Substitute $\chi_0^{(i)}\left(x, \boldsymbol{\tau}^{(k)}, \boldsymbol{\tau}'^{(k)}\right)$, $\boldsymbol{\tau}^{(k)}$, $\boldsymbol{\tau}'^{(k)}$ and π_i into (2.79)–(2.81) and (2.109)–(2.111) to find the first n eigenvalues for the SLP (3.1) for each i and denote it

as $\lambda_{\pi_i}^{(j)}(\boldsymbol{\tau}^{(k)}),\ j = 1 \ldots n$.

5. Substitute $\lambda_{\pi_i}^{(j)}(\boldsymbol{\tau}^{(k)})$ into (5.28) to get $\boldsymbol{R}(\boldsymbol{\tau}^{(k)})$. Using this and (5.33)–(5.34), find $\boldsymbol{R}'(\boldsymbol{\tau}^{(k)})$.

6. Find the gradient $\nabla D(\boldsymbol{\tau}^{(k)})$ and the Hessian $\nabla^2 D(\boldsymbol{\tau}^{(k)})$ using (5.30) and (5.31) respectively.

7. Depending on the algorithm that is used, find $\boldsymbol{d} = \boldsymbol{d}_k$ using (5.12), (5.18)–(5.20) or (5.22)–(5.23).

8. Find the residual $D(\boldsymbol{\tau}^{(k)})$ and the gradient norm $\|\nabla D(\boldsymbol{\tau}^{(k)})\|$.

9. If the Levenberg-Marquardt-Armijo method is used, then choose a $\delta \in (0, 2)$, and let $\gamma_k = \min\{1, \|\boldsymbol{R}\|^{\delta}\}$.

10. Fix a parameter $\xi \in (0, 1)$, say 0.5 and find the step length η_k such that

$$D(\boldsymbol{\tau}^{(k)} + \eta_k \boldsymbol{d}_k) - D(\boldsymbol{\tau}^{(k)}) < \theta \eta_k \nabla D(\boldsymbol{\tau}^{(k)})^T \boldsymbol{d}_k < 0. \tag{5.35}$$

11. Update $\boldsymbol{\tau}$ using $\boldsymbol{\tau}^{(k+1)} = \boldsymbol{\tau}^{(k)} + \eta_k \boldsymbol{d}_k$.

12. Fix tolerances t_r and t_a. Repeat Steps 1 – 11 until

$$\|\nabla D(\boldsymbol{\tau}^{(k)})\| \leq t_r \|\nabla F(\boldsymbol{\tau}^{(0)})\| + t_a. \tag{5.36}$$

1. Convergence

Theorem 8. *Let $\boldsymbol{\tau}_k := \boldsymbol{\tau}^{(k)}$ be the Levenberg-Marquardt-Armijo iterates of the least squares problem with the iteration step given by* (5.22)–(5.23). *Assume that $\boldsymbol{R}'(\boldsymbol{\tau}_k)$ is nonsingular, $\|\boldsymbol{R}'(\boldsymbol{\tau}_k)\|$ is uniformly bounded and*

$$\gamma_k = min(1, \|\boldsymbol{R}(\boldsymbol{\tau}_k)\|). \tag{5.37}$$

Then if $D(\boldsymbol{\tau}_k)$ is bounded from below,

$$\lim_{k\to\infty} \nabla D(\boldsymbol{\tau}_k) = 0 \tag{5.38}$$

and hence, any limit point $\boldsymbol{\tau}^*$ such that

$$\boldsymbol{\tau}^* = \lim_{k\to\infty} \boldsymbol{\tau}_k \tag{5.39}$$

is a stationary point. Furthermore, the stationary point is a minimum.

Proof. Since λ is continuously differentiable with respect to $\boldsymbol{\tau}$ by Proposition 1, $\boldsymbol{R}'(\boldsymbol{\tau}) = \frac{\partial \lambda}{\partial \boldsymbol{\tau}}$ is continuous. Also, since $\boldsymbol{R}'(\boldsymbol{\tau})$ is nonsingular, $\kappa\left(\boldsymbol{R}'(\boldsymbol{\tau}_k)^T \boldsymbol{R}'(\boldsymbol{\tau}_k)\right)$ is bounded. Furthermore, for the particular choice of γ_k given in (5.37), $\kappa(\boldsymbol{H}_k)$ is also bounded, that is

$$\kappa\left(\gamma_k \, diag\left[\boldsymbol{R}'(\boldsymbol{\tau}_k)^T \boldsymbol{R}'(\boldsymbol{\tau}_k)\right] + \boldsymbol{R}'(\boldsymbol{\tau}_k)^T \boldsymbol{R}'(\boldsymbol{\tau}_k)\right) \leq \hat{\kappa}.$$

Then Lemma 3 holds and the parameter η_k appearing in (5.35) satisfies (5.15). Now since $\|\boldsymbol{R}'(\boldsymbol{\tau}_k)\|$ is uniformly bounded,

$$\|\boldsymbol{R}'(\boldsymbol{\tau}_k)\| \leq \tilde{C}_1, \quad \text{for all } k.$$

Then,

$$\|\boldsymbol{H}_k\| = \|\gamma_k \, diag\left[\boldsymbol{R}'(\boldsymbol{\tau}_k)^T \boldsymbol{R}'(\boldsymbol{\tau}_k)\right] + \boldsymbol{R}'(\boldsymbol{\tau}_k)^T \boldsymbol{R}'(\boldsymbol{\tau}_k)\| \leq \tilde{C}_2 + \tilde{C}_1^2 \leq \tilde{C}_3.$$

Here, we use the fact that $\|\boldsymbol{R}'(\boldsymbol{\tau}_k)\| = \|\boldsymbol{R}'(\boldsymbol{\tau}_k)^T\|$ for the matrix norm induced by the Euclidean norm. Now, $D(\boldsymbol{\tau}_k)$ is a decreasing sequence by construction, and if it is bounded from below, $D(\boldsymbol{\tau}_k)$ converges and

$$\lim_{k\to\infty} D(\boldsymbol{\tau}_k) - D(\boldsymbol{\tau}_{k+1}) = 0. \tag{5.40}$$

Now by (5.10), (5.22) and (5.23),

$$\begin{aligned} D(\boldsymbol{\tau}_{k+1}) - D(\boldsymbol{\tau}_k) &< -\theta\eta_k \nabla D(\boldsymbol{\tau}_k)^T \boldsymbol{H}_k^{-1} \nabla D(\boldsymbol{\tau}_k) \\ &\leq -\theta\hat{\eta}\tilde{C}_3^{-1} \|\nabla D(\boldsymbol{\tau}_k)\|^2 \leq 0. \end{aligned}$$

Hence, by (5.40),

$$\|\nabla D(\boldsymbol{\tau}_k)\|^2 \leq \frac{\tilde{C}_3(D(\boldsymbol{\tau}_k) - D(\boldsymbol{\tau}_{k+1}))}{\theta\hat{\eta}} \to 0.$$

The fact that any limit point $\boldsymbol{\tau}^*$ is a minimum is clear from the fact that $\boldsymbol{H}_k$ is symmetric and positive-definite. □

Remark 4. We remark that although Theorem 8 states global convergence of the scheme, the functional (5.27) that we are interested in minimizing has multiple local minima. Due to this, the results of the iteration depend on the choice of the initial guess, and thus, we require the initial guess be close enough to the true solution. To demonstrate that the problem has multiple local minima, we consider the following two examples:

Consider Model Problem II and let $\boldsymbol{\tau} = (\tau^1, \tau^2) \in [0,1] \times [0,1]$ and the original function be $\tilde{\boldsymbol{\tau}} = (0.45, 0.67)$. In the first example, we consider the first eigenvalue $\{\lambda^0_{\pi_i}\}$ for four blood pressures 45 mmHg, 93 mmHg, 100 mmHg and 120 mmHg. The $\{\tilde{\lambda}^0_{\pi_i}\}_{i=1}^4$ are assumed to be given and $D(\boldsymbol{\tau})$ is plotted as a function of τ^1 and τ^2. (See Figure 10a).

In the second example, we consider the first three eigenvalues $\{\lambda^0_{\pi_i}, \lambda^1_{\pi_i}, \lambda^2_{\pi_i}\}$ for eight blood pressures 30mmHg, 45 mmHg, 54 mmHg, 93 mmHg, 100 mmHg, 120 mmHg, 130 mmHg and 150 mmHg. The $\{\lambda^0_{\pi_i}, \lambda^1_{\pi_i}, \lambda^2_{\pi_i}\}_{i=1}^8$ are assumed to be given and $D(\boldsymbol{\tau})$ is plotted as a function of τ^1 and τ^2 (See Figure 10b).

In Figure 10, we see that the multiple local minima of the objective functional

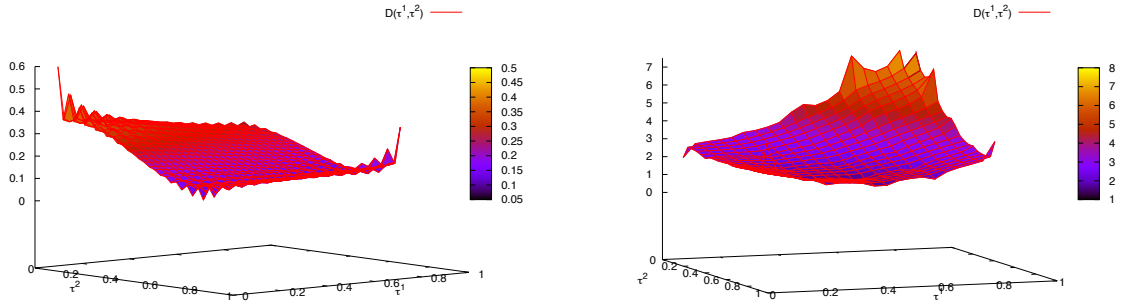

(a) First Eigenfrequency with $i = 4$ (b) First 3 Eigenfrequencies with $i = 8$

Fig. 10. Plot of $D(\boldsymbol{\tau})$ Showing Multiple Local Minima

$D(\boldsymbol{\tau})$ are very close to one another. This feature makes the inverse problem very ill-posed, and finding the true minima becomes very challenging. In order to get an accurate enough solution, the initial guess for the gradient based methods need to be close to the true solution. Also, note that the minima are further apart for a larger number of given eigenfrequencies. Thus, one can increase the accuracy of reconstruction of the residual stress by considering a higher number of eigenfrequencies from various blood pressures.

D. Numerical Examples

In this section, we present numerical simulations for Model Problems I and II of reconstructing several residual stresses $\boldsymbol{\tau}$ using the algorithms described in Section B and C and compare the results for different parameters. The values of other parameters involved in the model such as ρ, μ, ν, the stretches λ_0, η_0, α_0, and the inner and outer radii are chosen to be the same as in Chapter IV Section D. The Levenberg-Marquardt parameter is chosen as in (5.37), $\xi = 0.5$ and $\theta = 1.0 \times 10^{-3}$. The true value $\boldsymbol{\tau}_{true}$ and the returned value $\boldsymbol{\tau}_{final}$ of $\boldsymbol{\tau}$ at each node is given along with the

L^2 absolute error $\|\boldsymbol{\tau}_{true} - \boldsymbol{\tau}_{final}\|_{L^2}$ and the L^2 norm of the gradient $\nabla \boldsymbol{D}(\boldsymbol{\tau})$. A corresponding plot of the true $\boldsymbol{\tau}$ and the iterated $\boldsymbol{\tau}$ for each table is presented. Note that in the figures, the solid line represents the true $\boldsymbol{\tau}$ and the dotted line represents the iterated $\boldsymbol{\tau}$.

1. Model Problem I

Example 4. The function we want to approximate is $\boldsymbol{\tau} = 1 - \left(\frac{x-x_0}{x_1-x_0}\right)^2$ and we use the cubic spline interpolation of the function at 4 nodes. The initial guess is taken to be $(-0.03, 0.1, 0.12, -0.02)$. Table VIII shows the input and output for the iterations given the first eigenvalue $\{\lambda^0\}$ of 4 blood pressures, $\{45, 93, 100, 120\}$ mmHg, and 10 blood pressures, $\{30, 45, 54, 75, 93, 100, 105, 120, 130, 150\}$ mmHg, and the reconstructions are shown in Figure 11. Note that reconstructing the function with $\{\lambda^0\}$ of 4 blood pressures is equivalent to solving a system of nonlinear equations, and it already gives a sufficiently accurate estimation for this particular model problem given that the initial guess is close to the solution. Although the reconstruction is only slightly better with 10 blood pressures than with 4, the number of iterations required for the algorithm to converge is lower in this case.

For the next two examples, consider 10 blood pressures, $\{30, 45, 54, 75, 93, 100, 105, 120, 130, 150\}$ mmHg. In Table IX, we show the results for Example 4 with an initial guess far away from the true function, and plot the reconstruction in Figure 12. Two eigenvalues $\{\lambda^0, \lambda^1\}$ for each blood pressures is taken as data. This example shows that a high number of iterations is a trade off for higher accuracy. It is important to note that despite the existence of multiple local minima, the algorithm converges to the true solution for this particular choice of the initial guess. Next we take an initial guess further away from the solution and two cases, first with $\{\lambda^0\}$ given for each blood pressures, and second with $\{\lambda^0, \lambda^1\}$ given for each blood pres-

Table VIII. Numerical Example 4 Given $\{\lambda^0\}$ of 4 and 10 Blood Pressures

true value (kPa)	0.0	0.222	0.222	0.0
initial guess(kPa)	-0.02	0.12	0.1	-0.03
No. of pressures	4			
output (kPa)	-0.004	0.203	0.232	0.01
iteration number	40			
absolute L^2 error	$2.5\text{e}-02$			
$\|\nabla D\|_{L^2}$	$7.43\text{e}-05$			
No. of pressures	10			
output (kPa)	-0.003	0.2112	0.2311	0.006
iteration number	29			
absolute L^2 error	$1.0\text{e}-02$			
$\|\nabla D\|_{L^2}$	$7.76\text{e}-04$			

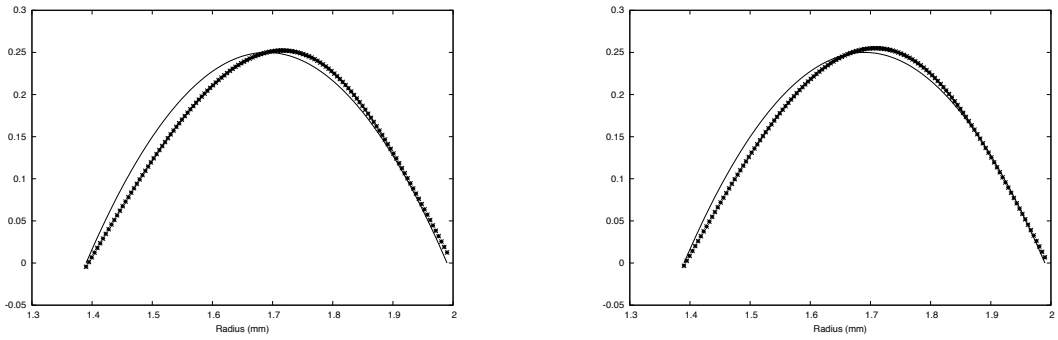

(a) Given 4 Pressures (b) Given 10 Pressures

Fig. 11. Reconstruction of Example 4

Table IX. Numerical Example 4 Given $\{\lambda^0, \lambda^1\}$ of 10 Blood Pressures

No. of pressures	10			
true value (kPa)	0.0	0.222	0.222	0.0
initial guess(kPa)	1	2.0	2.0	1.0
output (kPa)	-0.001	0.224	0.224	-0.001
iteration number	103			
absolute L^2 error	$1.88\text{e}-06$			
$\|\nabla D\|_{L^2}$	$5.0\text{e}-03$			

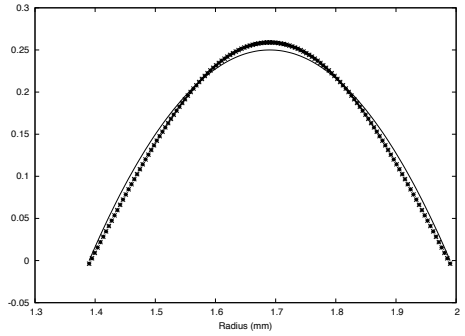

Fig. 12. Reconstruction of Example 4 for Initial Guess $\{1.0, 2.0, 2.0, 1.0\}$

.

sures. See Table X and Figure 13 for output and plots. This shows that the first eigenvalues $\{\lambda^0\}$ are not sufficient to get a good estimate of the function if the initial guess in far away from the solution, and may result in convergence to a different local minimizer. The first eigenvalues of the final solutions $\{0.217, -0.005, -0.005, 0.217\}$ and $\{0.217, -0.005, -0.005, 0.217\}$ were computed and found to be equal, which is why the line search was unable to locate the right direction of descent.

Example 5. In this example, the orginal function is $\boldsymbol{\tau} = \sin\left(2\pi\left(\frac{x-x_0}{x_1-x_0}\right)\right)$ and we use the cubic spline interpolation of the function at 7 nodes. The function is estimated

Table X. Numerical Example 4 Given $\{\lambda^0\}$ and $\{\lambda^0, \lambda^1\}$ of 10 Blood Pressures

No. of pressures	10			
Tolerance	$t_r = 1.0\text{e}-05$		$t_a = 1.0\text{e}-06$	
true value (kPa)	0.0	0.222	0.222	0.0
initial guess(kPa)	5.0	5.0	5.0	5.0
Eigenfrequencies	$\{\lambda^0\}$			
output (kPa)	0.217	-0.005	-0.005	0.217
iteration number	41			
absolute L^2 error	$2.4\text{e}-01$			
$\|\nabla D\|_{L^2}$	$8.5\text{e}-04$			
Eigenfrequencies	$\{\lambda^0, \lambda^1\}$			
output (kPa)	-0.001	0.223	0.223	-0.001
iteration number	94			
absolute L^2 error	$1.8\text{e}-03$			
$\|\nabla D\|_{L^2}$	$4.4\text{e}-04$			

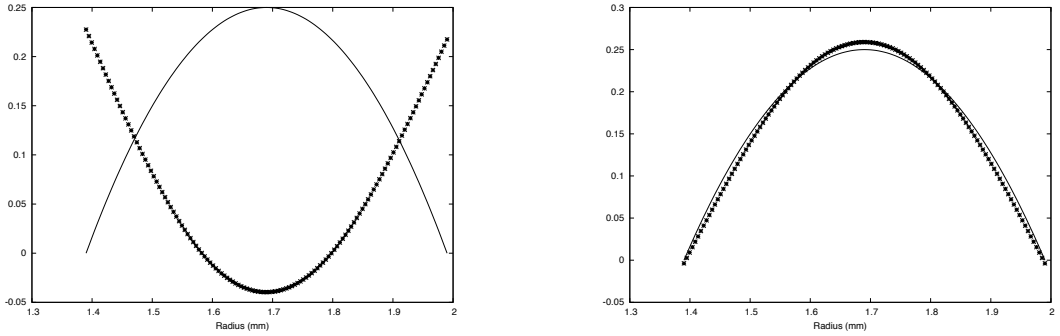

(a) Given $\{\lambda^0\}$ (b) Given $\{\lambda^0, \lambda^1\}$

Fig. 13. Reconstruction of Example 4 and Table X

given the first three eigenfrequencies of six blood pressures $\{45, 93, 100, 120, 130\}$ mmHg and the initial guess is taken to be $(-0.01, 2.0, 2.0, -0.3, -2.0, -2.0, 0.02)$. We employ two different methods for updating the matrix $\boldsymbol{H}_k$ in the Levenberg-Marquardt algorithm, namely, using (5.18) and (5.22) with all other parameters fixed and compare the results. We observe that although the initial guess is far away from the true solution, the objective function $D(\boldsymbol{\tau}^{(0)}) = \frac{1}{2}\sum_{l=1}^{m*n} |\lambda^l(\boldsymbol{\tau}^{(0)}) - \tilde{\lambda}^l|^2$ and the Jacobian norm $\|\boldsymbol{R}'(\boldsymbol{\tau}^{(0)})\|$ are very small. As a result, the value of $\gamma_k \, diag\,[\boldsymbol{R}'(\boldsymbol{\tau}^{(k)})^T \boldsymbol{R}'(\boldsymbol{\tau}^{(k)})]$ at the k-th iteration, with γ_k given by (5.37), is very small, and hence, (5.22) acts like a Gauss Newton iteration. This makes the algorithm very slow, and in cases where it converges, it requires a lot of iterations. On the other hand, if (5.18) is used to update the $\boldsymbol{H}_k$, the step lengths at each iteration are large enough for the algorithm to converge to the true solution efficiently. Our numerical experiment shown in Table XI depict this. We halt the iteration for (5.22) in 42 steps to compare it with the other case which converges in 42 iterations. The plots are shown in Figure 14.

2. Model Problem II

Example 6. The function we want to approximate is $\boldsymbol{\tau} = 1 - \left(\frac{x - x_0}{x_1 - x_0}\right)^2$ and we use the cubic spline interpolation of the function at 5 nodes. The initial guess is taken to be $(-0.01, 0.1, 0.1, 0.1, -0.02)$ and only the first eigenfrequency of each blood pressures are assumed to be given. Tables XII and XIII show the input and output for the iterations with 6 blood pressures, $\{45, 93, 100, 120, 130, 150\}$ mmHg, and 10 blood pressures, $\{30, 45, 54, 75, 93, 100, 105, 120, 130, 150\}$ mmHg, respectively, and the reconstructions are shown in Figure 15. This example shows that a higher number of blood pressures gives a better reconstruction.

Table XI. Numerical Example 5 with 6 Blood Pressures

No. of pressures	6						
Tolerance	$t_r = 1.0\text{e}-05$			$t_a = 1.0\text{e}-06$			
true value (kPa)	0.0	0.866	0.866	0.0	0.866	0.866	0.0
initial guess(kPa)	-0.01	2.0	2.0	-0.3	-2.0	-2.0	0.02
$\boldsymbol{H}_k$ updated with (5.22)							
output (kPa)	-0.04	1.923	1.976	-0.02	-1.99	-1.98	0.097
$\boldsymbol{H}_k$ updated with (5.18)							
output (kPa)	-0.08	0.832	0.894	-0.0118	-0.906	-0.858	0.146
iteration number	46						
absolute L^2 error	$1.7\text{e}-1$						
$\|\nabla D\|_{L^2}$	$7.23\text{e}-5$						

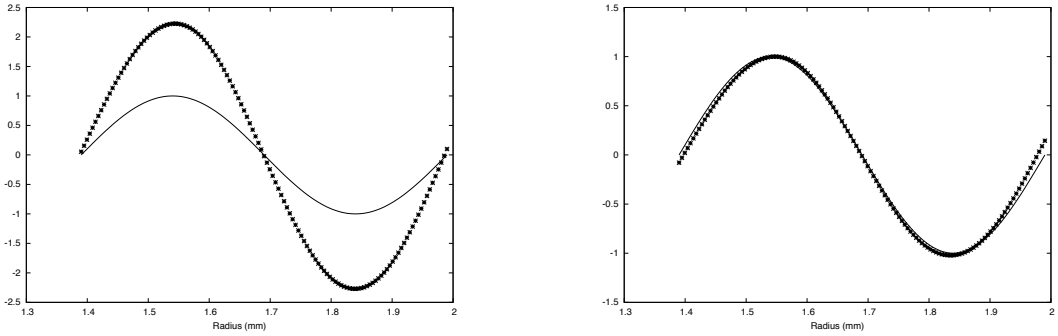

(a) $\boldsymbol{H}_k$ Updated with (5.22) (b) $\boldsymbol{H}_k$ Updated with (5.18)

Fig. 14. Reconstruction of Example 5 and Table XI

Table XII. Numerical Example 6 Given $\{\lambda^0\}$ of 6 Blood Pressures

No. of pressures	6				
true value (kPa)	0.0	0.1875	0.25	0.1875	0.0
initial guess(kPa)	-0.01	0.1	0.1	0.1	-0.02
output (kPa)	-0.04	0.131	0.15	0.136	0.02
iteration number	29				
absolute L^2 error	$1.4\text{e}-1$				
$\|\nabla D\|_{L^2}$	$8.35\text{e}-4$				

Table XIII. Numerical Example 6 Given $\{\lambda^0\}$ of 10 Blood Pressures

No. of pressures	10				
true value (kPa)	0.0	0.1875	0.25	0.1875	0.0
initial guess(kPa)	-0.01	0.1	0.1	0.1	-0.02
output (kPa)	-0.01	0.132	0.203	0.13	0.04
iteration number	35				
absolute L^2 error	$1.0\text{e}-1$				
$\|\nabla D\|_{L^2}$	$3.0\text{e}-2$				

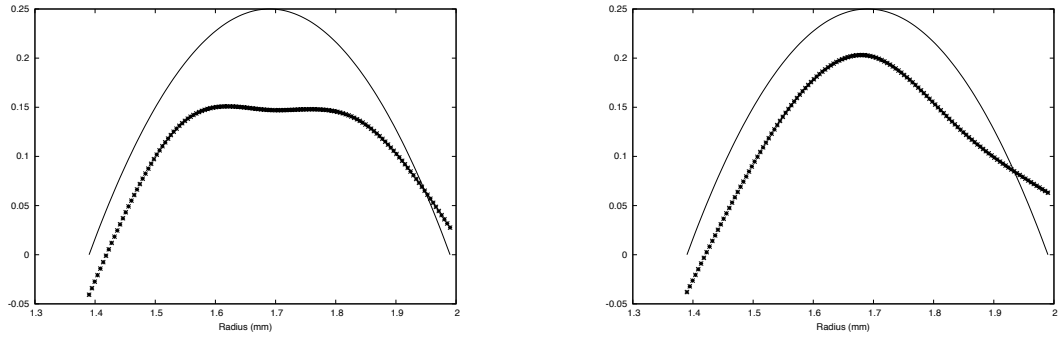

(a) Given 6 Pressures (b) Given 10 Pressures

Fig. 15. Reconstruction of Example 6

Table XIV. Numerical Example 7 with $\{\lambda^0\}$

No. of pressures	10				
true value (kPa)	0.0	0.1875	0.25	0.1875	0.0
initial guess(kPa)	-0.01	0.1	0.4	0.1	-0.02
output (kPa)	-0.02	0.15	0.225	0.15	0.04
iteration number	25				
absolute L^2 error	$5.22\text{e}-2$				
$\|\nabla D\|_{L^2}$	$2.0\text{e}-2$				

Table XV. Numerical Example 7 with $\{\lambda^0, \lambda^1\}$

No. of pressures	10				
true value (kPa)	0.0	0.1875	0.25	0.1875	0.0
initial guess(kPa)	-0.01	0.1	0.4	0.1	-0.02
output (kPa)	-0.0001	0.189	0.248	0.18	0.004
iteration number	34				
absolute L^2 error	$8.63\text{e}-3$				
$\|\nabla D\|_{L^2}$	$4.0\text{e}-2$				

Example 7. The original function and the number of nodes are the same as in Example 6. The initial guess was taken to be $(-0.01, 0.1, 0.4, 0.1, -0.02)$ and a total of 10 blood pressures $\{30, 45, 54, 75, 93, 100, 105, 120, 130, 150\}$ mmHg were used. Tables XIV and XV shows the input and output for the iterations with data $\{\lambda^0\}$ and $\{\lambda^0, \lambda^1\}$ respectively, and the reconstructions are shown in Figure 16. This example tells us that for a fixed number of blood pressures, a larger number of eigenvalues makes the approximation more accurate as desired.

Example 8. The function we want to reconstruct is $\boldsymbol{\tau}(x) = \cos\left(4\pi\left(\frac{x-x_0}{x_1-x_0}\right)\right)$. We assume we are given data for 10 blood pressures $\{30, 45, 54, 75, 93, 100, 105, 120, 130, 150\}$

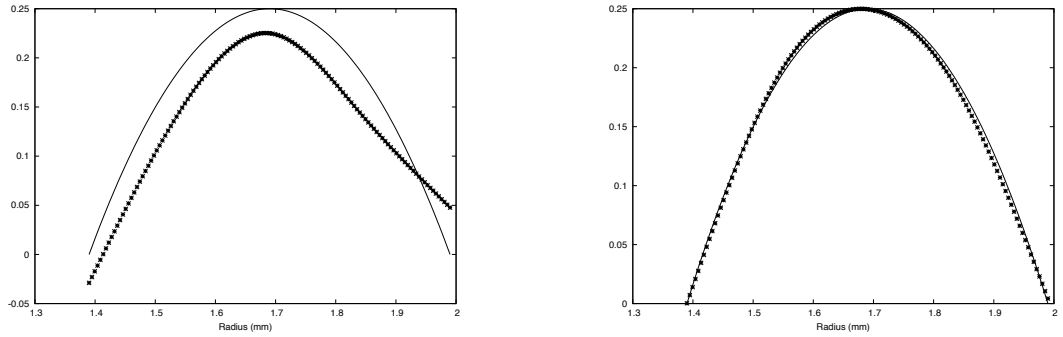

(a) Given $\{\lambda^0\}$ (b) Given $\{\lambda^0, \lambda^1\}$

Fig. 16. Reconstruction of Example 7

mmHg. We run numerical simulations for $\{\lambda^0\}$ and $\{\lambda^0, \lambda^1\}$. The inputs and outputs are shown in Table XVI, and the reconstructions are shown in Figure 17. It can be seen that only the sequence $\{\lambda^0\}$ is not enough to accurately reconstruct the function. An additional sequence of eigenfrequencies gives a much accurate reconstruction. In Figure 18(a), we show the semi-log plot of the the functional value $D(\boldsymbol{\tau})$ with respect to the iteration number and in Figure 18(b), the semi-log plot of $\|\nabla D(\boldsymbol{\tau})\|_{L^2}$ with respect to the iteration number for the case where the sequence $\{\lambda^0, \lambda^1\}$ are given. Both the graphs show that convergence of the algorithm is at least linear.

Table XVI. Numerical Example 8

No. of pressures	10				
true value (kPa)	1.0	-1.0	1.0	-1.0	1.0
initial guess(kPa)	0.0	0.0	0.0	0.0	0.0
Eigenfrequencies	$\{\lambda^0\}$				
Tolerance	$t_r = 1.0\text{e}-05$			$t_a = 1.0\text{e}-05$	
output (kPa)	0.973	-0.668	0.663	-0.491	-0.502
iteration number	41				
absolute L^2 error	$1.65\text{e}+0$				
$\|\nabla D\|_{L^2}$	$3.01\text{e}-2$				
Eigenfrequencies	$\{\lambda^0, \lambda^1\}$				
Tolerance	$t_r = 1.0\text{e}-03$			$t_a = 1.0\text{e}-04$	
output (kPa)	0.999	-0.989	1.002	-1.003	0.984
iteration number	49				
absolute L^2 error	$2.0\text{e}-2$				
$\|\nabla D\|_{L^2}$	$1.4\text{e}+0$				

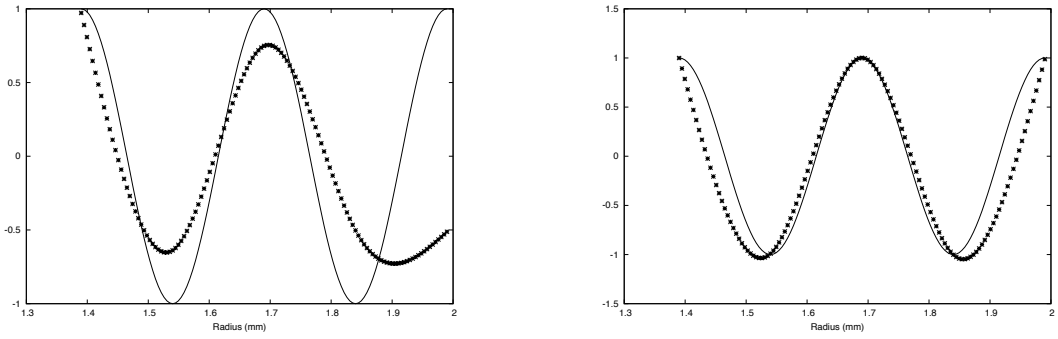

(a) Given $\{\lambda^0\}$ (b) Given $\{\lambda^0, \lambda^1\}$

Fig. 17. Reconstruction of Example 8

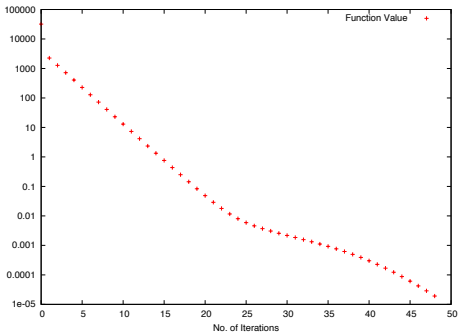

(a) Plot of Function Value $D(\boldsymbol{\tau})$

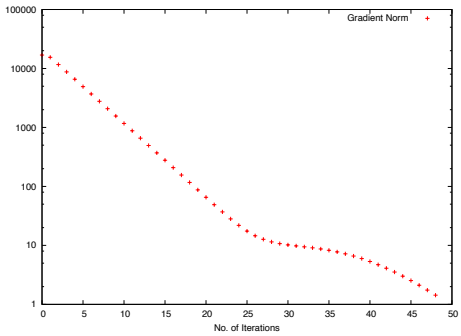

(b) Plot of $\|\nabla D(\boldsymbol{\tau})\|_{L^2}$

Fig. 18. Example 8

CHAPTER VI

SUMMARY

In this chapter, we summarize the contents of this dissertation and briefly discuss possible future work.

A. Conclusions

This dissertation focuses on developing numerical methods to estimate the residual stresses and pre-stresses in a nonlinear elastic body. In particular, we focus on an elastic body that has mechanical properties similar to the arterial wall, and formulate an inverse spectral problem by making use of Intravascular Ultrasound (IVUS) medical technology. In Chapter II, a modeling framework is developed, similar to one proposed in [19], for the response of the residually stressed, hyperelastic, rectangular body subjected to a time varying harmonic pressure on the boundary. A quasi-static boundary value problem is first formulated modeling the large deformation due to induced pressure, and then an idealized model for IVUS is developed such that small amplitude time harmonic vibrations are superimposed upon the static large deformation. The model is then studied for specific classes of deformations in an effort to utilize the semi-inverse approach. Two different forms of constitutive equations incorporating residual stresses are considered. The boundary value problems are constructed for each of the two cases, and the nonlinear inverse spectral problem is formulated to estimate one of the tensile residual stress τ_{11}. We remark that the other two tensile stresses τ_{22} and τ_{33} can be estimated in a similar way by rotating the experimental body in the appropriate direction.

In Chapter IV, the inverse problem is formulated as a system of nonlinear boundary value problems that correspond to different pressures, and an algorithm is con-

structed to estimate the residual stress given the first few eigenfrequencies of each pressure as data. It should be emphasized that this approach utilizes the first few eigenfrequencies of a large number of pressures instead of a large number of eigenfrequencies for a single pressure. This feature not only exploits the nonlinearity of the problem, but also makes the method more robust since the lower eigenfrequencies are the easiest to measure accurately via experiments. This is also the reason why we cannot employ most of the techniques developed in the literature to solve inverse spectral problems for second order boundary value problems. We present numerical simulations to show the viability of the method, discuss the advantages and limitations of the algorithm.

Chapter V provides an alternative approach of formulating the inverse problem as a nonlinear least squares problem, and an algorithm is constructed using optimization techniques for over-determined problems. The Levenberg-Marquardt method is employed along with a line search technique to enhance the robustness of the algorithm. Global and local convergence of the method is discussed, and numerical simulations are presented.

B. Future Work

There are many opportunities for future work motivated by this project that generalize the model to more complex problems. One could investigate the validity of the results for more realistic constitutive models, such as those that include anisotropy, and for more sophisticated geometries such as an asymmetrical tubular domain. Other research directions would be to seek solutions within other class of deformations, and to explore different models for incorporating residual stress, such as the multiplicative model introduced in [19]. An important step in continuing the numerical experiments

developed in this dissertation would be to test the algorithms against experimental data. This will not only help validate the model and verify its accuracy, but also be useful in determining to what extent the residual stress fields are affected by linearizing the problem. One could also investigate the presence of residual stresses by solving the full three dimensional nonlinear wave equation and comparing it with the linearized model.

Finally, the *Secant Method for the Inverse Spectral Problem* developed in Chapter IV is only locally convergent, and the nonlinear least squares algorithm developed in Chapter V is a local optimization method. It is sensitive to the initial guess that starts the iteration due to presence of multiple local minima of the objective functional. In order to find a global minimizer of the over determined problem, one needs to employ global deterministic or stochastic optimization methods.

REFERENCES

[1] L. E. Andersson, *Inverse eigenvalue problems for a Sturm-Liouville equation in impedance form*, Inverse Problems, 4 (1988), pp. 353–397.

[2] Larry Armijo, *Minimization of functions haveing lipschitz continuous first partial derivatives*, Pacific Journal of Mathematics, 16 (1966), pp. 1–3.

[3] W. Bangerth, R. Hartmann, and G. Kanschat, *deal.II Differential Equations Analysis Library, Technical Reference*. `http://www.dealii.org` accessed on 5/26/2010.

[4] W. Bangerth, R. Hartmann, and G. Kanschat, *deal.II—a general-purpose object-oriented finite element library*, ACM Trans. Math. Software, 33 (2007), pp. 24–27.

[5] Ake Bjorck, *Numerical Methods for Least Squares Problems*, SIAM, Philadelphia, 1996.

[6] Amin Boumenir and Vu Kim Tuan, *The Gelfand-Levitan theory revisited*, The Journal of Fourier Analysis and Applications, 12 (2006), pp. 257–267.

[7] R. Bustamante and G. A. Holzapfel, *Methods to compute 3d residual stress distributions in hyperelastic tubes with application to arterial wall*, International Journal of Engineering Science, 48 (2010), pp. 1066–1082.

[8] L Cardamone, A. Valentin, J. F. Eberth, and J. D. Humphrey, *Origin of Axial Prestretch and Residual Stress in Arteries.*, Springer, New York, 2002.

[9] K. Chadan, D. Colton, L. Paivarinta, and W. Rundell, *An Introduction to Inverse Scattering and Inverse Spectral Problems*, SIAM, Philadelphia, 1997.

[10] Ward Cheney and David Kincaid, *Numerical Analysis: Mathematics of Scientific Computing*, American Mathematical Society, Providence, RI, 3rd ed., 2002.

[11] C. J. Chuong and Y. C. Fung, *On residual stresses in arteries*, Journal of Biomechanical Engineering, 108 (1986), pp. 189–192.

[12] Alexander Ern and Jean-Luc Guermond, *Theory and Practice of Finite Elements*, Appl. Math. Sci., 159, Springer-Verlag, New York, 2004.

[13] Richard H. Fabiano, Roger Knobel, and Bruce D. Lowe, *A finite-difference algorithm for an inverse Sturm-Liouville problem*, IMA Journal of Numerical Analysis, 15 (1995), pp. 75–88.

[14] Y. C. Fung, *On the foundations of biomechanics*, ASME Journal of Applied Mechanics, 50 (1983), pp. 1003–1009.

[15] Y. C. Fung, *Biodynamics: Circulation*, Springer-Verlag, New York, 1984.

[16] Y. C. Fung, *Biomechanics. Motion, Flow, Stress, and Growth*, Springer-Verlag, New York, 1990.

[17] Y. C. Fung, *What are the residual stresses doing in our blood vessels?*, Annals of Biomedical Engineering, 19 (1991), pp. 237–249.

[18] I. M. Gel'fand and B. M. Levitan, *On the determination of a differential equation from its spectral function*, American Mathematical Society Translations, 1 (1951), pp. 253–304.

[19] Yuliya Gorb and Jay R. Walton, *Dependence of the frequency spectrum of small amplitude vibrations superimposed on finite deformations of a nonlinear cylindrical elastic body on residual stress.*, International Journal of Engineering Science, 48 (2010), pp. 1289–1312.

[20] Kun Gou, Sunnie Joshi, and Jay R. Walton, *Recovery of material parameters of soft hyperelastic tissue by an inverse spectral technique*, International Journal of Engineering Science, 56 (2012), pp. 1–16.

[21] A. Guillou and R. W. Ogden, *Growth in soft biological tissue and residual stress development*, Mechanics of Biological Tissue, (2006), pp. 47–62.

[22] M. E. Gurtin, *An Introduction to Continuum Mechanics*, Academic Press, New York, 1981.

[23] A. Hoger, *On the determination of residual stress in an elastic body*, Journal of Elasticity, 16 (1986), pp. 303–324.

[24] A. Hoger, *Residual stress in an elastic body: a theory for small strains and arbitrary rotations*, Journal of Elasticity, 31 (1993), pp. 1–24.

[25] J. D. Humphrey, *Cardiovascular Solid Mechanics: cells, tissues, and organs.*, Springer-Verlag, New York, 2002.

[26] B. E. Johnson and A. Hoger, *The use of a virtual configuration in formulating constitutive equations for residually stressed elastic materials*, Journal of Elasticity, 41 (1995), pp. 177–215.

[27] C. T. Kelley, *Iterative Methods for Linear and Nonlinear Equations*, SIAM, Philadelphia, 1995.

[28] C. T. Kelley, *Iterative Methods for Optimization*, SIAM, Philadelphia, 1999.

[29] P. D. Kiousis and G. Z. Voyiadjis, *A note on the reference frame indifference*, Acta Mechanica, 74 (1988), pp. 203–208.

[30] Q. Kong, H. Wu, and A. Zettl, *Dependence of the n-th Sturm-Liouville eigenvalue on the problem*, Journal of Differential Equations, 156 (1999), pp. 328–354.

[31] Q. Kong and A. Zettl, *Eigenvalues of regular Sturm-Liouville problems*, Journal of Differential Equations, 131 (1996), pp. 1–19.

[32] B. M. Levitan, *Inverse Sturm-Liouville Problems*, VNU Science Press, Utrecht, 1987.

[33] X. Li and K. Hayashi, *Alternate method for the analysis of residual strain in the arterial wall*, Biorheology, 33 (1996), pp. 439–449.

[34] Donald W. Marquardt, *An algorithm for least-squares estimation of nonlinear parameters*, SIAM, 11 (1963), pp. 431–441.

[35] T. Matsumoto, T. Furukawa, and K. Nagayama, *Microscopic analysis of residual stress and strain in the aortic media considering anisotropy of smooth muscle layer*, Mechanics of Biological Tissue, (2006), pp. 257–268.

[36] Jorge J. Moré and David J. Thuente, *Line search algorithms with guaranteed sufficient decrease*, ACM Transactions on Mathematical Software (TOMS), 20 (1994), pp. 286–307.

[37] Anuja Nair, Barry D. Kuban, E. Murat Tuzcu, Paul Schoenhagen, Steven R. Nissen, and D. Geoffrey Vince, *Coronary plaque classification with intravascular ultrasound radiofrequency data analysis*, Circulation, 106 (2002), pp. 2200–2206.

[38] J. W. Paine, *A numerical method for the inverse Sturm-Liouville problem*, SIAM Journal on scientific and statistical computing, 5 (1984), pp. 149–156.

[39] Jurgen Poschel and Eugene Trubowitz, *Inverse Spectral Theory*, Pure and Appl. Math., Academic Press, Inc., Orlando, FL, 1987.

[40] P. D. Richardson, *Mechanical properties of atherosclerotic tissues*, Mechanics of Biological Tissue, (2006), pp. 207–223.

[41] William Rundell and Paul E. Sacks, *The reconstruction of Sturm-Liouville operators*, Inverse Problems, 8 (1992), pp. 457–482.

[42] William Rundell and Paul E. Sacks, *Reconstruction techniques for classical inverse Sturm-Liouville problems*, Mathematics of Computation, 58 (1992), pp. 161–183.

[43] M. E. Safar and E.D. Frohlich, *Atherosclerosis, Large Arteries and Cardiovascular Risk*, Adv. Cardiology, 44, Karger Publishers, Basel, 2007.

[44] Jose Seabra, Francesco Ciompi, Petia Radeva, and Joao Miguel Sanches, *A rayleigh mixture model for ivus imaging*, Ultrasound Imaging: Advances and Applications, 1 (2012), pp. 25–47.

[45] J. Stalhand and A. Klarbring, *Parameter identification in arteries using constraints*, Mechanics of Biological Tissue, (2006), pp. 295–305.

[46] R. N. Vaishnav and J Vossoughi, *Estimation of residual strains in aortic segments*, In: Biomedical Engineering II, Recent Developments, (1983), pp. 330–333.

[47] J. Vossoughi, Z. Hedjazi, and F. S. Borris, *Intimal residual stress and strain in large arteries*, In: ASME Advances in Bioengineering, (1991), pp. 434–437.

[48] Philip Wolfe, *The secant method for simultaneous nonlinear equations*, Communications of the ACM, 2 (1959), pp. 12–13.

[49] Anton Zettl, *Sturm-Liouville Theory*, American Mathematical Society, Providence, RI, 2005.

[50] X Zhang, C.R. McKay, and M. Sonka, *Tissue characterization in intravascular ultrasound images*, IEEE Transactions on Medical Imaging, 17 (1998), pp. 889–899.

VITA

Sunnie Joshi was born in Kathmandu, Nepal. She studied at Randolph College beginning August 2003 and graduated in December 2006 with a Bachelor of Science degree in mathematics and a Bachelor of Arts degree in physics. She enrolled in the doctoral program in the Department of Mathematics, Texas A&M University in the fall of 2007. Sunnie can be contacted at:

Department of Mathematics

Texas A&M University

College Station, TX 77843-3368

U. S. A.

Email address: sjoshi@math.tamu.edu